TAMPEREEN TEKNILLINEN YLIOPISTO
TAMPERE UNIVERSITY OF TECHNOLOGY

Katrina Elizabeth Wendel

The Influence of Tissue Conductivity and Head Geometry on EEG Measurement Sensitivity Distributions

Julkaisu 900 • Publication 900

Tampere 2010

Tampereen teknillinen yliopisto. Julkaisu 900
Tampere University of Technology. Publication 900

Katrina Elizabeth Wendel

The Influence of Tissue Conductivity and Head Geometry on EEG Measurement Sensitivity Distributions

Thesis for the degree of Doctor of Science in Technology to be presented with due permission for public examination and criticism in Rakennustalo Building, Auditorium RG202, at Tampere University of Technology, on the 18th of June 2010, at 12 noon.

Tampereen teknillinen yliopisto - Tampere University of Technology
Tampere 2010

ISBN 978-952-15-2383-0 (printed)
ISBN 978-952-15-2537-7 (PDF)
ISSN 1459-2045

Abstract

Electrical neuroimaging is a contemporary functional imaging method that evolves electroencephalography (EEG) beyond traditional signal analysis. It exploits the millisecond temporal resolution of EEG and integrates it with its spatial resolution, which is mapped according to the measurement sensitivity distribution of the measurement leads. This thesis assesses the EEG measurement sensitivity distribution according to the influence of tissue conductivities, electrode placement, electrode type, and geometries upon volume conductor head models.

The conductivity of the skull is correlated with the age of the patient, recognizing that juveniles have higher spatial resolution than adults. Surface electrodes are compared with subdermal electrodes and are found to be non-interchangeable because the subdermal electrodes measure electric activity from one-eighth the volume of their surface-electrode counterparts. More accurate geometrical definitions naturally yield more precise forward and inverse calculations; however, a stochastically deformable generic head model based on anthropometric data addresses the void in imaged and segmented heads of different ages, genders and head shapes. Comprehensively, the investigation of these three key areas improves the knowledge of the EEG measurement sensitivity distributions, which will conceivably translate into clinical improvements in the diagnostics of brain functionality.

Acknowledgements

The work presented in this dissertation was performed at the Department of Biomedical Engineering, Tampere University of Technology, from 2006 to 2010. I gratefully acknowledge my four-year doctoral fellowship with the International Graduate School in Biomedical Engineering and Medical Physics (iBioMEP), Finland. I would also like to acknowledge additional support from the Academy of Finland through the High Resolution EEG Project, the Ragnar Granit Foundation, and grants sponsored by the European COST action NeuroMath (BM0601).

I would like to express my deepest gratitude to my supervisor, Professor Jaakko Malmivuo, for accepting me into his program, his invaluable research guidance, and his enthusiasm and motivation to instruct me how to write scientific literature. I also thank Professor Jari Hyttinen and Dr. Jari Viik for their continuous support and direction. I extend my thanks to the entire Department of Biomedical Engineering for fostering an environment that makes researching, learning, and teaching a pleasure.

I would like to thank my excellent past and present colleagues for invaluable discussions, co-authoring of papers, reviewing my work, and for inspiring me with many ideas. I would especially like to thank the following exceptional individuals, who not only work with me as a colleague, but also incite passion and bring joy to my life: Dr. Rauno Gordon, Dr. Asta Kybartaite, Nathaniel Narra, MSc, Michael Osadebey, MSc, Narayan Puthanmadam Subramaniyam, MSc, and Vladimir Villaseñor Herrera, MSc.

I wish to sincerely thank the examiners of this dissertation for their advice, constructive criticism, and evaluations: Dr. Sylvain Baillet (Medical College of Wisconsin, USA), Dr. Geertjan Huiskamp (University Medical Center

Utrecht, The Netherlands), Dr. Guido Nolte (Fraunhofer Institute FIRST, Berlin, Germany), and Dr. Thom Oostendorp (University Medical Center St. Radboud, Nijmegen, The Netherlands). I also thank Dr. Brian Canfield (University of Tennessee Space Institute, USA) for carefully proofreading this thesis.

Most importantly I would like to thank my parents, my sister Mollie, my brother Andrew, and my love Piotr. You have encouraged me to do my best, motivated me beyond my imagination, taught me that life is a wonderful adventure, and supported me at all times. Love y'all!!!

Tampere, Finland, June 2010

Katrina Wendel

Table of Contents

List of Publications

This doctoral thesis combines selected works of the author into a compendium to analyze the topic of EEG measurement sensitivity distributions. A letter and number comprise the publication key. "P" refers to the appended primary publications, and "S" refers to supplemental publications, which are briefly cited in this dissertation.

Primary Publications

P1 **K Wendel** and J Malmivuo, "Correlation between Live and Post Mortem Skull Conductivity Measurements," oral presentation and Open Finalist in the Student Paper Competition. In *Proceedings of the 28th Annual International Conference of the IEEE Engineering in Medicine and Biology Society*, New York City, USA, pp. 4285–4288, August 30 – September 3, 2006.

P2 **K Wendel**, NG Narra, M Hannula, P Kauppinen, J Malmivuo. The Influence of CSF on EEG Sensitivity Distributions of Multilayered Head Models. IEEE Transactions on Biomedical Engineering, vol. 55, no. 4, pp. 1454–1456, April 2008.

P3 **K Wendel**, M Osadebey, J Malmivuo. "Coupling Axis-Length Profiles with Bezier Splines in Finite Element Head Models," oral presentation and Finalist in the Young Investigators Competition. In *IFMBE Proceedings of the 14th Nordic-Baltic Conference on Biomedical Engineering and Medical Physics*, A Katashev, Y Dekhtyar, and J Spigulis (eds.).

Riga, Latvia, Springer-Verlag, vol. 20, pp. 465–468, June 16–20, 2008.

P4 **K Wendel**, O Väisänen, J Malmivuo, NG Gencer, B Vanrumste, P Durka, R Magjarevic, S Supek, ML Pascu, H Fontenelle, and R Grave de Peralta Menendez. EEG/MEG Source Imaging: Methods, Challenges, and Open Issues. Computational Intelligence & Neuroscience, vol. 2009, article ID 656092, 12 pages, 2009.

P5 **K Wendel**, M Osadebey, and J Malmivuo, "Incorporating Craniofacial Anthropometry into Realistically-Shaped Head Models," oral presentation. In *IFMBE Proceedings on the World Congress on Medical Physics and Biomedical Engineering*, O Dössel & WC Schlegel (eds.), Munich, Germany, vol. 25, pp. 1706–1709, September 7–12, 2009.

P6 **K Wendel**, J Väisänen, G Seemann, J Hyttinen, and J Malmivuo. The Influence of Age and Skull Conductivity on Surface and Subdermal Bipolar EEG Leads. Computational Intelligence & Neuroscience, vol. 2010, article ID 397272, 7 pages, 2010.

P7 **K Wendel**, J Väisänen, A Kybartaite, J Hyttinen, and J Malmivuo. The Significance of Relative Conductivity on Thin Layers in EEG Sensitivity Distributions. Biomedizinische Technik (Biomedical Engineering), vol. 55, no. 3, 2010. Published online ahead of print: 5/05/2010, DOI: 10.1515/BMT.2010.012.

Supplemental Publications

S1 T. Salmi, J. Malmivuo, P. Kauppinen, A. Salmi, **K Wendel**, T. Salpavaara, T. Silfvast, and P. Meriläinen, "Emergency EEG Development of Quick Application on site EEG." Abstract and poster session at the *Nordic Congress of Clinical Neurophysiology.* Helsinki, Finland, 21–24 May 2006.

S2 R Gordon, T Arola, **K Wendel**, O Ryynänen, J Hyttinen. "Accuracy of Numerical Methods in Solving Static and Quasistatic Electric Fields," in *Proceedings of the Estonian Academy of Sciences; Engineering. Special issue on Electronics (Guest ed. M.Min).* Estonian Academy Publishers, Tallinn, vol. 12, no. 3-2, pp. 262–283, September 2006.

S3 **K Wendel**, NG Narra, M Hannula, J Hyttinen, J Malmivuo. The Influence of Electrode Size on EEG Lead Field Sensitivity Distributions. IJBEM, vol. 9, no. 2, pp. 116–117, 2007.

S4 **K Wendel** and J Malmivuo. "The Effect of Electrode Size on Cortical EEG Sensitivity Distributions," oral presentation. In *IFMBE Proceedings of the 14th Nordic-Baltic Conference on Biomedical Engineering and Medical Physics*, A Katashev, Y Dekhtyar, and J Spigulis (eds.). Riga, Latvia, Springer-Verlag, vol. 20, pp. 350–352, June 16–20, 2008.

S5 **K Wendel**, J Väisänen, J Hyttinen, and J Malmivuo, "The Electric Phenomena of Multi-Layered Tissue in EEG Sensitivity Distributions." Abstract and poster presented at the *Advanced Methods for the Estimation of Human Brain Activity and Connectivity*, NeuroMath Cost Action BM0601, Leuven-Heverlee, Belgium. March 12–13, 2009.

S6 **K Wendel**, J Väisänen, J Hyttinen, and J Malmivuo, "The Influence of Age and Skull Conductivity on Surface and Subcutaneous Bipolar EEG Leads," oral presentation. 7^{th} *International Symposium on Noninvasive Functional Source Imaging of the Brain and Heart &* 7^{th} *International Conference on Bioelectromagnetism*, Rome, Italy, May 29–31, 2009.

S7 J Väisänen, **K Wendel**, G Seemann, J Malmivuo, and J Hyttinen. "Sensitivities of Bipolar Subcutaneous and Cortical EEG Leads, " oral presentation. In *IFMBE Proceedings on the World Congress on Medical Physics and Biomedical Engineering*, O Dössel & WC Schlegel (eds.), Munich, Germany, vol. 25, pp. 267–270, September 7–12, 2009.

S8 **K Wendel**, D Stoliar, J Malmivuo, and J Hyttinen. "Measuring Tissue Thicknesses of the Human Head Using Centralized and Normalized Trajectories," poster presentation. *Consciousness and its Measures*, NeuroMath Cost Action BM0601, Limassol, Cyprus, November 29 – December 1, 2009.

S9 N Puthanmadam Subramaniyam, O Väisänen, **K Wendel**, J Malmivuo, "Cortical Potential Imaging with Realistic Head Model using L-Curve and GCV Method," poster presentation. *Consciousness and its Measures*, NeuroMath Cost Action BM0601, Limassol, Cyprus, November 29 – December 1, 2009.

S10 NP Subramaniyam, ORM Väisänen, **KE Wendel**, JAV Malmivuo. Cortical Potential Imaging Using L-curve and GCV Method to Choose the Regularisation Parameter. Nonlinear Biomedical Physics, vol. 4, no. 1, 2010.

S11 A Joutsen, L Lyytikäinen, J Jurva, J Väisänen, **K Wendel**, O Väisänen, JM Tanskanen, V Jäntti, H Eskola, "Median Nerve Somatosensory Evoked Potential Recordings Using Surface and Needle Electrodes," poster presentation. In *The* 29^{th} *Intl. Congress of Clinical Neurophysiology*, ICCN 2010, Kobe, Japan, October 28 – November 2, 2010.

S12 **K Wendel**, ME Osadebey, A Jayasundara, P Dastidar, and J Malmivuo. Radial Vector Representation of MRI Data: Formulation of a Universal Geometric Descriptor for Human Anatomic Structures. Submitted to IEEE Transactions on Medical Imaging.

Author's Contribution

The author has designed the studies, analyzed all results, and composed [P1-P7]. She did receive some assistance in the writing of [P6] and substantial co-writing and assistance from her co-authors with special guidance from R Grave de Peralta Menendez in [P4]. In that article the author was primarily responsible for section 3 "Volume Conductor" and partially, section 2 "Preprocessing". The author made all the FEM models in [P2, P3, P7]. She incorporated profile data in [P3] and geometry generation in [P5] from M Osadebey. Additionally, she included the FDM models from J Väisänen and A Kybartaite into [P6, P7].

List of Abbreviations and Symbols

Abbreviations

2-D	two-dimensional
3-D	three-dimensional
aFDM	anisotropic finite difference method
BEM	boundary element method
BIS	bispectral index
CSF	cerebrospinal fluid
CT	computed tomography
ECG	electrocardiogram
ECoG	electrocorticogram
EEG	electroencephalogram
EIT	electrical impedance tomography
EP	evoked potential
FDM	finite difference method
FEM	finite element method
fMRI	functional magnetic resonance imaging
FSV	fifth sensitivity volume
GFS	global field synchronization
HSV	half sensitivity volume
iFDM	isotropic finite difference method
MEG	magnetoencephalogram
MRI	magnetic resonance imaging
NIH	National Institutes of Health
nonROI	brain source volume excluding the ROI volume

O_Z	occipital electrode location along the midsagittal surface
PET	positron emission tomography
ROI	region of interest
ROISR	region of interest sensitivity ratio
SPECT	single photon emission computed tomography
VHM	Visible Human Man
VHW	Visible Human Woman

Symbols

Γ_Ω	surface of the head
Φ_{LE}	lead field electric potential
σ	electrical conductivity tensor
Ω	volume of the head
$\mathbf{E_{LE}}$	reciprocal electric field
$\mathbf{J}$	total current density
$\mathbf{J}^i$	volume source current density
$\mathbf{J}_{LE}$	lead field current density
$\mathbf{n}$	vector normal to the surface
V_{LE}	lead voltage
v_B	volume of the brain source region
v_{nonROI}	volume of the brain source excluding the region of interest
v_{ROI}	volume of the region of interest
v_S	volume of a sphere

Chapter 1

Introduction

1.1 The Motivation to Understand EEG Leads

Interest in treating and healing neurological illnesses dates back thousands of years. A skull from 5100 B.C. shows signs of brain surgery in the form of trepanation from the Late Neolithic Age [Alt et al., 1997]. Evidence from Greek and Roman antiquity shows that early writers accompanied drawings with their descriptions of the nervous system [Clarke and Dewhurst, 1996]. British physician Richard Caton [1875] recorded the first electrocorticogram (ECoG) on exposed animal brains thereby advancing the field from anatomy to electrical physiology. Over 80 years ago Hans Berger [1929] recorded the first human electroencephalogram (EEG) on the surface of the scalp, which he described as a "window into the brain." Since then the field of electroencephalography has evolved to recording and analyzing the spatial and temporal dynamics of neuroelectric activity.

Neuroscientists ultimately aim to understand the nervous system, to evaluate its functional processes, to identify corresponding cortical areas regarding physiological functionality, to detect and investigate neurological diseases, and to learn how human beings perceive, think, store and process memories. Prior to deciphering the thought process, many researchers investigate neural storage, connectivity patterns, and dynamic oscillations within the brain [Buzsáki, 2006]. Our brains certainly are not static — they are dynamic environments. Therefore, EEG and magnetoencephalogram (MEG) recordings optimally capture the neuroelectrically-generated signals with millisecond temporal resolu-

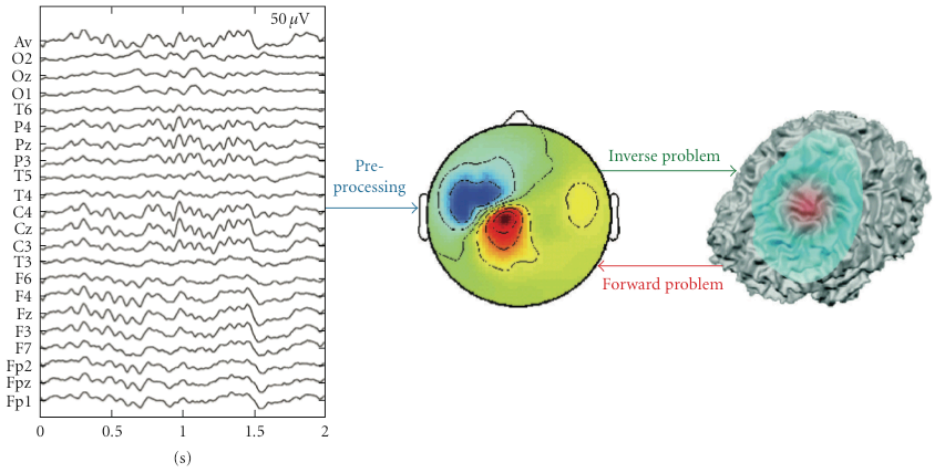

FIGURE 1.1: Key parts of source imaging. Preprocessing prepares the recorded signals for solving the inverse problem. The inverse problem attempts to locate the sources from recorded measurements, whereas the forward problem assumes a source definition in order to calculate a potential distribution map. Reproduced from [P4].

tion [Michel et al., 2004b]. Traditional EEG analysis evaluates frequency content and waveform morphology. Neuroimaging moves beyond traditional EEG as a functional imaging method, utilizing the millisecond temporal resolution with the spatial resolution influenced by the measurement leads [Gevins et al., 1990; Michel et al., 2004b, 2009]. Other functional imaging modalities offer better spatial resolution but worse temporal resolution, such as functional magnetic resonance imaging (fMRI), positron emission tomography (PET), and single photon emission computed tomography (SPECT) [Gevins et al., 1990; Babiloni et al., 2001; Michel et al., 2004b; Enderle et al., 2005]. Combined or considered separately, these five non-invasive techniques comprise the contemporary techniques used to evaluate brain functionality.

As we altruistically extend our curiosity beyond the laboratory, we apply our experimental research into clinical practice. Two primary applications of EEG bridge this gap — signal analysis and source imaging (Fig. 1.1). In signal analysis researchers evaluate cognitive and functional processes from recorded EEGs [Akhtari et al., 2000, 2002; Niedermeyer and Lopes Da Silva, 2005; Sörnmo and Laguna, 2005; Nunez and Srinivasan, 2006], [S11]. For instance, anesthesiology is one important area that relies upon the traditional signal analysis of the EEG as patients undergo different depths of anesthesia.

In this clinical application of EEG, a lack of knowledge exists in understanding the measurement sensitivity distributions of different EEG leads in terms of electrode dimensions, type, and placement. This example highlights that other fields ranging from neurology to ambulatory EEG [S1] to cognitive neuroscience do not have a clear understanding of what each EEG measurement lead, i.e. channel, truly measures. Moreover, this misunderstanding or lack of knowledge of the EEG measurement sensitivity resolution extends beyond anesthesiology into the current trend of establishing brain connectivity patterns or preprocessing the signal for inverse problems [Durka et al., 2005; Leal et al., 2006; Michel et al., 2009], [P4].

Over the last four decades researchers have experimentally tested the subdermal electrodes as a possible substitute for surface electrodes [Zablow and Goldensohn, 1969; Siivola and Järvilehto, 1982; Dumitru and Lester, 1991; Hemmerling et al., 2002; Young et al., 2006; Martz et al., 2009]. Many of the earlier studies claimed that the subdermal needle electrodes yielded similar waveform and latency data for evoked potential (EP) trials with a sufficient number of epochs as surface cup electrodes [Zablow and Goldensohn, 1969; Siivola and Järvilehto, 1982; Dumitru and Lester, 1991].

Bispectral index (BIS) studies began comparing surface and subdermal electrode types for ease of use and practicality and similarly concluded that amplitudes and latencies correlated between electrode types [Hemmerling and Harvey, 2002; Hemmerling et al., 2002; Akavipat et al., 2006]. However, Sebel et al. [2004] and McCulloch [2005] advised that cortical activity should be evaluated on an individual basis rather than relying upon a sole number to indicate depth of anesthesia because BIS suffers from the EEG inverse problem of non-uniqueness [Jäntti and Alahuhta, 2002]. Clearly, the intensive care unit and the operating room need subdermal electrodes due to their practical advantages such as extended periods of usage [Martz et al., 2009]. Patients even prefer the needle electrodes [Dumitru et al., 1992]. What these studies lack and medical doctors inquire about is a clear understanding of what various electrode shapes, montages, and configurations really measure.

Collectively, these wide-ranging clinical areas from anesthesiology to neurology to cognitive neuroscience necessitate an exposition upon the EEG measurement sensitivity distributions. To fulfill such a treatise benefiting the patients of these areas motivates an investigation of normative sensitivity volumes across different people, genders and ages. By aiming to study such a substantial patient base requires knowledge of the changes in tissue conductiv-

ity with respect to age as well as the geometrical knowledge of each patient's head geometry. Unfortunately, not all patients will require individual imaging, such as patients undergoing anesthesia for surgery of other body parts. Therefore, developing a generic head model fills the void in missing head geometries that are not already imaged or segmented. Deforming a proposed generic model according to anthropometric data will provide a comprehensive survey across age, gender, and head shape in order to minimize the misinterpretation of the EEG measurement sensitivity distributions.

Europe annually spends nearly 400 billion Euros (ca. 35% of the healthcare budget) on neurological diseases [Vukov-Colić, 2010]. The cost of creating personalized head models currently includes time, the related expenses for high resolution imaging modalities such as computed tomography (CT) and magnetic resonance images (MRI), and the cost for segmenting the image data and the construction of the volume conductor head model. Furthermore, it eliminates the need for any unnecessary MRIs or radiation-based CTs for anesthesia patients. The proposed models in this dissertation combines anthropometric data with pre-existing segmented clinical data.

The future goal of EEG sensitivity distributions includes better classification and characterization of a patient's measured source regions according to his or her age, gender, and head shape. Furthermore, such a tool will enable electroencephalographers to differentiate which sensitivity volumes to reference for healthy, neurologically diseased, and morphologically deformed patients, thus enhancing the diagnosis of neurological disorders that could be either congenital or environmentally acquired.

1.2 Objectives

The goal of this thesis is to understand how the accuracy of the EEG measurement sensitivity distribution depends on tissue conductivity values, geometry of modeled layers, electrode placement, and electrode type. As a consequence, researchers will be able to improve their source imaging studies, and clinicians may gain insight as to where and what a single EEG channel senses. As a secondary benefit of this thesis, the framework for building and evaluating adaptable generic head models improves the modeling efficiency, and a tertiary benefit reduces the overall cost.

The ensuing discussion of chapters 4–6 conveys the complex dependencies of EEG measurement sensitivity distributions upon tissue conductivities, the

geometrical juxtaposition of tissues, and electrode configurations. This thesis assesses which regions contribute and with what weight an EEG lead measures the neuroelectric activity, i.e., its measurement sensitivity distribution. This thesis hypothesizes that individual characteristics of the patient, such as age, gender, and head shape, as well as electrode characteristics, directly influence each model's forward solution and consequently each measurement lead's sensitivity distribution. In order to contribute and impart such an understanding to the medical community several key areas need to be investigated:

- To identify key modeling areas of EEG source imaging and discuss important open issues warranting further investigation [P4].
- To evaluate the key open issue of tissue conductivity values. These values are correlated with the influence of age and growth upon EEG sensitivity distributions [P1, P4, P6].
- To assess the influence of juxtaposed tissues according to conductivity values, and how they contribute to a lead's measurement sensitivity distribution [P2, P7].
- To identify the influence of surface and subdermal EEG electrodes have upon the measurement sensitivity distributions by understanding how their shape, size, and location detects the neurological source activity [P2, P6].
- To develop a method to examine the role of gender, ethnic group and head shape as it influences the EEG lead field measurement [P3–P7].

Chapter 2

Background

In order to understand the measurement sensitivity distributions of neuroelectric activity of the brain, this background chapter elucidates upon four key areas: EEG electrode systems, head volume conductor models, the underlying equations and the numerical methods that solve both the well-posed forward problems and the ill-posed inverse problems. The first section reviews various EEG montages in order to aid the reader in understanding the placement of the leads in the model as well as on patients. The second section appraises the volume conductor model, which entails the geometry and conductivities applied to the model. The third section explains the lead field and the reciprocity theorem applied to the model, and the last section provides a synopsis of the numerical methods available.

2.1 EEG Electrode Systems

Before analyzing electrode sensitivity distributions, this section reviews the present state of various EEG montages. The montages comprise an arrangement of EEG channels, i.e., leads. These leads can be individually placed or arranged in a cap. The composition of the effective electrode area is typically fabricated from silver, silver-chloride, tin, gold or stainless steel [Grimnes and Martinsen, 2000; Ollikainen et al., 2000]. The shape of the electrode classifies its type as either a surface or subdermal electrode. The surface electrodes consist of conductive cups usually measuring 10 mm in diameter, sponges or rubber cups embedded into a wired elastic cap, and disposable adhesive disc

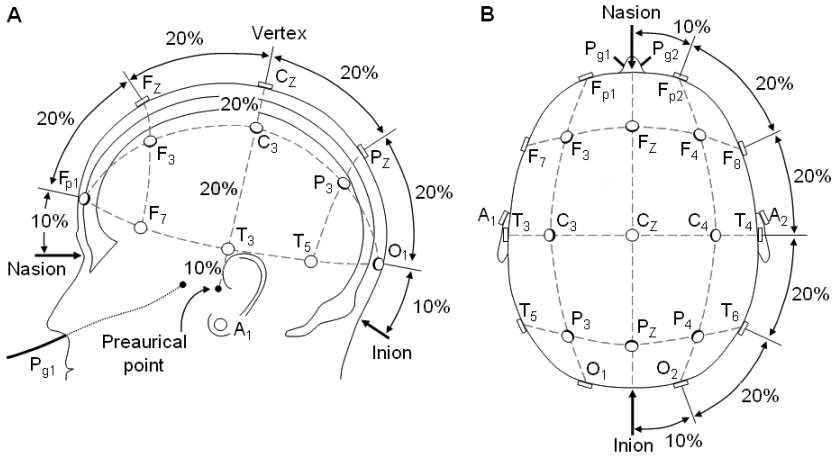

FIGURE 2.1: (a) The sagittal and (b) the superior transverse view of the 10-20 system. Reproduced from [Sharbrough et al., 1991].

electrodes. The disposable electrodes have two important dimensions: the pregelled area conventionally measures 10 mm in diameter, whereas the effective electrode area of the metal depends on the vendor.

There are two primary areas where the EEG montages differ in how they are positioned on the patient – craniometric landmarks and registered montages. The montages referencing the craniometric landmarks require knowledge by the technician to apply the elastic electrode caps [Felten and Shetty, 2010], whereas the registered systems detect the location of the electrodes either manually or automatically.

Currently, most clinical practices use the standard international 10-20 electrode system established by Jasper [1958a, b]. This 10-20 system initially defines four cranial landmarks to orient the electrodes in reference to the nasion, inion, and left and right preaurical points (Fig. 2.1). The nasion and inion are craniometric landmarks, i.e., discernible points on the skull. The nasion is the depression where the frontonasal and internasal sutures connect [Moore and Dalley, 2005], and the inion is the external occipital protusion felt along the lower midsagittal surface at the base of the skull [Moore and Dalley, 2005; Venes, 2005]. These points coupled with the vertex define the midsagittal plane passing through the patient's head. Furthermore, these locations aid the technicians applying the electrode caps as well as the researchers identifying the recorded electrode locations in patient-matched medical images.

Comprehensively, landmark-based montages reproduce accurate electrode locations from the anterior to the posterior of numerous patients. Moreover, computer algorithms can analyze the CT of a patient to detect these two landmarks in order to automate the actual location of the electrodes by projecting the local minima and maxima of the skull for the nasion and inion, respectively, onto the scalp surface [Darvas et al., 2006; Stoliar, 2009], [S8]. The dextral and sinistral preaurical points contain slightly more variance in their positioning. These points comprise either the tragus, which is the cartilaginous projection anterior to the ear [Venes, 2005; Stoliar, 2009], or the temporo-mandibular joint (i.e., mastoids) [Cacioppo et al., 2007; Stoliar, 2009]. Algorithms also rely upon local maxima for detection of either of these points.

The design of an electrode montage comprises the number, position, and size of the electrodes, thus influencing the measurement sensitivity of each channel. In the 10-20 system the separation distance between electrodes has been measured as a percentage of the interval between these four craniometric landmarks. Presently, clinical EEG recordings typically employ either 15 or all 21 electrodes of the standardized 10-20 system [Felten and Shetty, 2010], and the electrode contact area with the scalp measures 10 mm [Ollikainen et al., 2000]; however, modern brain research requires better spatial resolution than the 10-20 system yields [Gevins et al., 1995; Babiloni et al., 1997; Gevins et al., 1999; Babiloni et al., 2001; Michel et al., 2004b].

High resolution EEG meets the demand of improved spatial resolution by increasing the number of electrodes included within the system. These montages often consist up to 256 electrodes according to craniometrically-based montages or equidistant spacing, thus requiring registration of the electrodes. The landmark-based systems include the 10-10 system (a.k.a. 10% system) and the 10-5 system (a.k.a 5% system). The 10-10 and the 10-5 systems are extensions of the original 10-20 system comprising up to 74 and 345 electrode locations, respectively [Chatrian et al., 1985; Oostenveld and Praamstra, 2001; Oostenveld, 2006]. The American Electroencephalographic Society and the International Federation of Societies for Electroencephalography and Clinical Neurophysiology endorsed the 10-10 system [Sharbrough et al., 1991; American Encephalographic Society, 1994; Gilmore, 1994; Nuwer et al., 1998; Klem et al., 1999; Oostenveld and Praamstra, 2001; Oostenveld, 2006].

Contrastingly, the registration-based systems utilize either electromagnetic digitizers (Polhemus^{TM} FastTRACK) [Le et al., 1998; Koessler et al., 2007] or photogrammetric systems [Gilmore et al., 2005; Lamm et al., 2005; Russell

et al., 2005]. The registration process benefits the EEG application because precise positioning of the electrode cap is no longer required.

Several companies compete for a portion of the EEG market share. The 10-20 systems sell to both clinical and research facilities, whereas, mostly only the research institutes seek the high resolution montages. Research EEG caps on the market include the Brain Product, EasyCap, Electro-Cap [Blum and Anneveldt, 1982], Frauenhofer Institute's Speed Cap, Geodesic sensor net [Tucker, 1993], and Neuroscan Quik-Cap. Electric Geodesic Inc. also produces the Geodesic Photogrammetry System [Gilmore et al., 2005; Russell et al., 2005].

2.2 Head Volume Conductor Models

The geometry and conductivity values determine the measurement sensitivity distributions of a volume conductor. Simpler models often yield more generalized and theoretical results, while highly complex models tend to seek specific answers relevant to a smaller subset of models. Similarly, isotropic and anisotropic conductivity values affect the model simulations according to measurement values taken from live and *post mortem* tissue samples.

2.2.1 Forward and Inverse Problems

The forward and inverse problems are two types of mathematical problems that are available to study the physical phenomena of some branch of science. Both of these problems comprise three components (Fig. 1.1): the data, the model, and the model parameters. Applying these generalized problems to the field of electrical neurophysiology specifies the data as EEG, the model as the head model volume conductor, and the model parameters as the neuroelectric sources.

The forward problem assumes a distribution of sources (i.e., neuroelectric sources) and applies it to the volume conductor (i.e., the head model) to generate data (i.e., a surface potential map of estimated EEG data) (Fig. 1.1 red arrow.) Moreover, the reciprocity theorem according to Helmholtz [1853] may be applied to the forward problem, which states that the sources and measurement locations may by exchanged. Energizing the measurement lead as the source maps the measurement sensitivity distribution of the lead [McFee and Johnston, 1953, 1954a, b; Plonsey, 1963; Malmivuo and Plonsey, 1995].

This latter approach of the forward problem is the type discussed in this thesis. Furthermore, forward problems fulfill the following three conditions of well-posed problems: existence, uniqueness, and stability of the solution or solutions [Hadamard, 1902].

The inverse problem uses the data (i.e., the recorded EEG) and the volume conductor (i.e., the head model) to estimate the distribution of sources (i.e., neuroelectric sources) (Fig. 1.1 green arrow.) Contrastingly, the inverse problems are typically ill-posed and often ill-conditioned, requiring regularization. These problems do not have unique solutions; therefore, they necessitate a priori assumptions to reduce the set of solutions to reasonable estimated representations of the physiological phenomena [Michel et al., 2004b, 2009].

In the early inverse-problem models researchers attempted to locate one or more sources of neuroelectric activity via source localization [Koles, 1998; Leahy et al., 1998; Huiskamp et al., 1999; Pascual-Marqui, 1999; Vanrumste et al., 2001; Yao and Dewald, 2005]. Recently, source localization has evolved into source imaging where researchers identify regions within the brain that most likely contribute to both focal and nonfocal sources. The source imaging aids detecting epileptic centers for presurgical planning and cognitive regions [Gevins et al., 1991; Babiloni et al., 1997; Ollikainen et al., 2001; Michel et al., 2004b, 2009], [P4, S9, S10].

Using Green's theorem, Yamashita [1982] proved that the source compartment, i.e., the brain, can be removed from the model. This proof claims that the solution on a closed surface is unique even though it may still be ill-posed. To overcome the ill-posedness of the inverse problem, models with omitted source spaces apply a deblurring kernel to the scalp potentials to obtain a unique cortical potential image [Ryynänen et al., 2004a, 2006], [S9, S10].

2.2.2 Spherical and Elliptical Geometries

The forward problem has a unique solution [Malmivuo and Plonsey, 1995], [P4], but the model it is based upon is still only an estimate of the anatomy and physiology of the human head. One of the earliest estimates for the head model was constructed as three concentric spheres [Rush and Driscoll, 1969]. The three compartments referred to the brain, skull, and scalp. Later researchers concluded that a fourth shell is necessary — the cerebrospinal fluid (CSF) [Zhou and van Oosterom, 1992; Ferree et al., 2000]. Investigations that continued this pursuit of a general understanding of the neuroelectric phenomena involved often tailor spherical models to address specific issues such

as local variations [Cuffin, 1993], noise [Ryynänen et al., 2006], conductivity values [Ryynänen et al., 2006], electrode properties in 2-D and 3-D [Suesserman et al., 1991; Ollikainen et al., 2000], source localization [Vanrumste et al., 2001], and spatial resolution [Malmivuo et al., 1997; Malmivuo and Suihko, 2004].

The elegance of these simple models is inherent in that they can be solved analytically. The analytical method has a direct solution, hence it does not require an iterative numerical solver (Sec. 2.4). This simplicity is extended through to the ellipsoid and perturbed spheroid solutions [Nolte and Curio, 1999]. However, when realistically-shaped electrodes replace the point electrode model, a numerical method is necessary to solve either the forward or inverse problem using the spherical volume conductor model [Ollikainen et al., 2000], [P2, S2–S4].

2.2.3 Realistic Geometry

The poor sphericity of the viscerocranium and the frontal and temporal lobes of the brain led researchers into improving the geometry beyond the spherical model [Hämäläinen and Sarvas, 1989]. Realistically-shaped models increase the model complexity in order to reduce errors in source localization, source imaging, and scalp potentials [Gevins et al., 1991; Cuffin, 1995; Babiloni et al., 1997; Huiskamp et al., 1999; Michel et al., 2004b].

Realistic models are constructed from a set of segmented image slices, usually originating from one of the primary medical imaging modalities — CT or MRI. Considering their pros and cons, CT more accurately images the skull due to its sensitivity to hard tissue via radiation, whereas MRI better images soft tissues such as the skin, cortex, and the gray matter-white matter boundary and is safe. The differences between the three-layer CT- and MRI-based models in [Huiskamp et al., 1999] illustrate significant differences at the base of the skull.

Unfortunately, diagnostic equipment that is available to adults is not optimal for children in terms of safe radiation limits. Such imaging modalities include CT, PET, and SPECT, which use ionizing radiation or radioactive tracers. Due to the nature of these technologies, children will only obtain such screening in extreme cases [Yusof, 2007]. MEG is safe, but it is often limited by the availability of smaller helmets, which locate the gradiometers closer to the scalp surface. EEG is safe and readily adaptable to various head sizes due to the elastic nature of most EEG caps.

2.2.4 Tissue Conductivity Values

The basis for contemporary conductivity values stems from historical conductivity measurements. The initial attempt to explain the lead fields required an estimated conductivity value for the scalp, skull, and brain. Rush and Driscoll [1968, 1969] saturated a dried skull with saline solution to estimate a brain:skull conductivity ratio of 80:1 and equated the scalp conductivity to the brain conductivity. Nearly three decades passed before these estimated values were challenged and other tissues were added to EEG head models.

In 2000 Akhtari et al. [2000] reported low conductivity values for a skull sample ranging from 7.6 to 11.5 mS/m. Their measurements were performed on a 2-year-old cadaver. In the same year, Oostendorp et al. [2000] measured a fresh *post mortem* skull sample, concluding that the brain:skull conductivity ratio should shift to 15:1. In 2002 Akhtari et al. [2000] repeated their measurements on a fresh tissue sample measuring 16.2 to 41.1 mS/m on the diploë (cranial spongiform layer), and 5.4 to 7.2 mS/m on compact bone. Then Hoekema et al. [2003] suggested that the ratio could be as low as 5:1.

Both human as well as other mammalian tissues have been studied to acquire a broad spectrum of tissue conductivity values for modeling purposes [Geddes and Baker, 1967; Gabriel et al., 1996a, b, c; Gabriel, 2005; Gabriel et al., 2009; Peyman et al., 2001, 2002, 2007, 2009]. Controversy exists over the values reported in the literature due to live versus *post mortem* acquisition and the time in minutes and hours after death. Furthermore, the debate extends to the temperature and moisture presence of the tissues.

Additionally, anisotropy exists within the skull and white matter [Nicholson, 1965], where the literature reporting these values is limited. Several modeling studies reported the significance of these directional conductivity values, which should encourage further experimental studies to determine the live tissue conductivies [Haueisen et al., 2002; Hallez et al., 2005; Wolters et al., 2006]. In recent years researchers have investigated the shifting changes of reported tissue conductivity values [Haueisen et al., 1997, 1999, 2002; Ramon et al., 2006b]. Their findings include recommendations of incorporating many distinct tissues into the model as well as anisotropy.

2.3 Lead Field and the Reciprocity Theorem

The lead field maps the direction and sensitivity of each measurement lead [Plonsey, 1963; Malmivuo and Plonsey, 1995]. It is created by feeding a re-

ciprocal current I_R to the measurement lead. There are two ways to explain and depict the lead field – either as a current field or a potential field. Both methods contain the same information but depict it differently.

The density and direction of the lead field current indicates the measurement sensitivity distributions in a volume conductor [McFee and Johnston, 1953, 1954a, b]. The lead voltage relates the measured signal to the current sources in the volume conductor such that

$$V_{LE} = \int_v \frac{1}{\sigma} \mathbf{J}_{LE} \cdot \mathbf{J}^i dv, \tag{2.1}$$

where V_{LE} is the measured EEG voltage in the volume conductor v. The reciprocal current field $\mathbf{J}_{LE}$ is the lead field, $\mathbf{J}^i[A/cm^2]$ is the impressed current density field in the volume conductor, and σ is the conductivity tensor [S/m] [Malmivuo and Plonsey, 1995].

The lead field current clearly illustrates the direction of the lead pair (Fig. 2.2). The density and direction of the current flowlines indicate the magnitude and direction of the sensitivity of the measurement lead. One feature of these flowlines is that they are discontinuous in two-dimensional (2-D) figures attempting to depict three-dimensional (3-D) data [Malmivuo and Plonsey, 1995]. The addition of isosensitivity surfaces demarcating the current density can overcome the broken flowlines by displaying the regions of the lead field that have the same current density. Moreover, the lead field current flowlines in Fig. 2.2 unmistakably show that the EEG measurement sensitivity distribution primarily detects tangential electric source components when the lead pair is located in the vicinity of each other (Fig. 2.2a), and the radial components (Fig. 2.2b) when the electrodes are distant to each other [Malmivuo and Plonsey, 1995; Malmivuo et al., 1997], [P4].

When displaying the lead field as an electric potential field, the sensitivity of the lead is equivalent to its negative gradient (Eq. 2.2).

$$\mathbf{J}_{LE} = -\sigma \nabla \Phi_{LE} = \sigma \mathbf{E}_{LE}, \tag{2.2}$$

where Φ_{LE} is the reciprocal lead field potential, and $\mathbf{E}_{LE}$ is the reciprocal electric lead field [Plonsey, 1963; Rush and Driscoll, 1969].

The sensitivity distribution in the volume conductor can be established by applying the reciprocity theorem of Helmholtz with the Poisson equation (Eq. 2.3) to describe quasi-static bioelectric source-field problems [Helmholtz,

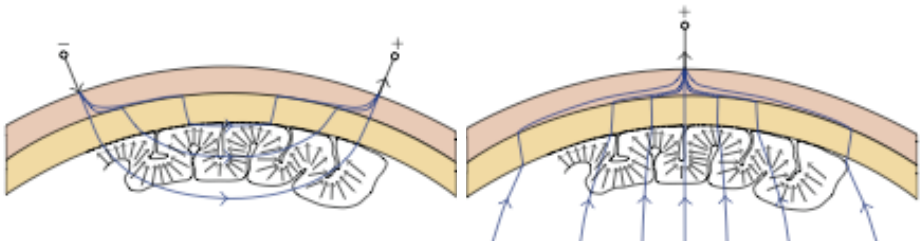

(a) 2 electrodes (tangential) (b) 1(+1) electrodes (radial)

FIGURE 2.2: The Sensitivity Distributions of EEG. (a) An EEG setup measuring the tangential components of neuroelectrical activity, where the electrodes are located relatively close to each other. (b) An EEG setup measuring the radial components of neuroelectric activity, where the measuring electrode is located far from the reference electrode. The arrows in both figures represent macrocolumns of cellular architecture, not dipolar sources. Reproduced from [P4].

1853; Sarvas, 1987].

$$\nabla \cdot (\sigma \nabla \Phi_{LE}) = \nabla \cdot \mathbf{J}^i \,(\text{in } \Omega), \tag{2.3}$$

where Ω is the volume of the head. The Neumann boundary conditions must be set equal to zero on the surface of the head Γ_Ω, i.e., the scalp such that

$$\sigma(\nabla \Phi_{LE}) \cdot \mathbf{n} = 0 \,(\text{on } \Gamma_\Omega), \tag{2.4}$$

where $\mathbf{n}$ is a vector normal to the surface [Johnson et al., 2003].

2.4 Numerical Methods

Advanced computational modeling requires numerical methods to obtain the solution. The analytical solution only works for spherical and mildly perturbed spheroids [Rush and Driscoll, 1969; Nolte and Curio, 1999]. Table 2.1 summarizes the key points of the four choices available: boundary element method (BEM), finite element method (FEM), and the two types of finite difference method (FDM) — isotropic FDM (iFDM) and anisotropic FDM (aFDM).

The BEM is a numerical method, where the mesh is defined on the boundaries. This includes the boundaries between each compartment as well as the external boundary, where each separate compartment demarcates an isotropic

TABLE 2.1: A comparison of the four methods for solving Poisson's equation in a realistic head model is presented: boundary element method (BEM), finite element method (FEM), isotropic finite difference method (iFDM), and anisotropic finite difference method (aFDM). Reproduced from [P4].

	BEM	FEM	iFDM	aFDM
Position of computational points	Surface	Volume	Volume	Volume
Free choice of computational points	Yes	Yes	No	No
System matrix	Full	Sparse	Sparse	Sparse
Solvers	Direct/iterative	Iterative	Iterative	Iterative
Number of conductivity domains/compartments	Small	Large	Large	Large
Requires tessellation	Yes	Yes	No	No
Handles anisotropy	No	Yes	No	Yes

conductivity region. Isotropic regions often represent one tissue, but sometimes multiple tissues comprise one compartment, such as the scalp, cranial muscles, and adipose tissue. The solutions of such calculations are computed at the nodes of the mesh [Meijs et al., 1989; Fuchs et al., 1998; Vanrumste et al., 2001]. The equations for the forward calculation using BEM are published in Oostendorp and van Oosterom [1989].

FEM is a method, where the entire volume can be meshed including all of the boundaries. The user selects the structure and discretization of the mesh to be regular or irregular per the defined mesh tesselation and node shape. Then, an interpolation function is applied such that the solution is calculated within the element [Czichos et al., 2006], [S2].

Finite difference method (FDM) can be considered as a special case of FEM, where the mesh is regular. The node shapes are either rectangular prisms or cubes (rectangles and squares for 2-D). FDM is commonly applied to medical images due to its convenience of aligning the grid to the voxels of the image sets. There are two choices to align the grid to the image data, which are corner-voxel and center-voxel formulations [Gordon, 2007], [S2]. FDM can be solved both isotropically and anisotropically as per the two right columns in Table 2.1.

Chapter 3

Design of the Head Models

The design, analysis, and forward solution of the EEG volume conductor model comprises five topics, recounting the model parameters used in publications [P1–P7]. The first section details the source and methods for obtaining the geometry in these models. The second section recounts the conductivity values applied to each investigation. The third section specifies the electrodes. The fourth section describes the numerical methods selected for the publications, and the fifth section summarizes three metrics for assessing the forward solutions of these models.

3.1 Model Geometries

There are three main classes of head-model geometries — all of which are included in this dissertation: spherical, generic, and realistic models. These three classes are devised to evaluate tissue conductivities, tissue layer significance, and head model significance.

3.1.1 Spherical Models

The spherical models are mathematically the simplest representations of the human head. The spherical models produced in [P2] and [P7] contain both three- and four-shell models. Table 3.1 recounts all seven spherical model variations. In these publications, all models are based upon the four-shell model having radii of $74.5, 78.0, 84.5$, and $90.0\,mm$ for the external surfaces of

TABLE 3.1: The external tissue radii and thicknesses (mm) are reported for the 3- and 4-shell spherical models. The model names corresponding to [P2] and [P7] are reported in the first and second rows of the table header, respectively. Modified from [P7].

	[P2] Model Names:	CSF	CT and CT2	MRI
	[P7] Model Names:	Control	Thin Skull	Thick Skull
Scalp	external radius	90.0	90.0	90.0
	thickness	5.5	5.5	5.5
Skull	external radius	84.5	84.5	84.5
	thickness	6.5	6.5	10
CSF	external radius	78.0	–	–
	thickness	3.5	0	0
Brain	external radius	74.5	78.0	74.5

the brain, CSF, skull, and scalp, respectively. These radii were selected based upon [Malmivuo and Plonsey, 1995; Ferree et al., 2000; Oostendorp et al., 2000]. The *CSF* and *Control* models refer to the four-concentric shells model in [P2] and [P7], respectively. Similarly, the *MRI* and *Thick Skull* models depict the three-shell models, where the CSF layer is merged into the skull layer. These theoretical models represent images segmented from the soft-tissue sensitive MRIs, whereas the *CT* and *Thin Skull* models[1] designate the hard-tissue sensitive CT images [Huiskamp et al., 1999; Enderle et al., 2005; Ramon et al., 2006b], [P2, P7]. In these models the brain is defined as the region inside the skull.

3.1.2 Realistic Models

The second class consists of realistic models directly segmented from an MRI, CT, or matched MRI-CT set. These models specifically correspond to a unique individual and are used for exact source localization. The realistic models in [P6, P7] are derived from the U.S. National Library of Medicine's Visible Human Project [National Institutes of Health (NIH), 1995; Ackerman, 1991; Sachse et al., 1998]. The Visible Human Man (VHM) was sampled and the Visible Human Woman (VHW) was downsampled to $1\,mm \times 1\,mm \times 1\,mm$

[1] The CT2 model was solved using the brain radius at $78.0\,mm$, but the sensitivity volumes only considered the results inside the brain radius of $74.5\,mm$.

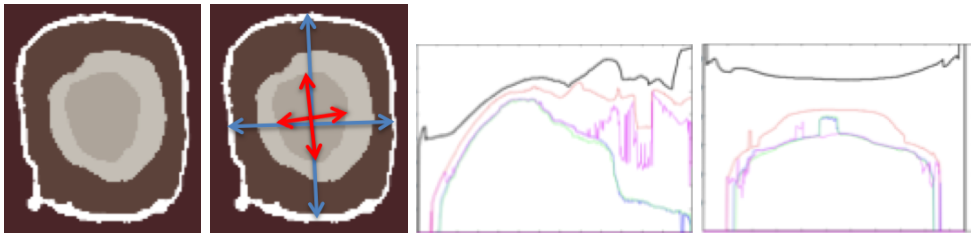

(a) Image Slice (b) Slice Analysis (c) Transverse (d) Sagittal

FIGURE 3.1: (a) The figure shows an original MRI slice from the calvarium of the VHW. (b) The major and minor axis lengths for the inner and outer tissues are not necessarily on the midline of each slice. This results from asymmetrical growth of the tissues. (c-d) Major axis lengths plotted in voxels ($0.33\,mm$) along the y-axis versus slice number plotted along the x-axis with slice separation of $0.33\,mm$. The scalp (black), skull (red), CSF (magenta), and brain (blue) tissues represent the plotted lines from maximum to minimum magnitude of the ordinate values . (c) Transverse major axis lengths. (d) Sagittal major axis lengths. Modified from [P3].

resolution in [P6, P7]. These two realistic models were selected to avoid the necessity of MRI-CT dataset registrations because these models were segmented from digital cryogenic slices.

3.1.3 Generic Models

The generic models constitute the continuum between spherical and realistic models in the following groups: simple, non-adaptable complex, and adaptable complex.

Simple Generic Models

The simple generic models consist of a set of realistic models smoothed and partially downsampled from the specific realistic images to fit wider groups of gender, race and age. The models in [P2, P3] were derived from the segmented VHW model into a four-tissue model. The brain, skull, CSF, and scalp were each separated, slice contoured, splined, and lofted into separate 3-D objects. Then all objects, each representing one tissue, were combined into one set to compose the 3-D model [P2]. The splines and layers that were lofted together are identified in [P3]. Radial-angular-axis lengths (Fig. 3.1) [P5, S12] through the transverse slices were used to define the Bezier-spline control points [P3].

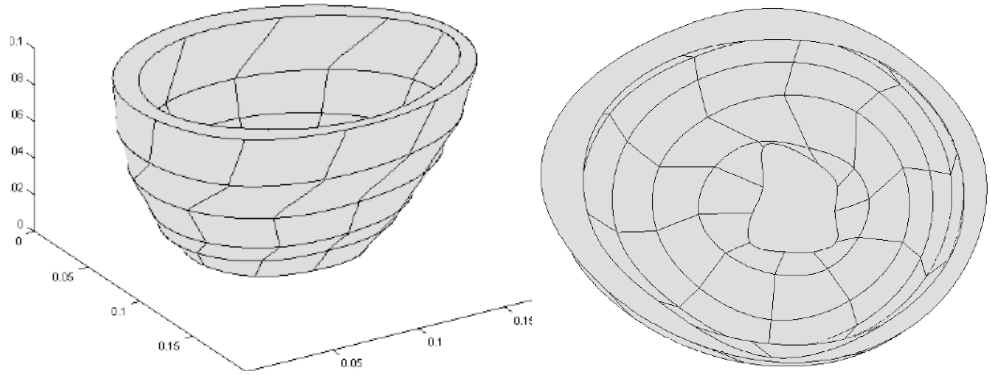

(a) Scalp — Inferior view (b) Skull — Superior view of the calvarium

FIGURE 3.2: (a) The scalp tissue is cut 115 mm from the vertex, and then it is inverted on the table. (b) The superior view of the skull faces sinistrally. The calvarium is cut at the same plane as the scalp. Reproduced from [P3].

The slices were selected based upon the slope change of the major and minor axis lengths that can be seen in Fig. 3.1(c, d). The criteria for the slice selection also eliminated distortion, warp, and twisting between the lofted slices. The result of the lofted slices can be seen in Fig. 3.2.

Non-Adaptable and Adaptable Complex Generic Models

The generic models can also be fixed, highly complex models such as the VHM and VHW (Fig. 3.3), which are used to represent moderate population sizes comprising people of the same gender, same ethnic group, and a similar age and size [P6, P7]. Additionally, the generic models can be adaptable, highly complex models representing smaller subpopulations having archetypal features such as similar head shapes [P5].

The non-adaptable complex generic models are the same as the realistic models interpreted in the context of wider population groups than the investigated individual. One additional model that joins this pair of models is the cortically enhanced VHW in [P7], where 6 layers of cortical tissue are modeled in the left parietal-occipital lobe [Rauber and Kopsch, 1955; Zilles, 1990; Matelli et al., 2003; Ross et al., 2003; Squire, 2003; Baehr and Frotscher, 2005; Kybartaite, 2006]. The adaptable complex model requires a base model (i.e. a template) with specific deformations made to it in order to form a set of

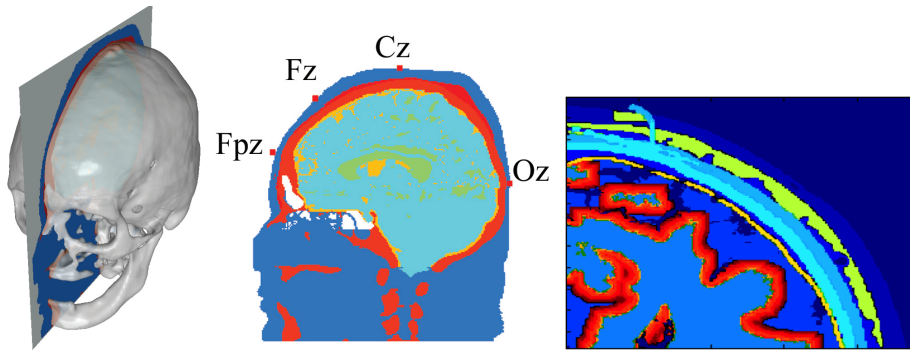

(a) (b) (c)

FIGURE 3.3: (a) Midsagittal slice of the Visible Human Woman (VHW) skull. (b) The selected cross section depicting electrodes F_{PZ}, F_Z, C_Z, and O_Z. (c) Zoomed-in view of the cortically enhanced left parietal-occipital lobe. Reproduced from [P7].

TABLE 3.2: Brain-to-skull conductivity ratios $\sigma_{Br} : \sigma_{Sk}$ discussed in [P1] and applied to the head models in [P2, P6, P7].

$\sigma_{Br} : \sigma_{Sk}$ Applied	Publications
3:1 – 14:1	[P1]
5:1, 10:1, 15:1, 20:1, 80:1	[P2, P7]
5:1, 8:1, 15:1, 30:1	[P6]

varied models. The VHW model was adapted according to anthropometric data in [P5] to generate other women of various ethnic origins [Howells, 1973; Farkas et al., 2005].

3.2 Model Conductivities

The selection of the tissue conductivity values directly impacts the solution of the model. These values influence the formation of the lead fields and so the ensuing discussion in Chapter 4 expounds upon the historical values and currently cited values for the brain, skull, scalp, and CSF conductivities. All other tissues for the complex models were derived from Ramon et al. [2004, 2006a, b]; Kybartaite [2006]. Concisely, Tables 3.2 and 3.3 list the conductivity ratios and values used in the appended primary publications.

TABLE 3.3: Tissue conductivity values $[S/m]$ applied to the discussion of the skull tissue [P1] and the head models in [P2, P6, P7].

Tissue	Conductivity Values [S/m]	Publications
Brain	0.25	[P2, P7]
Brain: Gray Matter	0.33	[P6, P7]
Brain: White Matter	0.14	[P6, P7]
CSF	1.54, 1.79	[P1, P2, P6, P7]
Scalp	0.43, 0.45	[P2, P6, P7]
Skull: Live	0.053, 0.063	[P1]
Skull	0.003, 0.013, 0.017, 0.025, 0.05	[P2, P7]
Skull	0.014, 0.029, 0.054, 0.087	[P6]

3.3 Montages and Lead Pairs

The EEG lead pairs in [P2, P3, P5–P7] simulated leads from the international 10-20 system, which comprises 21 electrodes, through high resolution EEG montages of 64, 128, 256, and 512 electrodes [P4]. Additionally, [P6-P7] evaluated the occipitally evoked potentials (EP) by moving the reference electrode along the midsagittal line through 10-20 locations F_{PZ}, F_Z, C_Z (Fig. 3.3).

3.4 Numerical Methods

In the appended publications, two numerical methods were used to solve the models. FDM was used in [P6, P7]. Those models were solved according to the conjugate gradient method [Nocedal and Wright, 2006] using the FDM solver of the Department of Biomedical Engineering, Tampere University of Technology. The present version was designed and scripted by Takano [2002]; however, the initial version was scripted by Walker [1985]; Walker and Kilpatrick [1987], and then it was evolved by Hyttinen [1994] and Kauppinen et al. [1999]. FEM was used in [P2, P3, P7, S2]. The models were implemented in COMSOL Multiphysics, COMSOL Group, Sweden (formerly Femlab) [COMSOL AB, 2004a, b, 2006]. These two methods are discussed in Sec. 2.4. Additionally, the boundary element method (BEM) is a third method discussed in [P4], but it was not applied to any model.

3.5 Evaluation Metrics

This thesis evaluates the appended works through sensitivity volumes and ratios.

3.5.1 The Half and Fifth Sensitivity Volumes

Malmivuo et al. [1997] and [P2] introduced the concept of the half-sensitivity volume (HSV) and fifth-sensitivity volume (FSV), respectively, to define the volume in which the sensitivity of the measurement lead is concentrated. The HSV and FSV are the sizes of the volumes within the source region of the volume conductor, where the magnitude of the sensitivity is at least half and one-fifth of the maximum current density in the source region, respectively. The size of the HSV reflects how focused is the region from which the lead measures bioelectric activity. Specifically, smaller volumes have a higher measurement resolution and, conversely, larger volumes have a lower measurement resolution. The HSV and FSV are applied to evaluate the ability of the lead to concentrate the measurement sensitivity.

3.5.2 The Region of Interest Sensitivity Ratio

Väisänen et al. [2008b] established the concept of the region of interest sensitivity ratio (ROISR), which provides a parameter to analyze the specificity of a measurement system. Subsequently, Väisänen et al. [2008a] and Väisänen and Hyttinen [2009] applied the concept to EEG and electrocardiogram (ECG) measurements. Equation 3.1 defines ROISR as a ratio between the average sensitivity of a predefined region-of-interest (ROI) volume v_{ROI} (Eq. 3.2) and the average sensitivity in the rest of the source volume, hereafter called as a nonROI volume. The ratio is formulated such that

$$\mathbf{ROISR} = \frac{\frac{1}{|v_{ROI}|}\int_{v_{ROI}} |\nabla \Phi_{LE}(\mathbf{y};\mathbf{x})| dy}{\frac{1}{|v_{nonROI}|}\int_{v_{nonROI}} |\nabla \Phi_{LE}(\mathbf{y};\mathbf{x})| dy}, \tag{3.1}$$

where v_{ROI} is the ROI source volume and v_{nonROI} is the nonROI source volume.

In the case of EEG, the nonROI volume consists of the entire brain source volume excluding the ROI volume. ROISR thus defines how well the measurement sensitivity is concentrated within the selected ROI, i.e., how specific the

measurement is to the signals generated within the ROI. We define the ROI volume as

$$v_{ROI} = v_B \cap v_S, \tag{3.2}$$

where v_B is the brain source volume containing the gray and white matter, and v_S is a sphere with a $20\,mm$ radius from the cortical electrode located on the occipital cortex surface (10/20 location, O_Z). Consequently, the ROI in [P6] contains both gray and white matter. We selected this location due to its relevance in visually evoked studies [Sörnmo and Laguna, 2005].

Chapter 4

The Influence of Tissue Conductivity Values

The previous chapter described the design of the EEG volume conductor model. It explained that the two parameters of geometry and conductivity affect the model experiments. This chapter applies tissue conductivity to age and growth in order to assess patient specific characteristics. The chapter begins with the relevance of live versus *post mortem* conductivity values and subsequently discusses age-appropriate conductivity values in the two following sections [P1, P2, P4, P6, P7].

4.1 Live vs. *Post Mortem* Skull Conductivities

Tissue conductivity values directly influence the formation of the lead field. The wrong electrical conductivities distort the shape and amplitude of the electrical surface potentials, thereby causing the modeler to draw incorrect conclusions regarding EEG source localization [Meijs et al., 1989; Malmivuo and Plonsey, 1995; Pohlmeier et al., 1997; van den Broek et al., 1998; Ollikainen et al., 1999; Akhtari et al., 2000], [P2, P4, P7]. However, partially accurate tissue conductivity values distort the lead field matrix less than completely inaccurate values. While these statements seem strong, they should lead the astute reader to contemplate one's own conductivity values. Therefore, more accurate conductivity values yield smaller source localization errors and better lead field matrices.

The conductivity of the skull perplexes many researchers, while some take it for granted. The originally reported skull conductivity values were not an absolute value but described by a relative 80:1 ratio of brain to skull conductivity [Rush and Driscoll, 1968, 1969]. In recent years fewer and fewer studies are using older values or ratios to positively reflect the outcome of the shift in reported skull conductivity values.

Should the skull be modeled as a single layer or a tri-layer? Law [1993] suggested that a single-layer conductivity could be estimated by the skull thickness and structure. This approach requires knowledge of the tri-layer skull as the compact inner and outer bones increase in skull thickness. Pohlmeier et al. [1997] varied the skull resistivity (i.e., conductivity) to check the influence of conductivity upon the inverse problem, i.e., source localization error. They concluded that the three-layer model of the skull is necessary to improve the accuracy of source localization.

Compact and cancellous bones compose the tri-layer skull [Law, 1993; Akhtari et al., 2000, 2002; Moore and Dalley, 2005; Venes, 2005]. The cancellous bone, i.e., the diploë, divides the internal and external tables of the cranial walls. This bone tissue layer consists of a reticular structure of spongy tissue containing red marrow [Moore and Dalley, 2005; Venes, 2005]. As patients age, gray gelatinous material replaces the red marrow, which is due to a loss of red blood cells and fat in the marrow [Moore and Dalley, 2005]. These physiological changes are reported in medical texts [Moore and Dalley, 2005] but are not discussed in biomedical engineering papers. This deficient understanding of age-related changes coupled with the difficulty to obtain such measurements leads most researchers to apply one universal skull bone conductivity value.

If the diploë changes as patients age, will there be significant changes in conductivity values for *post-mortem ex vivo* samples? Publication [P1] correlated live to *post mortem* values of rats according to Kosterich et al. [1983, 1984] with that of human skulls [Oostendorp et al., 2000; Hoekema et al., 2003] and found a factor of 2.5 to 3 change in skull conductivity post cellular death (circa 90 minutes *post mortem*). Kosterich's *post mortem* rat skull samples also reflected approximately a factor 2.5 to 3 change from immediately after death to ninety minutes.

Publication [P1] befittingly noted and [P4] reiterated that the temperature and time in minutes after death should be recorded as well as the moisture saturation i.e. bone preparation. The live (i.e. fresh) human and monkey skull tissue conductivity measurements [Tang et al., 2008, 2009] did not heed

this advice because they did not report the time after death of the conductivity measurements. The measurements of Tang et al. [2008] are the first since Hoekema et al. [2003] to measure the live human skull conductivity directly on the tissue; however, both their publications loose credibility in failing to document the time after death and that all samples were kept soaked in gauze during the non-specified waiting period and subsequently rewarmed in an incubator prior to measurements. Cells metabolize rapidly through their stored energy and consequently die within 90 minutes [Kosterich et al., 1983]. In an oral communication with Tang et al. [2009] following his congress presentation, he failed to provide an exact timeline but instead claimed the measurements were made approximately two hours *post mortem*.

So where do these values from Tang et al. [2008, 2009] fit in regarding other known measurements? Their values are not truly living but should be considered as nearly fresh *post mortem* specimens. Therefore, these values should be more conductive than that of Oostendorp et al. [2000] but less than those of Hoekema et al. [2003], which are plotted in Fig. 4.1. Thanks to the nearly fresh *post mortem* skull conductivity measurements of Oostendorp et al. [2000], the reported three-decade-old estimation brain to skull conductivity ratio of 80:1 shifted to 15:1. Publications [P1, P2, P6, P7, S3, S4] support this increase in the skull conductivity value because this value more closely reflects living *in vivo* and *in vitro* cellular conductivity properties. Furthermore, this increase in reported skull conductivity values refines the respective resolutions of the EEG lead fields. This refinement of the measurement sensitivity correlates with measuring smaller source regions. The smaller measurement region assesses EEG data with higher spatial resolution, than previously believed [Malmivuo and Plonsey, 1995; Malmivuo and Suihko, 2004].

Although the measurements of Oostendorp et al. [2000] were conducted on a skull fragment that was pre-soaked in saline and measured at body temperature, their fresh *post mortem* skull behaves electrically different than living tissue due to the changed intra- and extra-cellular matrix caused by a few days in the freezer. Dead specimens lack natural mobile ion carriers in the extracellular matrices. Unfortunately, literature lacks the conductivity correlation between freshly excised dead tissue and frozen tissue that is raised to body temperature.

The EEG signal senses the substantial content of the measured signal from the extracellular matrix in the dispersive range below $1\,kHz$ for living tissue. Comparatively, EIT measurements include more intracellular space as the fre-

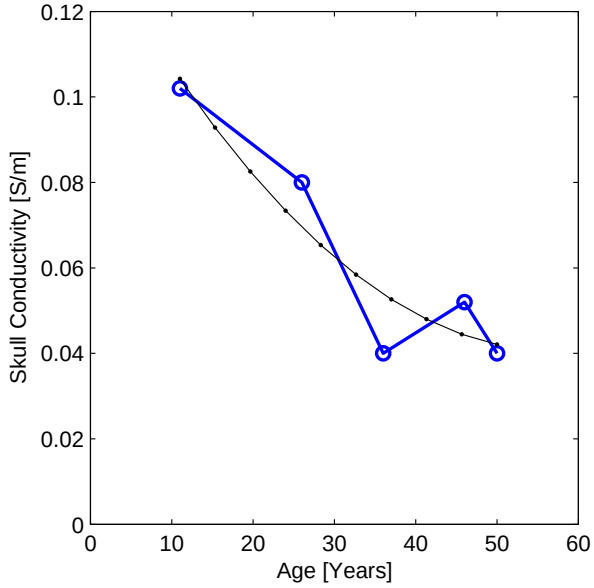

FIGURE 4.1: Reported conductivity values of live skull samples temporarily removed during epilepsy surgery plotted against patient age [Hoekema et al., 2003]. The thick blue trend with circles graphs raw data, and the thin gray trend with dots graphs the least squares fit. Reproduced from [P1].

quency of stimulation and measurement increases [Grimnes and Martinsen, 2000]. Either future studies should report the change in electrical behavior due to cellular death and forms of cadaver preservation, or they should report tissue conductivity measurements on only freshly excised living tissue specimens. Moreover, such studies should include the cranial thickness and location of measurement.

The age of the patient must be considered. What is the value of applying the wrong geometry or conductivity to a model that is supposed to represent the patient [Sadleir and Argibay, 2007; Nunez and Srinivasan, 2006]? It would seem to make as much sense as using a simple three-sphere model. As a natural consequence of childhood growth, the cranial plates expand along the fossae. Hoekema et al. [2003] opened the window into a range of conductivity values that could be applied to models justified by age (Fig. 4.1), [P1]. Recent skull conductivity measurements made on young pigs also yielded higher conductivity values than adult pigs [Gabriel et al., 2009; Peyman et al., 2009].

Although there is sparse statistical evidence to support this paucity of data, medical texts [Moore and Dalley, 2005; Venes, 2005] explain the developmental phases of the human body from birth onwards supporting the results of Hoekema et al. [2003] and [P1].

4.2 Correlating Tissue Conductivities with Age

In order to have a full discussion about age and growth we will first discuss the various growth phases primarily focusing on the human skull as the skull conductivity strongly influences the spatial content of the measurement sensitivity distribution. Furthermore, more emphasis is given to the section on juvenescence than adolescence because the early growth phases of the skull lend to more changes in the skull conductivity than during the late growth phase of adolescence.

4.2.1 Juvenescence

Ossification of the cranium is a process that begins by the eighth week of gestation and continues through birth. The face develops between the fourth and eighth gestational weeks [Yusof, 2007]. By the eighth week, most of the intramembranous ossification centers have developed. These centers create the cranial and facial bones [Moore and Dalley, 2005; Venes, 2005; Yusof, 2007]. The embryonic cranium is cartilaginious before ossification [Venes, 2005].

Calvarial bones grow superiorly and laterally to accommodate the growing brain. It is a process of deposition of new bone material on the external skull surface and resorption on the inner surface. There is also growth at the sutures [Yusof, 2007]. The viscerocranium is relatively smaller than the calvaria at birth, approximately one-eighth of the cranium (one third as an adult). The larger calvaria is due to growth of the brain and eyes [Moore and Dalley, 2005]. The face is small because of slower development of the maxillae, mandible, smaller cavities, and lacking teeth. The calvaria grows rapidly during the first 24 months to accommodate the brain growth.

At birth no diploë is present [Moore and Dalley, 2005]. In adults the skull bone conductivity decreases when there is no diploë [Tang et al., 2008]; however, this may not be true for children as their skulls have not ossified. During the first two years of growth, the child's frontal, occipital and sphenoidal bones connect via hyaline cartilage [Moore and Dalley, 2005]. The frontal bone is

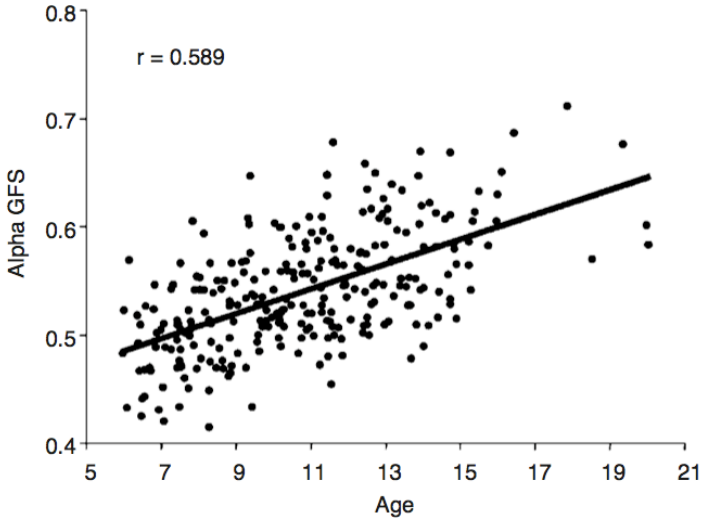

FIGURE 4.2: Reported alpha-band global field synchronization (GFS) as a function of age in healthy children. Koenig et al. claims this correlation indicates a progressively increasing degree of synchronization among brain regions. Reproduced from [Michel et al., 2009].

split into two parts on account of the frontal suture [Moore and Dalley, 2005]. The junction of the frontal suture with the sagittal and coronal sutures forms the anterior fontanelle. The posterior fontanelle is the large opening at the future site of the lambda, where the lambdoid and sagittal sutures merge. It begins growing closed a few months after birth and almost completely by age 12 months [Moore and Dalley, 2005; Venes, 2005]. By 18 months the anterior fontanelle will grow closed to form the bregma [Moore and Dalley, 2005]. The anterior fontanelle ossifies between 18 and 24 months of age [Venes, 2005].

The facial skeleton grows in an anteroinferior direction from the cranium [Yusof, 2007]. The sutural growth continues though age 4; afterwards follow apposition and remodeling phases [Yusof, 2007]. Therefore, the spatial resolution should also decrease due to the growing cranial circumference.

From age 1 to 8 years the frontal bone fuses at the frontal suture to form a single bone. The fontanelles grow closed by the age of two years [Yusof, 2007]. As the bregma and lamda grow closed, the conductivity over these landmarks decreases because the lower conducting bone divides the scalp from the meninges, blood, and cortical tissues. This change will be reflected in EEG sensitivity distributions. As the skull conductivity decreases with age [P1] due

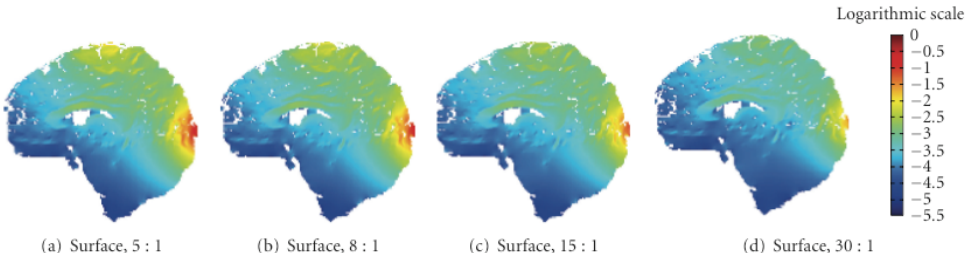

FIGURE 4.3: Measurement sensitivity distributions of the Visible Human Woman mapped in the logarithmic scale: (a–d) bipolar surface electrodes placed on the scalp at the apex (10/20 location C_Z) and over the occipital cortex (10/20 location O_Z). Scalp-to-skull conductivity ratios are specied in each subcaption: (a) 5:1, (b) 8:1, (c) 15:1, and (d) 30:1. Reproduced from [P6].

to ossification, the spatial resolution decreases [P2, P6, P7, S3, S4, S6].

It is plausible that the cranial development and growth causing a decline in skull conductivity explains the results printed in Fig. 4.2. Koenig et al. [Michel et al., 2009] claims that age is coupled with a progressively increasing degree of global field synchronization (GFS) among the brain regions. The desynchronization correlates with younger juveniles if the skull conductivity is higher than their older peers; therefore, an EEG lead would measure a smaller HSV and FSV, thus equating to higher spatial resolution. Consequently, the measured sensitivity distribution would measure smaller source volume areas (Fig. 4.2). Leads that measure active neuroelectric content from smaller brain regions would naturally cause the results to be less connected, i.e., more desynchronized than older juveniles. As the juveniles approach maturity, the decreased skull conductivity coupled with the larger cranial volume would smear the EEG signal as it propagates to the scalp.

Through the application of the reciprocity theorem [Helmholtz, 1853], the enlarged HSV and FSV for the higher brain-to-skull conductivity ratios (Fig. 4.3) map larger volumes from where the neuroelectric activity is measured. As the HSV expands with age (and perhaps the measurement sensitivity distributions overlap for neighboring measurement channels), then it is possible that synchronization can be caused by the increasingly smearing skull as the juvenile ages. This supposition enhances the position on GFS explained as, "a useful measure of synchronization of brain functions when no clear hypothesis about the distribution of sources of interest exists [Michel et al., 2009]."

4.2.2 Adolescence

The cranial base grows from cartilage remnants between bones and at the sutures because of the growth forces created by the growing brain. Growth continues in the cranial base through midadolescence. The calvaria reaches internal capacity around age 15 to 16 years. After that the cranial walls thicken for a few years until the ages 18 to 20 depending on growth maturity [Moore and Dalley, 2005]. The ossification process completes around 20 years of age (Figs. 4.1 and 4.2), [P1], which means that the conductivity of the cranial base decreases from birth through adulthood [Yusof, 2007]. This assessment correlates with the reported downward trend of cranial vault conductivity measurements Hoekema et al. [2003], [P1]. Applying these skull tissue conductivity changes to the head model simulations in Fig. 4.3 confirms the declining spatial resolution with age [P6, P7]. The selection of which subfigure to reference, i.e., the brain-to-skull conductivity ratio, depends on the researcher's assessment of the ongoing skull conductivity debate.

Chapter 5

The Influence of Tissue Layers

The previous chapter discussed the influence of conductivity upon the EEG volume conductor model. It explained the difference between live and *post mortem* conductivity values. This chapter applies these values to thin tissue layers and the significance to tissues regarding geometry and conductivity are discussed. The chapter begins with the relevance of tissue layers upon an EEG lead. Significant results are presented and discussed to explicate the measurement sensitivity distribution of an EEG lead [P1, P2, P4, P6, P7].

5.1 The Influence of Tissues on EEG Leads

EEG volume conductor head models range in construction from concentric spheres to realistically-shaped models. This wide scope of models usually includes the brain, skull and scalp, whereas more detailed models additionally contain the CSF, white matter, gray matter, diploë, fat, and eyes [Ramon et al., 2004, 2006b]. With these different tissue compositions, modeled surface EEG leads will calculate the sensitivity distributions differently [P2, P7]. So in order to understand the true influence of the electrodes upon the measurements, it is necessary to investigate the sensitivity distributions for different ways of modeling tissue layers.

With this purpose in mind, it is necessary to assess the electrical influence various tissues have upon the forward (and inverse) solution to the lead field

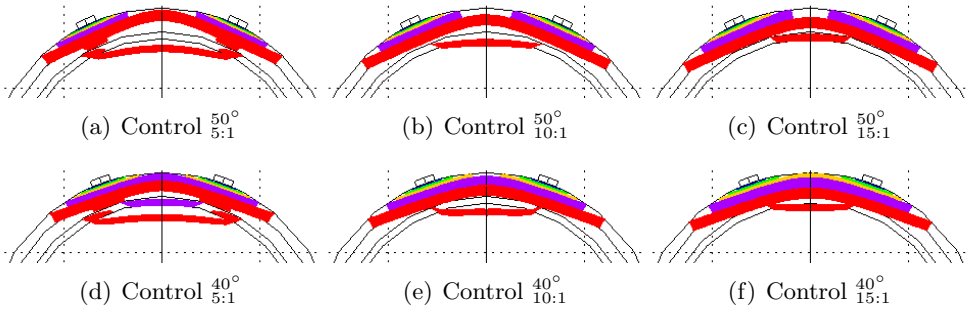

(a) Control $^{50^\circ}_{5:1}$ (b) Control $^{50^\circ}_{10:1}$ (c) Control $^{50^\circ}_{15:1}$

(d) Control $^{40^\circ}_{5:1}$ (e) Control $^{40^\circ}_{10:1}$ (f) Control $^{40^\circ}_{15:1}$

FIGURE 5.1: 3-D Isosensitivity Surfaces of the Lead Field: (a - f) all configurations show electrodes as the two small cylindrical disks in each figure. The whole head isosensitivity surfaces use brain-to-skull conductivity ratios as follows: 5 (a & d), 10 (b & e), and 15 (c & f). All subcaptions list the model with the electrode angle superscripted and the brain-to-skull conductivity ratio subscripted. The isosurface colors designate the five increments diminishing from 10% (blue), 5% (green), 3% (yellow), 2% (purple) to 1% (red) current density values. Modified from [P7].

current. This identification essentially evaluates different EEG studies. In [P2] and [P7] we use both spherical and realistic models to show how various tissues influence the measurement sensitivity distribution. In the first experiment of [P7], three sets of spherical models with different skull conductivity values of 0.05 S/m, 0.025 S/m, and 0.017 S/m were used to show the lead field current density $\mathbf{J}_{LE}$ of bipolar EEG lead pairs (Fig. 5.1). These isosensitivity maps of the whole head identify the influence of one tissue, the skull, according to its relative conductivity ratios of 5:1, 10:1, and 15:1.

When one layer is experimentally changed, its effect upon the lead field current can be identified. In Fig. 5.1 less than 2% of the lead field current enters the cortical region for models using the brain-to-skull conductivity ratio of 15 proposed by Oostendorp et al. [2000]; however, more lead field current concentrates in the CSF [P2] and cortical layers [P7] for models using a lower brain-to-skull conductivity ratio between 5 to 10 [Hoekema et al., 2003], [P1, P6]. Although studies with accurate realistically-shaped geometries and literature-based average conductivities still yield satisfactory results [Michel et al., 2004a; Gonzalez Andino et al., 2009], forward and inverse solution models using more accurate conductivity values for an identical geometry will shape the lead field current more closely to the realistic situation, assuming that the geometry does not significantly diverge from the patient's actual

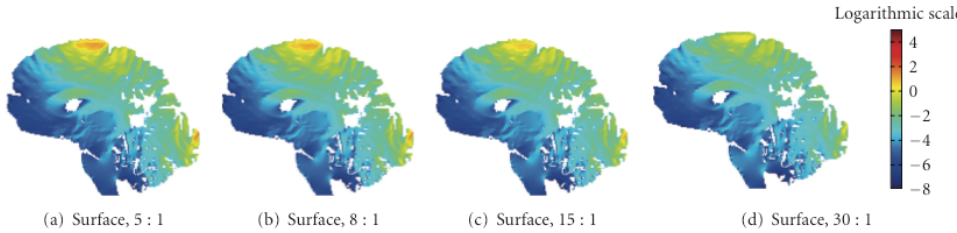

FIGURE 5.2: Measurement sensitivity distributions of the Visible Human Man mapped in the logarithmic scale: (a–d) bipolar surface electrodes placed on the scalp at the apex (10/20 location C_Z) and over the occipital cortex (10/20 location O_Z). Scalp-to-skull conductivity ratios are specied in each subcaption: (a) 5:1, (b) 8:1, (c) 15:1, and (d) 30:1. Reproduced from [P6].

anatomical structure.

Applying only this experimental change to the skull conductivity of the VHM dataset (Fig. 5.2, [P6]), the spatial resolution of the lead's measurement sensitivity distribution improves as the skull conductivity increases, i.e., the brain-to-skull conductivity ratio decreases. Figure 5.2 shows the region of the brain that each lead measures and the sensitivity of the measurement according to the lead field current density distribution within the brain. Clearly, the realistic results using higher skull conductivity values focus the bipolar measurement sensitivity distributions to the neocortex between the electrodes. Therefore, appropriate conductivity values are necessary to formulate a valid assessment of an EEG measurement lead. Consequently, volume conductor head models could further benefit from age-specific conductivities [P6].

Any variation in conductivity of any layer will affect the measurement lead fields, which are dependent on the ordering of the tissue layers. Specifically, the depth of the experimental layer diminishes in significance to the lead field measurements. In [P7] we explicate upon the electrical contribution of layered tissues to the whole head isosensitivity distributions. These cumulative effects are explained in the relative juxtaposition of layered tissues that either act as attractive or shunting layers. The attractive layers are identified as higher conducting layers juxtaposed to lower conducting layers. Examples of attractive layers and sublayers are the diploë relative to the internal and external compact bone of the skull [Lynnerup et al., 2005; Venes, 2005] and the CSF located proximal to the skull bone [P2, P7, S5]. In opposition to an attractive sublayer, the shunting sublayer forms from positioning an electrically higher-conducting tissue superior to a lower-conducting tissue such as

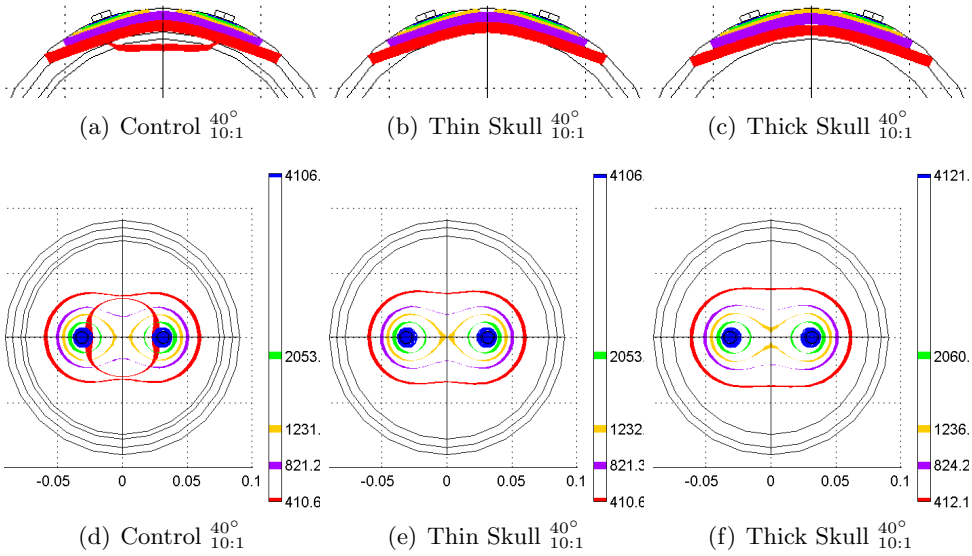

(a) Control $^{40^\circ}_{10:1}$ (b) Thin Skull $^{40^\circ}_{10:1}$ (c) Thick Skull $^{40^\circ}_{10:1}$

(d) Control $^{40^\circ}_{10:1}$ (e) Thin Skull $^{40^\circ}_{10:1}$ (f) Thick Skull $^{40^\circ}_{10:1}$

FIGURE 5.3: Spherical Whole Head Isosensitivity Surfaces of the Lead Field: (a–c) ZX-plane and (d–f) XY-plane. Each figure in the first row uses the same brain current density scale [%] shown in the figure below it. All subcaptions list the type of isosensitivity surface and the model type with the electrode angle superscripted and the brain-to-skull conductivity ratio subscripted. The isosurface colors designate five increments of current density values: 10% (blue), 5% (green), 3% (yellow), 2% (purple) to 1% (red) current density values. Modified from [P7].

the scalp superficial to the skull bone.

Considering the interaction of these attractive and shunting layers, the electrical contribution of a layer (tissue) can be assessed. These contrasting phenomena were identified by including and excluding the CSF layer from spherical models containing the scalp, skull, CSF, and brain [P7]. Models including the CSF are designated as *Control*, whereas models excluding CSF have either a *Thick* or *Thin* skull (Fig. 5.3). The isosensitvity maps of the whole head elucidate the cumulative effect of including or excluding a thin layer. Comprehensively, these maps illustrate the influence that the highly conductive CSF layer attracts the lead field current more so than either the *Thick* or the *Thin* models (i.e. models without CSF).

Naturally, these attractive and shunting layers act oppositely to each other. The basis for interpreting these layers comes from the divergence of a homogenous layer split into a piecewise volume conductor [Malmivuo and Plonsey,

1995], representing the oldest and simplest volume conductor models. So in this basic derivation of the interactive layers, a tissue can either be considered as a relative shunt or a more conductive path, when compared with another tissue of different conductivity value. Nesting these layers together (especially as they are heterogeneous mixtures of various cellular types), certain kinds of tissues should be included in models because they channel the lead field current, such as the CSF or the diploë of the skull and, partially, the gray matter [Ramon et al., 2004], [P7]. Both of these layers attract more lead field current, thereby reducing the lead field that enters the cortex.

Effectively, the neuroelectric activity is measured from the whole head. In some regions and in some tissues the sensitivity decreases to zero due to either the position of the measurement lead or the lack of electric sources in the tissue. Ideally, this whole head sensitivity distribution seems to improve the spatial resolution of the lead; however, the maximum cortical density (Fig. 5.4a) that enters the cortex is lower than models excluding the highly conductive tissues. Therefore, the calculated HSV and FSV (Fig. 5.4b,c) are greatest for the model that includes the CSF and lesser for the models that exclude the CSF. The CT model has the same dimensions as *Thin* models from [P7], and the MRI model mimics the *Thick* models of [P7]. Effectively, models including a highly attractive layer superior (external) to the cortical surface is expected to yield a lower maximum current density than models omitting such a layer. Consequently, the HSV and FSV should increase, thereby decreasing the spatial resolution with the inclusion of such a highly conductive layer.

5.2 The Effect of Subdermal Electrodes on the Skin

Although the skin itself is the outermost tissue of the human body, the scalp overlying the skull actually consists of five layers: skin, dense connective tissue, aponeurosis, loose connective tissue, and pericranium. Furthermore, the scalp extends to the natural hairline just above the inion to the eyebrows (supraorbital boundary) to the zygomatic arches [Moore and Dalley, 2005].

A new perspective on the skin reveals that skin effects can be minimized with the use of needle electrodes. Needle electrodes have existed for decades; however, the understanding of their sensitivity distributions previously were not modeled. With these simulations the needle electrodes clearly bypass the skin and concentrate the measurement sensitivity distribution to the neocortex [P6, S7, S11]. The skin should not be eliminated from the model but

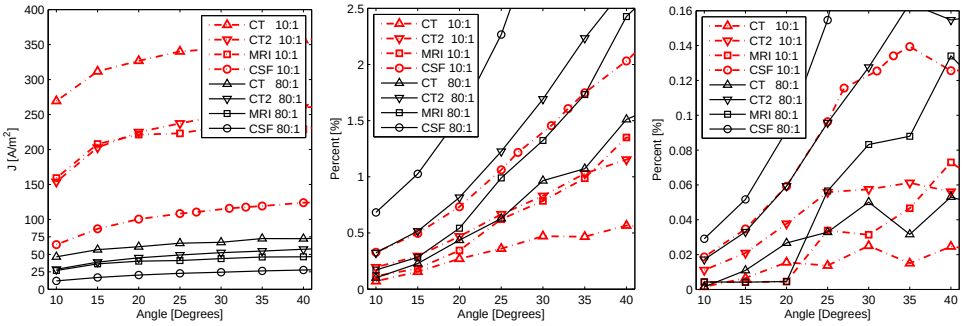

(a) Current Densities (b) HSV Percentages (c) FSV Percentages

FIGURE 5.4: Spherical model results for $\sigma_{Br}/\sigma_{Sk} = 10$ and 80. (a) Maximum Cortical Current Density $\mathbf{J}$ $[A/m^2]$ versus electrode separation angle. (b,c) Percentage of the brain filled by the (b) HSV and the (c) FSV versus electrode separation angle. Angles $11^\circ, 18^\circ, 23^\circ$, and 31° approximate 256, 128, 64, and 32 EEG electrode montages, respectively[Oostenveld and Praamstra, 2001]. Reproduced from [P2].

efforts to improve the knowledge of the point of electrode insertion as well as skin conductivity experiments will further improve EEG head volume conductor models. Comparing these electrodes with traditional EEG electrodes leads to the conclusion that they serve different purposes primarily in the resolution of the sensitivity distributions. Therefore, they cannot be equated as interchangeable electrodes. Truly, both types of electrodes add value to the field.

Chapter 6

The Value of Head Volume Conductor Models

The two previous chapters discussed the influence of conductivity and then applied it towards tissue layers. This chapter integrates these previous discussions into the value of an EEG volume conductor model and considers the question, "How does each type of geometrical model contribute to the goal of source localization? [P4]" There is significance in the spherical models just as there is in the realistic models; however, the continuum between these models is vaguely documented in the literature. This chapter examines the role of the generic model in bridging this continuum [P3, P4, P5, P7].

6.1 Spherical and Elliptical Models

The spherical model was introduced by the seminal works of Rush and Driscoll [1968, 1969]. They proposed three concentric spheres to represent the brain, skull, and scalp. In the last four decades, several studies have used this configuration [Malmivuo et al., 1997; Ryynänen et al., 2004a, b], [P2, P7, S2, S3, S4]. The CSF has been added as the fourth shell to the spherical model [Zhou and van Oosterom, 1992; Ferree et al., 2000] [P2, P7, S3, S4]. Consequently, these models are referred to as 3-shell and 4-shell models.

These 3- and 4-shell spherical models contribute to the field by theoretically explaining the lead field and volume conductor currents. Although their

resolution is of a few centimeters [Roth et al., 1993; Crouzeix et al., 1999], they explain the general theory.

6.2 Generic Models

Generic models comprise a wide range of models attempting to encompass a range of ages, genders, and ethnic groups. From the models that exist in literature, two classes of generic models exist – simple and complex. For the purpose of this discussion, the complex models are additionally referred to as adaptable.

In order to investigate a range of electrode types across various patient groups, we must rely upon a small number of normative three-dimensional (3-D) atlases of large data sets [Yusof, 2007].

6.2.1 Simple Generic Models

Simple generic models simulate down-sampled and smoothed tissue boundaries such as models similar to Fig. 3.2, which follow the methodology in Fig. 3.1 [P2, P3]. These models offer a representation of a wider group of people through their approximated shapes and sizes.

Whether researchers build spherically or realistically shaped models, it is important to obtain measurement data representative of a population when making observations about that particular population. Clearly, the best model for a particular patient matches his image data exactly; however, it is not always possible or feasible to have an exact model that fits every patient, so an appropriate generic model is warranted [Darvas et al., 2006], [P5]. Therefore, it is of utmost importance to obtain data representive of the population that a patient can be represented by in order to make quick utility of the likely closest-fitting, realistic model.

Several EEG or related head modeling publications consistently reference the same or similar measurements all relating to a larger male head of Northern European caucasian descent. These correlations match hat and wig sizes [HatsUK, 2005; TheHatSite, 2005; BestWigOutlet, 2005, 2009; WigSalon, 2005], which correlates with anthropometric, craniometric, and cephalometric data [Howells, 1973; Department of Defense, 1997; Donelson and Gordon, 1991; Farkas et al., 2005]. This implies that there is a paucity of analysis for head sizes that are not represented [Yusof, 2007]. Furthermore, the sensitivity distri-

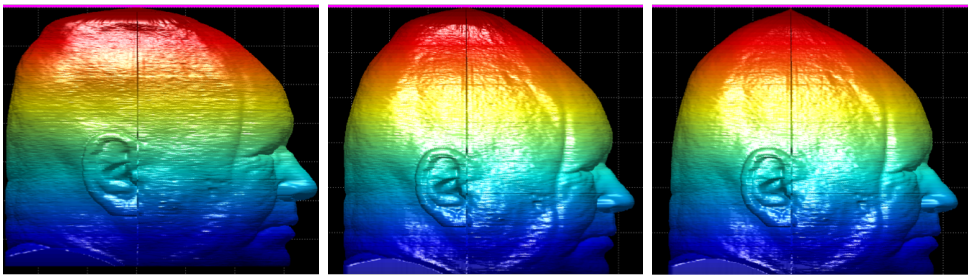

(a) (b) (c)

FIGURE 6.1: (a) Visible Human Woman used as the complex template. (b) The VHW template modified according to a power function with exponent of 0.01. (c) The VHW template modified according to the parabolic function using an angle of 10°.

butions for smaller models should yield smaller, i.e., better, spatial resolution according to the same set of conductivity values. If these models follow conductivity changes according to the aging skull as per the discussion in Ch. 4, then likewise the spatial resolution should further improve. However, if other conductivity-related changes occur in the skin due to environmental exposure or aging, then future studies could explore this area.

6.2.2 Adaptable Complex Generic Models

The current and near future of time-efficient and cost-effective EEG source localization models lies in the progression of deformable head geometries (Fig. 6.1) [P5, S12]. Anthropometric data currently exists detailing deformations in craniometric landmarks [Howells, 1973; Department of Defense, 1997; Donelson and Gordon, 1991; Farkas et al., 2005]; however, a database of landmark sizes coupled with age [P1, P6], gender [P5, P6], ethnic origin [P5], and head shape [P5] would improve the accuracy beyond the overly used fixed-geometry of highly complex models such as from the Visible Human Project [Ackerman, 1991; National Institutes of Health (NIH), 1995].

6.2.3 The Future of Adaptable Head Models

Future studies that will advance the field of source imaging will save time and money. They will optimize the deformation, i.e., adaptability, of head models by minimizing the need for expensive MRIs and CTs, and eliminating the seg-

mentation time. As scalp and skull tissue atlases are compiled and analyzed across age, gender, and ethnicity, the understanding of how to apply changes to a template will improve a model to match the non-imaged patient [S12]. Ultimately, incorporating the exact electrode locations to guide the deformation according to the patient's scalp surface would improve this method [van 't Ent et al., 2001; Darvas et al., 2006].

Chapter 7

Conclusions

This thesis provides a roadmap for the development of more accurate, time-efficient, and cost-effective head models for the EEG source localization community. The roadmap discusses the improvement of the conductivity and geometry of the model through the correlation of individual characteristics.

Considered collectively, the ideas presented in the three part discussion of Chapters 4–6 integrated the results and discussions from [P1–P7]. The results from the application of different skull conductivities [P1] to different electrode types [P6] reveal that juveniles experience higher spatial resolution EEG measurement sensitivity distributions than adults using the same electrode type. The subdermal needle electrodes focus the measurement sensitivity volume to a region approximately eight times smaller than that of the corresponding traditional surface electrodes for both juveniles and adults.

Skull Conductivity Ratio

Although the skull tissue conductivity relies on a sparse number of fresh human tissue *in vitro* measurements, strong correlations exist between past studies of animal models to support higher reported conductivity values of living tissues compared with *post mortem* tissues. This key open issue remains to be fulfilled with substantial living tissue measurements of all age groups from neonates to the elderly. From the exegsis on fresh and *post mortem* skull conductivity values, the optimal brain-to-skull conductivity ratio ranges from 4 to 8 for juveniles and from 8 to 12 for adults [P1, P6]. The collaborative effort of the

scientific community would improve both the forward and inverse solutions of EEG source localization to within a few millimeters [Oostendorp et al., 2000; Michel et al., 2009], [P4].

Effect of Conductive Tissue Layers

This dissertation expounds upon the value of tissue layers in a model. The inclusion of thin tissue layers directly impacts the formation of the lead field; however, the contrast in relative conductivity of neighboring tissues justifies whether the layer will significantly perturb the calculated lead field if it is removed. Improving the accuracy of the sensitivity distributions necessitates more accurate knowledge of the conductive properties of the tissues. Although this thesis excluded the discussion of anisotropy, the effects of its inclusion would only amplify the findings relevant to these thin tissue layers.

Subdermal Electrodes Focus the Measurement Sensitivity

The simulations of the needle electrodes demonstrate that the measurement sensitivity is more focused than with traditional surface electrodes [P6]. The message from these simulations explain what type of measurement sensitivity distribution belongs to different electrode types. These electrodes serve a different purpose than the traditional ones and, therefore, should not be considered as interchangeable electrodes for clinical purposes. The future aim of investigating different head shapes will further reveal its focusing ability beneath thicker and thinner skulls of differing subpopulations.

Constructing Head Models According to Anthropometric Data

The current and near future of an exposition on EEG measurement sensitivity distributions will benefit many clinical neurophysiologists such as anesthesiologists, neurologists, and cognitive neuroscientists. These benefits will come from the adaptation of highly detailed volume conductor models assessing different electrode types and locations [P6]. Anthropometric data applied to the VHW in [P5] demonstrates that various subpopulations in terms of head shape and size may be modeled without matching to representative MRIs or CTs.

Bibliography

Ackerman, M. 1991. The visible human project. *J. Biocommun.*, 18(14).

Akavipat, P., Dumrongbul, K., and Neamnak, P. 2006. Can electrocardiogram electrodes replace bispectral index electrodes for monitoring depth of anesthesia? *J Med Assoc Thai*, 89(1):51–55.

Akhtari, M., Bryant, H., Mamelak, A., Flynn, E., Heller, L., Shih, J., Mandelkern, M., Matlachov, A., Best, E., DiMauro, M., Lee, R., and Sutherling, W. 2002. Conductivities of three-layer live human skull. *Brain Topogr*, 14(3):151–167.

Akhtari, M., Bryant, H., Mamelak, A., Heller, L., Shih, J., Mandelkern, M., Matlachov, A., Ranken, D., Best, E., and Sutherling, W. 2000. Conductivities of three-layer human skull. *Brain Topogr*, 13(1):29–42.

Alt, K., Jeunesse, C., Buitrago-Téllez, C., Wächter, R., Boës, E., and Pichler, S. 1997. Evidence for stone age cranial surgery. *Nature*, 387:360.

American Encephalographic Society 1994. Guideline thirteen: Guidelines for standard electrode position nomenclature. *J Clin Neurophysiol*, 11(1):111–113.

Babiloni, F., Babiloni, C., Carducci, F., Fattorini, L., Anello, C., Onorati, P., and Urbano, A. 1997. High resolution EEG: a new model-dependent spatial deblurring method using a realistically-shaped MR-constructed subject's head model. *Electroencph. Clin. Neurophysiol.*, 102:69–80.

Babiloni, F., Cincotti, F., Carducci, F., and Babiloni, C. 2001. Spatial enhancement of EEG data by surface Laplacian estimation: the use of magnetic resonance imaging-based head models. *Clin Neurophysiol*, 112:724–727.

Baehr, M. and Frotscher, M. 2005. *Duus' Topical Diagnosis in Neurology: Anatomy, Physiology, Signs, Symptoms*. Thieme, Stuttgart & New York, 4th edition.

Berger, H. 1929. Über das Elektrenenkephalogramm des Menschen. *Archiv für Psychiatrie und Nervenkrankheiten*, 87:527–570.

BestWigOutlet 2005. How to find your head size. `http://www.bestwigoutlet.com/_e/page/1031/How_to_find_your_Head_Size.htm`.

BestWigOutlet 2009. How to find your head size. `http://www.bestwigoutlet.com/_e/page/1031/How_to_find_your_Head_Size.htm`.

Blum, J. and Anneveldt, M. 1982. An Electro-Cap tested. *Electroencph. Clin. Neurophysiol.*, 54:591–594.

Buzsáki, G. 2006. *Rhythms of the Brain*. Oxford University Press.

Cacioppo, J., Tassinary, L., and Berntson, G., editors 2007. *Handbook of Psychophysiology*. Cambridge University Press, Cambridge.

Caton, R. 1875. The electric currents of the brain. *Br Med J*, 2:278.

Chatrian, G., Lettich, E., and Nelson, P. 1985. Ten percent electrode system for topographic studies of spontaneous and evoked EEG activity. *Am J EEG Technol*, 25:83–92.

Clarke, E. and Dewhurst, K. 1996. *An Illustrated History of Brain Function: Imaging the Brain from Antiquity to the Present*. Norman Pub., San Francisco, 2nd edition edition.

COMSOL AB 2004a. *FEMLAB* modeling guide 3.1.

COMSOL AB 2004b. *FEMLAB* user's guide 3.1.

COMSOL AB 2006. COMSOL Multiphysics: Command Reference.

Crouzeix, A., Yvert, B., Bertrand, O., and Pernier, J. 1999. An evaluation of dipole reconstruction accuracy with spherical and realistic head models. *IEEE Trans Biomed Eng*, 110(12):2176–2188.

Cuffin, B. 1993. Effects of local variations in skull and scalp thickness on EEG's and MEG's. *IEEE Trans Biomed Eng*, 40(1):42–48.

Cuffin, B. 1995. A method for localizing EEG sources in realistic head models. *IEEE Trans Biomed Eng*, 42(1):68–71.

Czichos, H., Saito, T., and Smith, L. 2006. *Handbook of Materials Measurement Methods*, pages 973–1000. Springer.

Darvas, F., Ermer, J., Mosher, J., and Leahy, R. 2006. Generic head models for atlas-based EEG source analysis. *Human Brain Mapping*, 27:129–143.

Department of Defense 1997. Department of Defense Handbook: Human Engineering Design Guidelines. MIL-HDBK-759C.

Donelson, S. and Gordon, C. 1991. 1988 Anthropometric Survey of U.S. Army Personnel: Pilot Summary Statistics. Technical Report TR-91/040, pp. 184-185, U.S. Army Natick Research, Development, and Engineering Center, Natick, MA, U.S.A.

Dumitru, D. and Lester, J. 1991. Needle and surface electrode somatosensory evoked potential normative data: a comparison. *Arch Phys Med Rehabil*, 72(12):989–992.

Dumitru, D., Powell, G., and King, J. 1992. The effect of different needle recording electrodes on somatosensory-evoked potentials and intertrial waveform variation. *Am J Phys Med Rehabil*, 71(3):164–169.

Durka, P., Matysiak, A., Montes, E., Sosa, P., and Blinowska, K. 2005. Multichannel matching pursuit and EEG inverse solutions. *J Neuroscience Methods*, 148(1):49–59.

Enderle, J., Blanchard, S., and Bronzino, J. 2005. *Introduction to Biomedical Engineering*. Academic Press, second edition.

Farkas, L., Katic, M., and Forrest, C. 2005. International anthropometric study of facial morphology in various ethnic groups/races. *Journal of Craniofacial Surgery*, 16(4):615–646.

Felten, D. and Shetty, A. 2010. *Netter's Atlas of Neuroscience*. Saunders, 2nd edition edition.

Ferree, T., Eriksen, K., and Tucker, D. 2000. Regional head tissue conductivity estimation for improved EEG analysis. *IEEE Trans Biomed Eng*, 47(12):1584–1592.

Fuchs, M., Drenckhahn, R., Wischmann, H., and Wagner, M. 1998. An improved boundary element method for realistic volume-conductor modeling. *IEEE Trans Biomed Eng*, 45(8):980–997.

Gabriel, C. 2005. Dielectric properties of biological tissue: Variation with age. *Bioelectromagnetics Supplement*, 7:S12–S18.

Gabriel, C., Peyman, A., and Grant, E. 2009. Electrical conductivity of tissue at frequencies below 1 MHz. *Phys. Med. Biol.*, 54:4863–4878.

Gabriel, S., Gabriel, S., and Corthout, E. 1996a. The dielectric properties of biological tissues: I. literature survey. *Phys. Med. Biol.*, 41(11):2231–2249.

Gabriel, S., Lau, R., and Gabriel, C. 1996b. The dielectric properties of biological tissues: II. measurements in the frequency range of 10 Hz to 20 GHz. *Phys. Med. Biol.*, 41(11):2251–2269.

Gabriel, S., Lau, R., and Gabriel, C. 1996c. The dielectric properties of biological tissues: III. parametric models for the dielectric spectrum of tissues. *Phys. Med. Biol.*, 41(11):2271–2293.

Geddes, L. and Baker, L. 1967. The specific resistance of biological materials—a compendium of data for the biomedical engineer and physiologist. *Med. Biol. Eng.*, 5:271–293.

Gevins, A., Brickett, P., Costales, B., Le, J., and Reutter, B. 1990. Beyond topographic mapping: towards functional-anatomical imaging with 124-channel EEGs and 3-D MRIs. *Brain Topogr*, 3(1):53–64.

Gevins, A., Le, J., Brickett, P., Reutter, B., and Desmond, J. 1991. Seeing through the skull: advanced EEGs use MRIs to accurately measure cortical activity from the scalp. *Brain Topogr*, 4(2):125–131.

Gevins, A., Le, J., Leong, H., McEvoy, L., and Smith, M. 1999. Deblurring. *J Clin Neurophysiol*, 16(3):204–213.

Gevins, A., Leong, H., Smith, M., Le, J., and Du, R. 1995. Mapping cognitive brain function with modern high-resolution electroencephalography. *Trends in Neurosciences*, 18(10):429–436.

Gilmore, C., Clementz, B., and Buckley, P. 2005. Stimulus sequence affects schizophrenia–normal differences in event processing during an auditory oddball task. *Cognitive Brain Research*, 24(2):215–227.

Gilmore, R. 1994. American Electroencephalographic Society guidelines in electroencephalography, evoked potentials, and polysomnography. *J Clin Neurophysiol*, 11(1):147.

Gonzalez Andino, S., Grave de Peralta Menendez, R., Khateb, A., Landis, T., and Pegna, A. 2009. Electrophysiological correlates of affective blindight. *NeuroImage*, 44(2):581–589.

Gordon, R. 2007. *Modelling of Cardiac Dynamics and Intracardiac Bioimpedance*. PhD Dissertation, Tallinn University of Technology, Tallinn, Estonia.

Grimnes, S. and Martinsen, O. 2000. *Bioimpedance and Bioelectricity Basics*. Academic Press.

Hadamard, J. 1902. Sur les problèmes aux dérivées partielles et leur signification physique. *Princeton University Bulletin*, pages 49–52.

Hallez, H., Vanrumste, B., van Hese, P., D'Asseler, Y., Lemahieu, I., and van de Walle, R. 2005. A finite difference method with reciprocity used to incorporate anisotropy in electroencephalogram dipole source localization. *Phys. Med. Biol.*, 50:3787–3806.

Hämäläinen, M. and Sarvas, J. 1989. Realistic conductivity geometry model of the human head for interpretation of neuromagnetic data. *IEEE Trans Biomed Eng*, 36(2):165–171.

HatsUK 2005. The hat bible: Head and hat sizing. `http://www.hatsuk.com/hatsuk/hatsukhtml/bible/hatsize.htm`.

Haueisen, J., Bottner, A., Nowak, H., Brauer, H., and Weiller, C. 1999. The influence of conductivity changes in boundary element compartments on the forward and inverse problem in electroencephalography and magnetoencephalography. *Biomed. Tech.*, 44(6):150–157.

Haueisen, J., Ramon, C., Eiselt, M., Brauer, H., and Nowak, H. 1997. Influence of tissue resistivities on neuromagnetic fields and electric potentials studied with a finite element model of the head. *IEEE Trans Biomed Eng*, 44(8):727–735.

Haueisen, J., Tuch, D., Ramon, C., Schimpf, P., Wedeen, V., George, J., and Belliveau, J. 2002. The influence of brain tissue anistropy on human EEG and MEG. *NeuroImage*, 15(1):159–166.

Helmholtz, H. 1853. Über einige Gesetze der Vertheilung elektrischer Ströme in körperlichen Leitern mit Anwendung auf die thierischelektrischen Versuche. *Ann Phys Chem*, 89:211–233, 354–377.

Hemmerling, T., Coimbra, C., Harvey, P., and Choinière, M. 2002. Needle electrodes can be used for bispectral index monitoring of sedation in burn patients. *Anesthesia Analgesia*, 95:1675–1677.

Hemmerling, T. and Harvey, P. 2002. Electrocardiographic electrodes provide the same results as expensive special sensors in the routine monitoring of anesthetic depth. *Anesth Analg*, 94:369–371.

Hoekema, R., Huiskamp, G., Wieneke, G., Leijten, F., van Veelen, C., van Rijen, P., and van Huffelen, A. 2003. Measurement of the conductivity of the skull, temporarily removed during epilepsy surgery. *Brain Topogr*, 16(1):29–38.

Howells, W. 1973. *Cranial Variation in Man: A Study by Multivariate Analysis of Patterns of Difference Among Recent Human Populations*. Peabody Museum of Archaeology and Ethnology, Cambridge, Massachusetts.

Huiskamp, G., Vroeijenstijn, M., van Dijk, R., Wieneke, G., and van Huffelen, A. 1999. The need for correct realistic geometry in the inverse EEG problem. *IEEE Trans Biomed Eng*, 46(11):1281–1287.

Hyttinen, J. 1994. *Development of regional aimed ECG leads especially for myocardial ischemia diagnosis*. Doctor of Technology Dissertation, Publication 138, Tampere University of Technology, Tampere, Finland.

Jäntti, V. and Alahuhta, S. 2002. The BIS inverse problem and pharmacodynamics. *Anesthesiology*, 97(3):756–757.

Jasper, H. 1958a. Report of the committee on methods of clinical examination in electroencephalography. *Electroencph. Clin. Neurophysiol.*, 10(370–371).

Jasper, H. 1958b. The ten-twenty electrode system of the international federation. *Electroencph. Clin. Neurophysiol.*, 10:371–375.

Johnson, C., Mohr, M., Rude, U., Samsonov, A., and Zyp, K. 2003. *Multiscale and Multiresolution Methods in Computational Science and Engineering*, chapter Multilevel methods for inverse bioelectric field problems. Springer, Berlin.

Kauppinen, P., Hyttinen, J., Laarne, P., and Malmivuo, J. 1999. A software implementation for detailed volume conductor modelling in electrophysiology using finite difference method. *Computer Methods and Programs in Biomedicine*, 58:191–203.

Klem, G., Länders, H., Jasper, H., and Elger, C. 1999. The ten-twenty electrode system of the international federation. *Electroencph. Clin. Neurophysiol.*, Supplement 52:3–6.

Koessler, L., Maillard, L., Benhadid, A., Vignal, J., Braun, M., and Vespignani, H. 2007. Spatial localization of EEG electrodes. *Clin Neurophysiol*, 37(2):97–102.

Koles, Z. 1998. Trends in EEG source localization. *Electroencph. Clin. Neurophysiol.*, 106:127–137.

Kosterich, J., Foster, K., and Pollack, S. 1984. Dielectric properties of fluid-saturated bone — The effect of variation in conductivity of immersion fluid. *IEEE Transactions on Biomedical Engineering*, 31(4):369–373.

Kosterich, J. D., Foster, K., and Pollack, S. 1983. Dielectric permittivity and electrical conductivity of fluid saturated bone. *IEEE Transactions on Biomedical Engineering*, 30(2):81–86.

Kybartaite, A. 2006. Developing an accurate head model and simulating EEG signals. Master's thesis, Tampere University of Technology, Tampere, Finland.

Lamm, C., Fischmeister, F., and Bauer, H. 2005. Individual differences in brain activity during visuo-spatial processing assessed by slow cortical potentials and LORETA. *Cognitive Brain Research*, 25(3):900–912.

Law, S. 1993. Thickness and resistivity variations over the upper surface of the human skull. *Brain Topogr*, 6(2):99–109.

Le, J., Lu, M., Pellouchoud, E., and Gevins, A. 1998. A rapid method for determing standard 10/10 electrode positions for high resolution EEG studies. *Electroencph. Clin. Neurophysiol.*, 106:554–558.

Leahy, R., Mosher, J., Spencer, M., Huang, M., and Lewine, J. 1998. A study of dipole localization accuracy for MEG and EEG using a human skull phantom. *Electroencph. Clin. Neurophysiol.*, 107:159–173.

Leal, A., Dias, A., and Vieira, J. 2006. Analysis of the EEG dynamics of epileptic activity in gelastic seizures using decomposition in independent components. *Clin Neurophysiol*, 117(7):1595–1601.

Lynnerup, N., Astrup, J., and Sejrsen, B. 2005. Thickness of the human cranial diploe in relation to age, sex and general body build. *Head & Face Med*, 1(13).

Malmivuo, J. and Plonsey, R. 1995. *Bioelectromagnetism — Principles and Applications of Bioelectric and Biomagnetic Fields*. Oxford University Press, New York.

Malmivuo, J. and Suihko, V. 2004. Effect of skull resistivity on the spatial resolution of EEG and MEG. *IEEE Trans Biomed Eng*, 51(7):1276–1280.

Malmivuo, J., Suihko, V., and Eskola, H. 1997. Sensitivity distributions of EEG and MEG measurements. *IEEE Trans Biomed Eng*, 44(3):196–208.

Martz, G., Hucek, C., and Quigg, M. 2009. Sixty day continuous use of subdermal wire electrodes for EEG monitoring during treatment of status epilepticus. *Neurocrit Care*, 11:223–227.

Matelli, M., Luppino, G., and Zilles, K. 2003. *The Human Nervous System*. Academic Press, 2nd edition.

McCulloch, T. 2005. Use of BIS Monitoring Was Not Associated with a Reduced Incidence of Awareness. *Anesth Analg*, 100(4):1221.

McFee, R. and Johnston, F. 1953. Electrocardiographic leads I. Introduction. *Circulation*, 8(10):554–568.

McFee, R. and Johnston, F. 1954a. Electrocardiographic leads II. Analysis. *Circulation*, 9(2):255–266.

McFee, R. and Johnston, F. 1954b. Electrocardiographic leads III. Synthesis. *Circulation*, 9(6):868–880.

Meijs, J., Weier, O., Peters, M., and Oosterom, A. 1989. On the numerical accuracy of the boundary element method. *IEEE Trans Biomed Eng*, 36(10):1038–1049.

Michel, C., Koenig, T., Brandeis, D., Gianotti, L., and Wackermann, J., editors 2009. *Electrical Neuroimaging*. Cambridge University Press, New York.

Michel, C., Lantz, G., Grave de Peralta Menendez, R., Landis, T., and Seeck, M. 2004a. 128-channel EEG source imaging in epilepsy: clinical yield and localization precision. *J Clin Neurophysiol*, 21(2):71–83.

Michel, C., Murray, M., Lantz, G., Gonzalez, S., and Grave de Peralta, R. 2004b. EEG source imaging. *Clin. Neurophysiol.*, 115:2195–2222.

Moore, K. and Dalley, A. 2005. *Clinically Oriented Anatomy*. Lippincott Williams & Wilkins, fifth edition.

National Institutes of Health (NIH) 1995. Visible human project. U.S. National Library of Medicine.

Nicholson, P. 1965. Specific impedance of cerebral white matter. *Exp. Neurol.*, 13:386–401.

Niedermeyer, E. and Lopes Da Silva, F., editors 2005. *Electroencephalography: Basic Principles, Clinical Application, and Related Fields*, volume Fifth. Lippincott Williams & Wilkins, Philadelphia.

Nocedal, J. and Wright, S. 2006. *Numerical Optimization*. Springer, 2nd edition.

Nolte, G. and Curio, G. 1999. Perturbative analytical solutions of the electric forward problem for realistic volume conductors. *J App Phy*, 86(5):2800–2811.

Nunez, P. and Srinivasan, R. 2006. *Electric Fields of the Brain: The Neurophysics of EEG*. Oxford University Press, New York, second edition edition.

Nuwer, M., Comi, C., Emerson, R., Fuglsang-Frederiksen, A., Guäcrit, J., Hinrichs, H., Ikeada, A., Luccas, F., and Rappelsburger, P. 1998. IFCN standards for digital recording of clinical EEG. *Electroencph. Clin. Neurophysiol.*, 106:259–261.

Ollikainen, J., Vauhkonen, M., Karjalainen, P., and Kaipio, J. 1999. Effects of local skull inhomogeneities on EEG source estimation. *Med Eng & Phys*, 21(3):143–154.

Ollikainen, J., Vauhkonen, M., Karjalainen, P., and Kaipio, J. 2000. Effects of electrode properties on EEG measurements and a related inverse problem. *Med Eng & Phys*, 22(8):535–545.

Ollikainen, J., Vauhkonen, M., Karjalainen, P., and Kaipio, J. 2001. A new computational approach for cortical imaging. *IEEE Trans Med Img*, 20:325–332.

Oostendorp, T., Delbeke, J., and Stegeman, D. 2000. The conductivity of the human skull: Results of in vivo and in vitro measurements. *IEEE Trans Biomed Eng*, 47(11):1487–1492.

Oostendorp, T. and van Oosterom, A. 1989. Source parameter estimation in inhomogeneous volume conductors of arbitrary shape. *IEEE Transactions on Biomedical Engineering*, 36(3):382–391.

Oostenveld, R. 2006. High-density EEG electrode placement. `http://robertoostenveld.ruhosting.nl/index.php/electrode/#more-5`.

Oostenveld, R. and Praamstra, P. 2001. The five percent electrode system for high-resolution EEG and ERP measurements. *Clin Neurophysiol*, 112:713–719.

Pascual-Marqui, R. 1999. Review of methods for solving the EEG inverse problem. *IJBEM*, 1(1):75–86.

Peyman, A., Gabriel, C., Grant, E., Vermeeren, G., and Martens, L. 2009. Variation of the dielectric properties of tissue with age: the effect on the values of SAR in children when exposed to walkie-talkie devices. *Phys. Med. Biol.*, 54:227–241.

Peyman, A., Holden, S., Watts, S., Perrott, R., and Gabriel, C. 2007. Dielectric properties of porcine cerebrospinal tissues at microwave frequencies: *in vivo, in vitro* and systematic variation with age. *Phys. Med. Biol.*, 52:2229–2245.

Peyman, A., Rezazadeh, A., and Gabriel, C. 2001. Chnages in the dielectric properties of rat tissue as a function of age at microwave frequencies. *Physics in Medicine and Biology*, 46:1617–1629.

Peyman, A., Rezazadeh, A., and Gabriel, C. 2002. Changes in the dielectric properties of rat tissue as a function of age at microwave frequencies. *Phys. Med. Biol.*, 47:2187–2188.

Plonsey, R. 1963. Reciprocity applied to volume conductors and the EEG. *IEEE Trans Biomed Electron*, 10(1):9–12.

Pohlmeier, R., Buchner, H., Knoll, G., Rienacker, A., Beckmann, R., and Pesch, J. 1997. The influence of skull-conductivity misspecification on inverse source localization in realistically shaped finite element head models. *Brain Topogr*, 9:157–162.

Ramon, C., Haueisen, J., and Schimpf, P. 2006a. Influence of head models on neuromagnetic fields and inverse source localizations. *BioMedical Engineering Online*, 5(55).

Ramon, C., Schimpf, P., and Haueisen, J. 2006b. Influence of head models on EEG simulations and inverse source localizations. *BioMedical Engineering Online*.

Ramon, C., Schimpf, P., Haueisen, J., Holmes, M., and Ishimaru, A. 2004. Role of soft bone, CSF and gray matter in EEG simulations. *Brain Topogr*, 16(4):245–248.

Rauber, A. and Kopsch, F. 1955. *Lehrbuch und Atlas der Anatomie des Menschen*, volume 2. Thieme, Stuttgart, 19 edition.

Ross, M., Kaye, G., and Pawlina, W. 2003. *Histology a text and atlas*, page 875. 4th. Lippincott Williams & Wilkins, Philadelphia, 4th edition.

Roth, B., Balish, M., Gorbach, A., and Sato, S. 1993. How well does a three-sphere model predict positions of dipoles in a realistically shaped head? *Electroencph. Clin. Neurophysiol.*, 87:175–184.

Rush, S. and Driscoll, D. 1968. Current distribution in the brain from surface electrodes. *Anesthesia Analgesia*, 47:717–723.

Rush, S. and Driscoll, D. 1969. EEG electrode sensitivity — An application of reciprocity. *IEEE Trans Biomed Eng*, 16(1):15–22.

Russell, G., Eriksen, J., Poolman, P., Luu, P., and Tucker, D. 2005. Geodesic photogrammetry for localizing sensor positions in dense-array EEG. *Clin Neurophysiol*, 116(5):1130–1140.

Ryynänen, O., Hyttinen, J., Laarne, P., and Malmivuo, J. 2004a. Effect of electrode density and measurement noise on the spatial resolution of cortical potential distribution. *IEEE Trans Biomed Eng*, 51(9):1547–1554.

Ryynänen, O., Hyttinen, J., Laarne, P., and Malmivuo, J. 2004b. Effect of measurement noise on the spatial resolution of EEG. *Biomed Tech*, 48(2):94–97.

Ryynänen, O., Hyttinen, J., and Malmivuo, J. 2006. Effect of measurement noise and electrode density on the spatial resolution of cortical potential distribution with different resistivity values for the skull. *IEEE Transactions on Biomedical Engineering*, 53(9):1851–1858.

Sachse, F., Werner, C., Meyer-Waarden, K., and Dössel, O. 1998. Applications of the visible man dataset in electrocardiology: Calculation and visualization of body surface potential maps of a complete heart cycle. In *Proc. of the Second Users Conference of the National Library of Medicine's Visible Human Project*, pages 47–48.

Sadleir, R. and Argibay, A. 2007. Modeling skull electrical properties. *Annals of Biomedical Engineering*, 35(10):1699–1712.

Sarvas, J. 1987. Basic mathematical and electromagnetic concepts of the biomagnetic inverse problem. *Phys. Med. Biol.*, 32(1):11–22.

Sebel, P., Bowdle, T., Ghoneim, M., Rampil, I., Padilla, R., Gan, T., and Domino, K. 2004. The incidence of awareness during anesthesia: a multicenter United States study. *Anesth Analg*, 99:833–839.

Sharbrough, F., Chatrian, G., Lesser, R., Lüders, H., Nuwer, M., and Picton, T. 1991. American Electroencephalographic Society guidelines for standard electrode position nomenclature. *J Clin Neurophysiol*, 8:200–202.

Siivola, J. and Järvilehto, M. 1982. Spinal evoked potentials evaluated with two relevant electrode types. *Acta Physiol Scan*, 115(1):103–107.

Sörnmo, L. and Laguna, P. 2005. *Bioelectrical Signal Processing in Cardiac and Neurological Applications*. Academic Press.

Squire, L. 2003. *Fundamental of Neuroscience*, page 1426. Academic Press, San Diego, 2nd edition.

Stoliar, D. 2009. Measuring tissue thicknesses derived from medical images of the human head. Master's thesis, Tampere University of Technology, Tampere, Finland.

Suesserman, M., Spelman, F., and Rubinstein, J. 1991. In vitro measurement and characterization of current density profiles produced by nonrecesed, simple recessed, and radially varying recessed stimulating electrodes. *IEEE Trans Biomed Eng*, 38(5):401–408.

Takano, N. 2002. *Reduction of ECG leads and equivalent sources using orthogonalization and clustering techniques*. Phd dissertation, publication 382, Tampere University of Technology, Tampere, Finland.

Tang, C., You, F., Cheng, G., Gao, D., Fu, F., and Dong, X. 2009. Resistivities of the live monkey skulls. In Dössel, O. and Schlegel, W., editors, *IFMBE Proceedings*, volume 25, pages 130–132. World Congress 2009.

Tang, C., You, F., Cheng, G., Gao, D., Fu, F., Yang, G., and Dong, X. 2008. Correlation between structure and resistivity variations of the live human skull. *IEEE Trans Biomed Eng*, 55(9):2286–2292.

TheHatSite 2005. Hat sizing and how to measure your head. `http://www.thehatsite.com/measuring.html`.

Tucker, D. 1993. Spatial sampling of head electrical fields: the geodesic sensor net. *Electroencph. Clin. Neurophysiol.*, 87:154–163.

Väisänen, J. and Hyttinen, J. 2009. Region of interest sensitivity ratio in analyzing sensitivity distributions of electrocardiographic measurements. *Annals Biomed Eng*, 37(4):692–701.

Väisänen, J., Malmivuo, J., and Hyttinen, J. 2008a. Correlation between signal-to-noise ratios and region of interest sensitivity ratios of bipolar EEG measurements. *Med Biol Eng Comput*, 46:381–389.

Väisänen, J., Väisänen, O., Malmivuo, J., and Hyttinen, J. 2008b. New method for analysing sensitivity distributions of bioelectric measurements. *Med. Biol. Eng. Comput.*, 46(2):101–108.

van den Broek, S., Reiders, F., Donderwinkel, M., and Peters, M. 1998. Volume conduction effects in EEG and MEG. *Electroencph. Clin. Neurophysiol.*, 108:522–534.

van 't Ent, D., de Munck, J., and Kaas, A. 2001. A fast method to derive realistic BEM models for E/MEG source reconstruction. *IEEE Trans Biomed Eng*, 48(12):1434–1443.

Vanrumste, B., Van Hoey, G., Van de Walle, R., D'Havé, M., Lemahieu, I., and Boon, P. 2001. The validation of the finite difference method and reciprocity for solving the inverse problem in EEG dipole source analysis. *Brain Topogr*, 14(2):83–92.

Venes, D. 2005. *Taber's Cyclopedic Medical Dictionary*. F. A. Davis Company, Philadelphia, 20th edition.

Vukov-Colić, D. 2010. Images of the working brain and heart. *Croat Air*, Spring:140–144.

Walker, S. 1985. *Epicardial potential distributions calculated from body surface measurements using multiple torso models*. PhD Dissertation, University of Tasmania, Hobart, Tasmania, Australia.

Walker, S. and Kilpatrick, D. 1987. Forward and inverse electrocardiographic calculations using resistor network models of the human torso. *Circulation Research*, 61(4):504–513.

WigSalon 2005. Head sizes for wigs. `http://www.wigsalon.com/prowig.html`.

Wolters, C., Anwander, A., Tricoche, X., Weinstein, D., Koch, M., and MacLeod, R. 2006. Influence of tissue conductivity anistropy on EEG/MEG

field and return current computation in a realistic head model: a simulation and visualization study using high-resolution finite element modeling. *NeuroImage*, 30:813–826.

Yamashita, Y. 1982. Theoretical studies on inverse problems of electrocardiography and the uniqueness of solution. *IEEE Trans Biomed Eng*, 29(11):719–725.

Yao, J. and Dewald, J. 2005. Evaluation of different cortical source localization methods using simulated and experimental EEG data. *NeuroImage*, 25:369–382.

Young, G., Ives, J., Chapman, M., and Mirsattari, S. 2006. A comparison of subdermal wire electrodes with collodion-applied disk electrodes in long-term EEG recordings in ICU. *Clin. Neurophysiol.*, 117:1376–1379.

Yusof, A. 2007. *Craniofacial Growth Changes in Malaysian Malay Children and Young Adults: A Cross-Sectional 3-Dimensional CT Study.* PhD thesis, University of Adelaide, Adelaide, Australia.

Zablow, L. and Goldensohn, E. 1969. A comparison between scalp and needle electrodes for the EEG. *Electroencph. Clin. Neurophysiol.*, 26:530–533.

Zhou, H. and van Oosterom, A. 1992. Computation of the potential distribution in a four-layer anisotropic concentric spherical volume conductor. *IEEE Transactions on Biomedical Engineering*, 39(2):154–158.

Zilles, K. 1990. *The human nervous system.* Academic Press, San Diego, 1st edition.

Primary Publications

Publication P1

K Wendel and J Malmivuo, "Correlation between Live and Post Mortem Skull Conductivity Measurements." In *Proceedings of the 28th Annual International Conference of the IEEE Engineering in Medicine and Biology Society*, New York City, USA, pp. 4285–4288, August 30 – September 3, 2006.

Oral presentation and Open Finalist in the Student Paper Competition.

Publication P2

K Wendel, NG Narra, M Hannula, P Kauppinen, J Malmivuo. The Influence of CSF on EEG Sensitivity Distributions of Multilayered Head Models. IEEE Transactions on Biomedical Engineering, vol. 55, no. 4, pp. 1454-1456, April 2008.

Publication P3

K Wendel, M Osadebey, J Malmivuo. "Coupling Axis-Length Profiles with Bezier Splines in Finite Element Head Models." In *IFMBE Proceedings of the 14th Nordic-Baltic Conference on Biomedical Engineering and Medical Physics*, A Katashev, Y Dekhtyar, and J Spigulis (eds.). Riga, Latvia, Springer-Verlag, vol. 20, pp. 465–468, June 16–20, 2008.

Oral presentation and Finalist in the Young Investigators Competition.

Publication P4

K Wendel, O Väisänen, J Malmivuo, NG Gencer, B Vanrumste, P Durka, R Magjarevic, S Supek, ML Pascu, H Fontenelle, and R Grave de Peralta Menendez. EEG/MEG Source Imaging: Methods, Challenges, and Open Issues. Computational Intelligence & Neuroscience, vol. 2009, article ID 656092, 12 pages, 2009.

Hindawi Publishing Corporation
Computational Intelligence and Neuroscience
Volume 2009, Article ID 656092, 12 pages
doi:10.1155/2009/656092

Review Article

EEG/MEG Source Imaging: Methods, Challenges, and Open Issues

Katrina Wendel,[1] Outi Väisänen,[1] Jaakko Malmivuo,[1] Nevzat G. Gencer,[2] Bart Vanrumste,[3,4] Piotr Durka,[5] Ratko Magjarević,[6] Selma Supek,[7] Mihail Lucian Pascu,[8] Hugues Fontenelle,[9] and Rolando Grave de Peralta Menendez[10,11]

[1] *Department of Biomedical Engineering, Tampere University of Technology, 33101 Tampere, Finland*
[2] *Department of Electrical and Electronics Engineering, Middle East Technical University, 06531 Ankara, Turkey*
[3] *SCD, Department of Electrical Engineering (ESAT), Katholieke Universiteit Leuven, Kasteelpark Arenberg 10, B-3001 Leuven, Belgium*
[4] *MOBILAB, Biosciences and Technology Department, Katholieke Hogeschool Kempen, Kleinhoefstraat 4, B-2440 Geel, Belgium*
[5] *Department of Biomedical Physics, University of Warsaw ul. Hoża 69, 00-681 Warszawa, Poland*
[6] *Faculty of Electrical Engineering and Computing, University of Zagreb, 10000 Zagreb, Croatia*
[7] *Department of Physics, Faculty of Science, University of Zagreb, 10000 Zagreb, Croatia*
[8] *National Institute for Laser, Plasma and Radiation Physics, Laser Department, 077125 Bucharest, Romania*
[9] *Department of Medical Physics, School of Medicine, University of Patras, 26504 Patras, Greece*
[10] *Electrical Neuroimaging Group, Department of Clinical Neurosciences, Geneva University Hospital, 1211 Geneva, Switzerland*
[11] *Neurodynamics Laboratory, Department of Psychiatry and Clinical Psychobiology, University of Barcelona, 08035 Barcelona, Catalonia, Spain*

Correspondence should be addressed to Katrina Wendel, katrina.wendel@tut.fi and
Rolando Grave de Peralta Menendez, rolando.grave@hcuge.ch

Received 25 November 2008; Revised 31 March 2009; Accepted 29 April 2009

Recommended by Laura Astolfi

We present the four key areas of research—preprocessing, the volume conductor, the forward problem, and the inverse problem—that affect the performance of EEG and MEG source imaging. In each key area we identify prominent approaches and methodologies that have open issues warranting further investigation within the community, challenges associated with certain techniques, and algorithms necessitating clarification of their implications. More than providing definitive answers we aim to identify important open issues in the quest of source localization.

1. Introduction

Electroencephalography (EEG) and magnetoencephalography (MEG) represent two noninvasive functional brain imaging methods, whose extracranial recordings measure electric potential differences and extremely weak magnetic fields generated by the electric activity of the neural cells, respectively. These recordings offer direct, real time, monitoring of spontaneous and evoked brain activity and allow for spatiotemporal localization of underlying neuronal generators. EEG and MEG share the following characteristics: (1) they have a millisecond temporal resolution; (2) potential differences and magnetic fields are linear functions of source strengths and nonlinear functions of the source support (e.g., dipole locations); (3) they are caused by the same neurophysiological events, that is, currents from synchronously activated neuronal tissue often referred to as the primary or impressed current source density, and thus both can be used equivalently for the localization of neuronal generators.

The three-dimensional reconstruction of neural activity is commonly misconstrued as *tomography*, which is defined [1] as "*any technique that makes detailed predetermined plane sections of an object while blurring out the images of other planes*." The physics governing the propagation of the electromagnetic fields depends on the composition of the volume conductor, which means that the source activity outside the predetermined plane also influences the readings

of the sensors lying in the plane. So, actually the procedures applied in tomography and inverse solutions are somehow reversed: in tomography we reconstruct a 3D image by combining separately obtained slices, whereas, inverse solutions calculate the whole 3D distribution, which can be later presented as slices. While tomographic techniques (e.g., CT, PET, MRI, etc.) are associated with well-posed mathematical problems, the noninvasive estimation of the brain activity is essentially an ill-posed problem due to the infinite number of solutions.

In the subsequent sections we remark about some important issues for the understanding, selection, and evaluation of source imaging methods; hence our emphasis is on general approaches rather than particular solutions. These sections reflect upon our group discussion held at a NeuroMath workshop. As a group we acknowledge that we have differences of opinion regarding the selection of methods, we face various challenges as separate research centers, and we differ on what are the key open issues due to our different interests. Therefore, we have attempted to write an article that benefits the novice, aligns disparate parts of the source imaging community, and focuses much needed attention to several open issues.

1.1. Theory. The relationship between the sources inside the head and the external measurements d is described as

$$d = Lj, \tag{1}$$

where L is the linear operator representing the lead field (also known as the gain model or the direct model), and j represents the sources. The two mathematical properties of (1) reflect the attributes of the physical magnitudes involved. Firstly, the homogeneity property states that the image of an amplified source $k * j$ is an amplified measurement $k * d$, and secondly, the additive property states that the sum of the two sources $j = j_1 + j_2$ produces a measurement equal to the sum of each measurement alone $d = d_1 + d_2$. Together these two properties follow the superposition principle, that is, $L(k_1 * j_1 + k_2 * j_2) = k_1 * d_1 + k_2 * d_2$, where $d_1 = Lj_1$ and $d_2 = Lj_2$.

The ill-posed nature of this problem arises from the fact that two different sources j_1 and j_2 might produce the same measurement d, that is, $d = Lj_1 = Lj_2$, which is trivially equivalent to say that there exists a "silent" source h such that $Lh = 0$. In order to see the equivalence, note that if $d = Lj_1 = Lj_2$, therefore, the silent source $h = j_1 - j_2$ fulfils $Lh = Lj_1 - Lj_2 = d - d = 0$. In the other direction, if we assume that $Lh = 0$ and the existence of source j_1 such that $Lj_1 = d$, we can always build a new source $j_2 = j_1 + h$ that yields the same data, that is, $Lj_2 = L(j_1 + h) = Lj_1 + Lh = Lj_1 = d$.

That being said, we can establish one of the main properties of EEG/MEG scalp distributions (maps). While similar scalp maps cannot rule out the possibility of different subjacent source distributions, different maps are necessarily due to different source distributions. Importantly, we do not need to resort to any inverse method to conclude that.

Building on linearity and in the absence of a priori information to justify otherwise, we can represent the solution of (1) with a linear operator G that "estimates" j as follows:

$$j_{\text{est}} = G * d. \tag{2}$$

Substituting d by its value defined in (1) yields a fundamental equation of linear operators relating to the estimated and the original source distribution

$$j_{\text{est}} = G * L * j \; = R * j, \tag{3}$$

where $R = G * L$ is the resolution operator [2, 3]. In practice both the sensors and the geometry are made of discrete measurements, and thus it can be assumed that L, G, and R are finite dimensional matrices approximating the continuous (integral) operators.

2. Preprocessing

In this section, we discuss some relevant issues related to the preparation of the data identifying some useful preprocessing and things to avoid. In general, the philosophy of preprocessing is to prepare the signal for solving. Typically, these steps decompose complex signals and reduce the noise from the sensors as well as other undesirable sources.

The EEG and MEG inverse problems (Figure 1, green arrow) start with the time series (Figure 1) recorded at the scalp sensors. Therefore, the localizations based on the distribution of scalp amplitudes in single time instants might be improved by the application of signal processing techniques to the measured time series (Figure 1, blue arrow). In particular the input noise can be reduced by selective and sensitive extraction of relevant activities from the EEG/MEG data. This can be achieved by localizing signal components extracted by a blind source separation (e.g., ICA [4]). Other approaches rely on the information derived from the time-frequency representations, corresponding to the relevant phenomena we want to localize (e.g., sleep spindles [5]). A similar but more sensitive and selective preprocessing was proposed in [6] using the multichannel matching pursuit algorithm. Overall, most preprocessing algorithms are expected to benefit the quality and accuracy of the inverse solution.

2.1. Epochs. We should weigh the advantages and disadvantages of the role epochs play in the recordings of event-related potentials. So far there has been no standard on the number of trials, jitter, averaging amplitudes, or the appropriateness of single trial analysis. For instance, the signal-to-noise ratio (SNR) increases with the number of trials, that is, the number of epochs; however, habituation can affect the results of some studies. We propose that a document outlining these categories would benefit future studies in terms of comparison and regularization.

The neuroelectric signals are buried in spontaneous EEGs with signal-to-noise ratios as low as 5 dB. In order to decrease the noise level and find a *template* Evoked Potential (EP) signal, an ensemble-average (EA) is obtained using a large number of repetitive measurements [7]. This approach

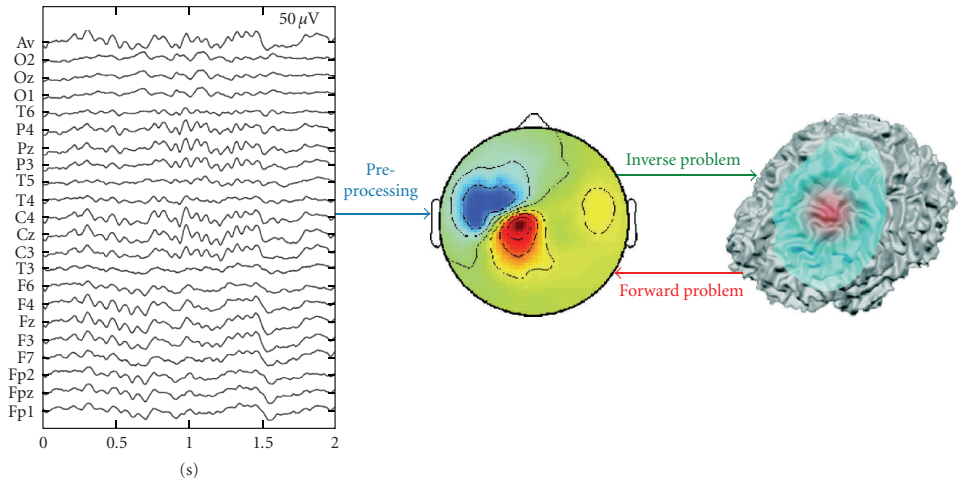

Figure 1: Key parts of source imaging. Preprocessing prepares the recorded signals for solving the inverse problem. The inverse problem attempts to locate the sources from recorded measurements, whereas the forward problem assumes a source definition in order to calculate a potential distribution map.

[8] treats the background EEG as additive noise and the EP as an uncorrelated signal. The magnitudes and latencies of EP waveforms display large interindividual differences and changes depending on the psychophysiological factors for a given individual [9]. Consequently, one goal in the methodological EP research is to develop techniques to extract the true EP waveform from a *single sweep*.

For clinical evaluations, either the template EP signal or possible amplitude and/or latency variations on single sweeps are used [9]. To observe such variations, the specific features are identified from a reference/template EP based on various estimation approaches. Since there are relatively tight constraints related to the available recording time or cooperativeness of the subject, the use of EA (as a reference EP signal) is usually impractical. This has led to the development of the alternative SNR improvement methods based on the additive model. Some of these algorithms are the weighted averaging approach, the subspace averaging method, the parametric filtering, the adaptive filtering, and Wiener filtering. In all these methods, it is assumed that the EP (i.e., signal) is stationary throughout the experiment. However, such assumptions are also questioned in some reports describing the event related potentials as superposition of some phase modulated rhythmic activities which may be related to different cognitive processes of the brain [10].

2.2. Things to Avoid. Contrary to the benefits of most preprocessing algorithms, there are certain algorithms that we should avoid before the application of source localization algorithms. In particular, the following choices threaten the integrity of the inverse solution.

(1) Baseline correction. Varying the values of individual electrodes either by "arbitrary" baseline shifting or by scaling factors changes the surface maps and thus the estimated sources. Although linear inverse solutions are rather stable (continuity with respect to the data), the application of base line correction to two conditions (that will be compared on the basis of their sources) can produce artificial differences induced by the correction and not by the real sources.

(2) Artificial maps produced by grand mean data or segmentation algorithms. Statistical averages (e.g., mean) yield values that are usually not present in the original data. It would not be surprising if the average maps are not present in any of the subject averages. Furthermore, this effect can be amplified by the differences in latencies of the subjects.

(3) The use of very high density of sensors might also jeopardize the source analysis due to different kinds of noise at different sensors. Moreover, no significant information is added after approximately 128 electrodes due to the noise levels. Lastly, some sensors might measure more artifacts than others due to their location near active muscles.

3. Volume Conductor

The head model as a volume conductor is a key element in source localization. The configuration of the volume conductor directly affects the solutions to the forward and inverse solutions. The three nearly equally important areas are head geometry, tissue conductivities, and electrode placement.

3.1. Geometry and Segmentation. The seminal study by Rush and Driscoll [11] used three concentric spheres, whereas, contemporary studies implement realistic models. We find that the differing models within the community are necessary, but how does each type of geometrical model contribute to the goal of source localization? The spherical models answer general questions of theory providing EEG

localization accuracy of a few centimeters, while the realistic models attempt to pinpoint exact locations but actually improve dipole localization by a few centimeters [12–14]. On the other hand, the spherical geometry is sufficient for most MEG-based numerical simulations. Only the localization of the deep sources near the bottom of the skull in the frontotemporal and the frontal areas requires a realistically-shaped-head-volume conductor model for MEG-based simulations [15].

The geometry is directly related to the imaging modality, computed tomography (CT) or magnetic resonance imaging (MRI), and the quality of the segmentation. Naturally, we will question which modality to segment—CT, MRI, or fused CT-MRI images [16]. We are encouraging the modelers to understand the significance of the boundaries defined by a particular modality and are not in any way suggesting the medical community to provide any unsafe and unnecessary radiation to any patient. We must remember that the modality we select influences the segmentation due to its sensitivity to hard or soft tissues accordingly. Furthermore, how many tissues, which tissues, and which cavities should the models include? We foresee that we are nearing a plateau to the improvement in localization accuracy as our segmentation resolution increases along with the inclusion of too many small tissue regions. One avenue of research that could plausibly benefit from the development of the head-model geometry is the integration of anthropometric and craniometric data [17]. This path could justify individual models that claim to represent a subpopulation and repudiate studies that misrepresent an identified subpopulation beyond statistical significance. Moreover, it could lead us to establishing the statistical significance of the shape and size of the geometrical features within individual and groups of models.

3.2. Conductivity Values. The electrical characteristics of many biological tissues are inhomogeneous, anisotropic, dispersive, and nonlinear. Head tissues such as the skull, scalp, muscles, cerebrospinal fluid, and gray and white matter have different conductivities σ, permittivities ε, and magnetic permeabilities μ (in most cases it is considered equal to the permeability of water, which is in turn close to the permeability of free space μ_o). The skull as well as the scalp has a multilayer structure, with each layer possessing different electrical properties. This fact leads either to multilayer modeling of the geometry of the tissue [18] or to attributing inhomogeneous properties to the tissue, that is, assigning tensors for $\sigma = \sigma(x, y, z)$ and $\varepsilon = \varepsilon(x, y, z)$. The values and distributions of inhomogeneities are an even more acute problem in patient populations where pathological processes are likely to significantly influence conductivities in affected brain regions. Could there exist an equivalent hybrid isotropic model that represents multiple anisotropy layers? How significantly would such approximations affect source localization within healthy individuals compared with patients with head pathologies?

The conductivity values of any model influence the lead fields of forward problems and the solutions of the inverse problems. Consequently, it is critical that we must assign as accurate conductivity values as reported from previous literature studies and extrapolate and interpolate the rest. As a community we have established electrical-property ranges for most head tissues in terms of conductivity σ and permittivity ε; however, we have to determine the actual electrical-conductivity distribution of an individual's head. As a result of these ranges, many historical studies assign average values to their tissues [15, 18–26]. Using an average value may not be appropriate for individualized models since those models may result in inaccurate solutions due to a function of position [27] or of age [28, 29]. Nevertheless, studies with patients [30, 31] have shown that using approximate conductivities ratios with an accurate geometrical description of the head (i.e., based on a subject's MRI) might yield reasonable, verifiable results for both cortical and deep EEG sources. Still, future models could benefit from using age-specific conductivities. We speculate that the application of age-based conductivity values applied to the skull tissues—most especially the trilayer skull tissue—would mostly benefit the models of youth, whose ossification centers change rapidly in the first two years and plateau in conductivity value around 18 to 20 years of age when the calvarial ossification process is completed [32].

In order to solidify our motivation for highlighting the significance of the skull conductivity, we must briefly delve into its history. The pioneering work [11] introduced a standard conductivity ratio for the brain-to-skull-to-scalp of 1:80:1, which is a historical value still used by some researchers over four decades later. In [33] are reported measurements on postmortem cadavers yielding a ratio of brain-to-skull conductivity values of 15:1. Three years later [28] presented conductivity values on live tissue as low as a ratio of 4:1. Subsequently, Wendel and Malmivuo [29] correlated *postmortem* to live tissue measurements as a way to incorporate and evaluate past data due to the lack in live tissue measurements. Their previous work used a scaling ratio of 0.33 to 0.4 to accommodate the change in conductivity from living to *postmortem* tissue based upon the conductivity recordings of dying tissue samples [34, 35]. In that previous paper they presented an open issue to the community to make more measurements on live tissue samples—most especially live skull samples—at normal body temperature and moisture, which still remains as an open issue today. Therefore, it is pertinent that we discriminate the conditions under which tissue conductivity and permittivity values were and will be acquired. Values obtained by in vivo or living in vitro measurements should be preferred over *postmortem* measurements. In the case of *postmortem* measurements, the time and temperature of acquisition should be specified since tissue properties change rapidly after cellular death.

3.3. Acquisition of Conductivity Values. In the last two decades, a number of approaches have been proposed to image the electrical conductivity of the human body. In conventional Applied Current Electrical Impedance Tomography (ACEIT) low-frequency-sinusoidal currents are applied

via electrodes attached to the body surface [36]. In Induced Current Electrical Impedance Tomography (ICEIT), time-varying magnetic fields with different spatial-field patterns are applied to induce current in the body. In both cases, surface electrodes are used to make voltage measurements.

Recently, two new approaches were proposed that utilize magnetic measurements in determining the conductivity distribution. In Magnetic Induction Imaging (MII), a transmitter coil is driven by a sinusoidal current to provide time varying magnetic fields [37, 38]. When a body is brought nearby these coils, eddy currents are induced in the body. The distribution of these currents is a function of the body's conductivity distribution. These currents create secondary magnetic fields, and the electromotive force induced in a receiver coil is measured. In Magnetic Resonance Electrical Impedance Tomography (MR EIT), low-frequency currents are applied from the body surface, and the resulting magnetic fields are measured using an MR system [39, 40]. Since magnetic fields are measured inside the body, high-resolution images can be measured. Note that all methods are still in the investigation phase, and none of them can provide the requirements of high-resolution conductivity information required for source localization.

3.4. Electrode Montages. EEG has been traditionally measured using the standard 10–20 electrode system including only 21 measurement electrodes. It has been widely acknowledged that the spatial resolution of the 10–20 system is not sufficient for modern brain research [41–44]. The first step in improving the spatial resolution of EEG is to increase the number of EEG electrodes, which the market has responded to with commercially available systems including up to 256 electrodes.

During the last two decades several studies have investigated the benefits of increasing the number of EEG electrodes. The effect on the accuracy of both the forward solutions and inverse solutions has been evaluated. In several articles, an increase in the number of electrodes to at least 128 has been shown to improve the accuracy of the results [45–50].

Different factors affect the appropriate number of electrodes. These include, for example, the widely debated value of the skull's relative conductivity, which has a great impact on the accuracy of inverse solutions. Additionally, the spatial resolution of especially the dense EEG systems (128–512 electrodes) is extremely sensitive to measurement noise. Thus, for different EEG measurements conducted in different environments, the appropriate number of electrodes may vary considerably [48]. Using active electrodes will reduce the noise.

4. Forward Problem

The 1969 study by Rush and Driscoll [11] on EEG electrode sensitivity ushered in the new era of source localization. Their work analytically solved Maxwell's equations to map the lead field, which is only possible with at least elliptical symmetry. Contemporary models consist of a combination of complex geometry and/or electrical parameters, thus necessitating numerical solutions such as the boundary element method (BEM), finite element method (FEM), and the finite difference method (FDM) (Table 1). In this section we aim to identify some of the complications, advantages, and disadvantages of these numerical methods. Through the following explanations we hope the reader gains an understanding of the differences presented, adopts one or more appropriate methods specific to his/her requirements, and refers to the references for specific information.

Most models are unable to obtain the direct solution so they rely upon iterative solvers such as the successive over-relaxation (SOR), conjugate gradients (CG), preconditioned conjugate gradient method (PCG), and algebraic multigrid (AMG) solvers. While these methods have been developed for regular linear systems, they can also be applied in our semidefinite case. In the case of a consistent right-hand side, semiconvergence can be guaranteed for SOR and (P)CG, while the AMG theoretical results are more complicated [51]. A summary of each method is given based on [52] for the first three methods and [53, 54] for the last method.

A first difference between BEM and FEM or FDM is the domain in which the solutions are calculated. In the BEM the solutions are calculated on the boundaries between the homogeneous isotropic compartments while in the FEM and FDM the solution of the forward problem is calculated in the entire volume. Subsequently, the FEM and FDM lead to a larger number of computational points than the BEM. On the other hand, the potential at an arbitrary point can be determined with FEM and FDM by interpolation of computational points in its vicinity, while for the BEM it is necessary to reapply the Barnard formula [55] and numerical integration.

Another important aspect is the computational efficiency. In the BEM, a full matrix $(\mathbf{I} - \mathbf{C})$, represented in

$$V = CV + \mathbf{V}_0, \tag{4}$$

needs to be inverted. When the scalp potentials need to be known for another dipole, $\mathbf{V}_0$ in (4) needs to be recalculated and multiplied with the already available $(\mathbf{I} - \mathbf{C})^{-1}$. Hence once the matrix is inverted, only a matrix multiplication is needed to obtain the scalp potentials. This limited computational load is an attractive feature when solving the inverse problem, where a large number of forward evaluations need to be performed. Alternatively, an accelerated BEM approach increases the speed considerably by calculating only m (i.e., the number of electrodes) rows of the corresponding inverse, whereas, the normal inversion process requires a lot more time due to the dimensionality of the matrix as $n \times n$ (i.e., n equals the number of nodes) [56, 57]. Projective methods [58] based on the parametric representation of the surfaces also allow for a drastic reduction of the computational load.

For the FEM and the FDM, a direct inversion of the large sparse matrices is not possible due to the dimension of the matrices. Typically at least 500 000 computational points are considered thus leading to system matrices of 500 000 equations with 500 000 unknowns, which cannot be solved in a direct manner with the computers currently

Table 1: A comparison of the four methods for solving Poisson's equation in a realistic head model is presented: boundary element method (BEM), finite element method (FEM), isotropic finite difference method (iFDM), and anisotropic finite difference method (aFDM).

	BEM	FEM	iFDM	aFDM
Position of computational points	Surface	Volume	Volume	Volume
Free choice of computational points	Yes	Yes	No	No
System matrix	Full	Sparse	Sparse	Sparse
Solvers	Direct/iterative	Iterative	Iterative	Iterative
Number of compartments	Small	Large	Large	Large
Requires tessellation	Yes	Yes	No	No
Handles anisotropy	No	Yes	No	Yes

available. However, matrices found in FEM and FDM can be inverted for a given source configuration or right-hand side term, utilizing iterative solvers such as the successive over-relaxation method (SSOR), the conjugate gradient (CG) method [59], or algebraic multigrid (AMG) methods [60, 61]. A disadvantage of the iterative solvers is that for each source configuration the solver has to be reapplied. The FEM and FDM would be computationally inefficient when an iterative solver would need to be used for each dipole. To overcome this inefficiency the reciprocity theorem is used [62].

When a large number of conducting compartments are introduced, a large number of boundaries need to be sampled for the BEM. This leads to a large full system matrix, thus lower numerical efficiency. In FEM and FDM modeling, the heterogeneous nature of realistic head models will make the stiffness matrix less sparse and badly conditioned. Moreover, the incorporation of anisotropic conductivities will decrease the sparseness of the stiffness matrix. This can lead to an unstable system or very slow convergence if iterative methods are used. To obtain a fast convergence or a stable system, preconditioning should be used. Preconditioning transforms the system of equations $Ax = b$ into a preconditioned system $M^{-1}Ax = M^{-1}b$, which has the same solution as the orignal system. M is a preconditioning matrix or a preconditioner, and its goal is to reduce the condition number (ratio of the largest eigenvalue to the smallest eigenvalue) of the stiffness matrix toward the optimal value of 1. Basic preconditioning can be used in the form of Jacobi, Gauss-Seidel, Successive Over-Relaxation (SOR), and Symmetric Successive Over-Relaxation (SSOR). These are easily implemented [63]. More advanced methods use incomplete LU factorization and polynomial preconditioning [63, 64].

For the FDM in contrast with the BEM and FEM, the computational points lie fixed in the cube centers for the isotropic approach and at the cube corners for the anisotropic approach. In the FEM and BEM, the computational points, the vertices of the tetrahedrons and triangles, respectively, can be chosen more freely. Therefore, the FEM can better represent the irregular interfaces between the different compartments than the FDM, for the same amount of nodes. However, the segmented medical images used to obtain the realistic volume conductor model are constructed out of cubic voxels. It is straightforward to generate a structured grid used in FDM from these segmented images. In the FEM and the BEM, additional tessellation algorithms [65] need to be used to obtain the tetrahedron elements and the surface triangles, respectively, although cubic and rectangular prism elements are possible in FEM like FDM.

Finally, it is known that the conductivities of some tissues in the human head are anisotropic such as the skull and the white matter tissue. Anisotropy can be introduced in the FEM [66] and in the FDM [67], but not in the BEM.

5. Inverse Problem

While previous sections focused on the different steps preceding the application of inverse procedures, that is, head geometry approximations, conductivity, geometry profile, accuracy of conductivity values, and so forth, this section discusses some open issues including the selection of the recording modality, the source model, and possible post processing to improve the robustness of the inverse solution estimates.

5.1. Recording Modality: MEG versus EEG. The introduction of the Superconducting Quantum Interference Device (SQUID) made it possible to measure the very low magnetic fields induced by the electric activity of the brain, called magnetoencephalography, MEG.

In the beginning of biomagnetic research, there was a lot of hope that biomagnetic signals would include information independent on the bioelectric signals. As described by Plonsey [68], the fact that according to the Helmholtz theorem the scalar and the vector potential fields could be selected independently was considered as evidence for the independence of the electric and magnetic measurements. On the other side, considering the origin of the bioelectric currents it is concluded that the divergence and the curl of the primary current could not be really arbitrarily assigned. Further experiments described in [68] pointed to the relevant contribution of the secondary sources to both electric and magnetic fields. Thus, while we cannot claim that measures of bioelectric or biomagnetic fields alone are enough to define the other [69], we should not expect important differences on the information recorded by them.

The conclusion that electric and magnetic measurements provide comparable information has been confirmed on theoretical and simulation grounds. Using the novel concept

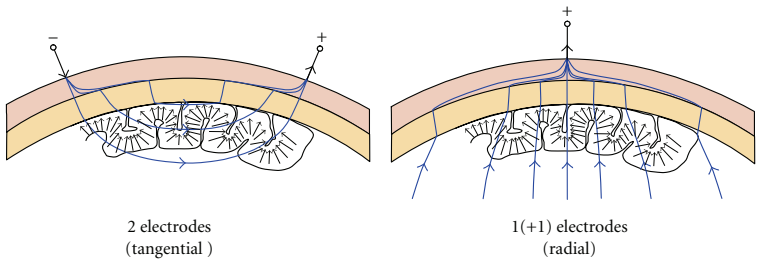

Figure 2: The Sensitivity Distributions of EEG. (Left) An EEG setup measuring the tangential components of neuroelectrical activity, where each bipolar lead is located relatively close to each other. (Right) An EEG setup measuring the radial components of neuroelectric activity, where the measuring electrode is located far from the reference electrode. The arrows in both figures represent macrocolumns of cellular architecture not dipolar sources.

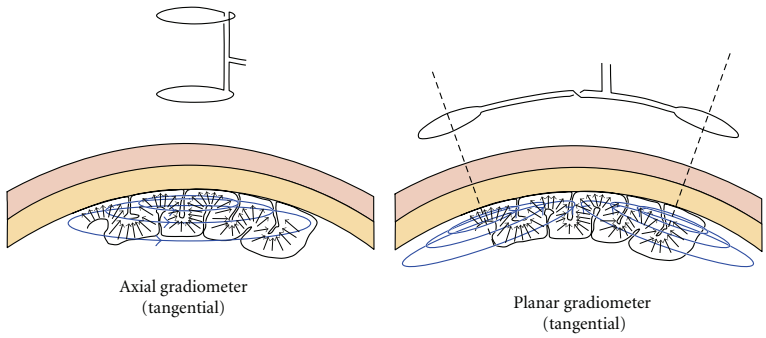

Figure 3: The Sensitivity Distributions of MEG. (Left) An MEG setup measuring the tangential components of neuroelectrical activity, using an axial gradiometer. (Right) An MEG setup measuring the tangential components of neuroelectric activity, using a planar gradiometer. The arrows in both figures represent macrocolumns of cellular architecture not dipolar sources.

of the half sensitivity volume, Malmivuo et al. [70] demonstrated that EEG and MEG record the electric activity in a very similar way, that is, the differences between the EEG and the MEG in the size of the half sensitivity volumes and the form of the sensitivity distributions are very small. Further evaluations of the spatial resolution for cortical sources in the spherical model led to better results for the EEG [71]. Using simulations [72] confirmed also a slight advantage of the EEG over many source locations and orientations with best results for the combined EEG/MEG measurements. More recently [73] applied pattern recognition techniques to decode hand movement directions from simultaneous EEG/MEG measurements, concluding that the inference of movement direction works equally well for both techniques.

Therefore, it may be beneficial to consider also the cost effect of the recording modality. The MEG instrumentation costs about 20 times more than the EEG instrumentation with the same number of channels. Thus, for improving the accuracy of the inverse solution it might be beneficial to first improve all aspects of the EEG technology, that is, number of channels, electrode location accuracy, head model geometry, and tissue resistivity accuracy, and so forth, because improving all these cost much less than the MEG instrumentation.

In summary we can confirm to the reader that besides the cost differences, these two techniques offer similar information about brain sources in what concerns accuracy of source localization, spatiotemporal resolution, and decoding or predictive power. We would like to highlight that although similar information is detected, the EEG and MEG measurement sensitivities are orthogonal. The EEG primarily detects electric sources that are radial to the scalp surface with sufficiently distant electrodes and tangential components when the leads are located near to each other (Figure 2); however, the MEG primarily senses magnetic currents generated by electric sources in the radial direction (Figure 3).

5.2. Source Models. There is vast literature reviewing the arsenal of methods available for the solution of the so-called bioelectromagnetic-inverse problem dealing with the estimation of the electrical activity (i.e., the distribution of sources) inside the head given external measurements of the electric and magnetic fields, for example, [44, 74, 75]. Nevertheless, before applying an inverse solution we must decide about the type of sources and their possible distribution (i.e., locations) inside the head.

The inverse solution estimators differ in source modeling assumptions. By comparing the number of unknowns of the source model with the amount of data, we can differentiate two main type of problems (i.e., of solutions). Firstly, overdetermined problems (e.g., dipolar solutions) with more data than unknowns can differ in minimization algorithms and their efficiency to escape local minima, measures of goodness of fit as well as the use of physiological and/or mathematical constraints often required in the solution estimation/selection process. These models require assumptions regarding the number and location of the brain sources modeled as point-current dipoles giving a unique solution provided that the global minimum is identified. Such approaches require a model order search in addition to a source parameter optimization [76]. Numerical simulation studies have demonstrated that an accurate estimation of the temporal dynamics of dipolar models is critically dependent on the ability to resolve and accurately localize all active brain regions [77]. While there is a range of physiological and anatomical reasons, animal studies as well as already converging evidence from the human hemodynamic and/or metabolic fMRI and PET studies suggest that the sensory and cognitive process can be considered as a network of distributed focal activity; possibility of extended activations of neuronal tissue in some conditions cannot be disregarded. In-depth electrode recordings used to be the primary evidence for the latter assumption, demonstrating activity over wide brain regions. However, even with such recordings, the summed contributions of the primary source contributions and volume currents are to be expected, and inverse models should be considered instead of taking such measures as strong evidence for extended brain activations.

On the other hand, we have the underdetermined problems (e.g., distributed inverse solutions) with more unknowns than data associated with the linear-minimum-norm approaches that is suggested [75, 78, 79] for cases when focal source assumptions are not justified. Such an approach is challenging as it might require further weighting and regularization to compensate for depth bias, selected by imposing mathematical criteria or physiological ones.

In order to help the reader make the correct choice, we describe four primary source models obtained by restriction on the source type and/or their location together with their main assumptions.

(1) *The equivalent-current dipole model.* It assumes that measurements are due to a single concentrated source. It is primarily valid for strong and spatially limited sources (e.g., some focal epilepsy) or sources observed from a far away measurement surface. It is probably more useful to summarize the measured field than the source itself, which is a particular case of the following source model.

(2) *Dipolar models as used in overdetermined problems.* These models consider that the measured fields are due to a small number of sources with unknown locations and orientations. They are very well suited for low-rank data as produced by filtered and averaged-evoked responses [80, 81].

(3) *Cortical model.* Under the extreme assumption that deep sources do not contribute to the external fields of the head, it assumes that the primary sources are located only in the cortical mantel with a direction constraint. It is probably very well suited for the analysis of measurements associated with the activation of some primary cortical areas [82].

Previous models can be considered as data driven in the sense that they can be only used under very specific and restrictive experimental conditions that will not be acceptable as a general model for the EEG and MEG sources. Furthermore, there is scarce experimental evidence in favor of the dipole. In fact a dipole would imply an indefinitely increasing potential when we approach its location. Hopefully, this has never been reported because that would correspond to an undefined potential at that location. Nevertheless, a more complete source model must contain, as a particular case, previous source models while incorporating those elements that are out of discussion so far, that is as follows.

(4) *Potential distribution inside the head.* The electromagnetic measurements at/near the scalp are due to the potential distribution inside the brain. These (intracranial) potentials that represent the primary source are generated in at, at least, the entire gray matter and not only at the cortex. This source model is compatible with all previous geometrical constraints while including the dipoles as a particular case. Importantly, this source model implies significant theoretical and numerical simplifications, solving also the issue of focal versus extended sources, since the potential is always a continuous function defined at all points of the head.

After defining the adequate preprocessing and source model for our data, we face the problem of the inverse procedure selection. The following issues might be relevant at this stage.

5.3. The Dipole Localization Error. The evaluation of the overdetermined-dipolar models seems to have a straightforward solution by comparing target and estimated sources with measures as the dipole localization error. Unfortunately, these measures cannot be directly extrapolated to underdetermined distributed solutions. This is probably why the evaluation of the distributed solutions remains as an open issue in this field. Obviously, this might influence the selection of the inverse solution. While we do not want to tell the reader what he/she should do/use, we would like to discuss some things to avoid.

It has been suggested that the zero dipole localization might be the way to select the inverse solution. This is likely motivated by genuine applications where the data is dominated by single focal sources (e.g., epilepsy focus localization) as well as by the long experience accumulated from overdetermined (dipolar) models. It is probably an abuse of language, which brings people to believe that "if we correctly localize each single source alone, then by the principle of superposition we should correctly localize any combination of sources". There are two clear inaccuracies with this statement.

(1) In this case, correct localization only means that the maximum of the modulus of the current source density coincides with the target site. This ignores that the amplitude will be, as is almost always the case for linear methods and multiple sources, misestimated due to the unavoidable off-diagonal elements on the resolution matrix (3).

(2) As the definition clearly states, the dipole localization error (DLE) is estimated from the modulus of the current source density, which means that the DLE is not a linear function of the data d, and thus the principle of superposition does not hold. Consequently, linear system theory, that characterizes the system by their response to (Delta like) input impulses, cannot be invocated.

Given previous theoretical flaws, it is not surprising that the DLE fails to predict the performance of an inverse solution in the presence of multiple sources. In fact it can be proved that correct localization of single sources is a trivial property of simple yet robust methods (see the work by Grave de Peralta et al. for this issue) that, we insist, are only applicable if the concentrated single source hypothesis holds.

5.4. Inverse Solutions and Spatial Filters. A sound approach for the inverse-problem solution in physical volumes is the estimation of spatial filters, which "filters out" the activity that arises from one special location, while trying to suppress the activity from all others. These methods that have reappeared nowadays under the name "beamformers" are very appreciated, among other things, because the solution can be computed independently for each solution point. Continuing with the original descriptions of these methods [83, 84], it was clear that minimizing crosstalk (i.e., distance to the ideal resolution matrix) between sources does not necessarily imply an optimal resolution kernel. Nevertheless, current applications suggest that the solution provided by these methods is not affected by the crosstalk.

There are very good reasons to select a Backus-Gilbert (i.e., beamformer) method such as its adaptive properties to deal with specific noise structures [85]. However, we cannot emphasize enough that the only way to assess the estimates provided by a linear inversion procedure is to look at the resolution kernels [2, 3, 86]. The fact that we build an independent estimate for each point alone does not mean that this estimate is not contaminated by the effect of simultaneously active sources.

In order to conclude the issue of the inverse procedure selection on a positive note, we mention that there is a sound theoretical way to select, and more importantly, to build an inverse solution. It is enough to note that infinitely-many-linear-inverse methods can be described by the equation $G = C * L' * (L * C * L')^{+}$. The source j_{est} estimated with this method will belong to the space spanned by the columns of $C * L'$ for both the noiseless and the noisy case. On the other hand, it is clear from (3) that the only way to change the rows of the resolution matrix (i.e., the resolution kernels) is by right transformations of the lead field. These two procedures together yield meaningful source estimates, when C is selected according to sound a priori information and when an appropriate right-hand transformation of the lead field is made [87].

5.5. Robust Methods for the Analysis of EEG/MEG Sources. The problem with the estimation of the EEG/MEG sources can be interpreted as follows. The measured data provides precise (up to the noise level) but local information. In order to know more about the whole system (i.e., the brain), we need to ascend to qualitatively higher levels corresponding to the surface maps and the 3D distribution of sources. By doing this we obtain a more complete global descriptor but probably also with a higher incertitude (if compared with the sensor data).

As it is also the case for the fMRI signal [88], in general we cannot rely on the amplitudes provided by the inverse solution to compare the neural activity at two different locations. For the same reason, ghost and lost sources appear in every reconstruction mixed with real sources. Thus, differentiating true sources from artifacts is almost impossible unless we know the real distribution. Consequently, we can say that the source distribution obtained from a single map is probably the most imprecise picture that we can have of brain activation.

What can we do to increase the reliability of these functional images? As for a partial answer, we suggest the following points.

(1) Select your inverse solution keeping in mind the previously discussed points about the spatial filters and the zero dipole localization error and consider with caution source distributions estimated from a single map (as produced, e.g., by segmentation algorithms).

(2) Use source models that reduce the underdetermination of the inverse problem. Give preference to physically sound transformations that reduce the problem to the estimation of scalar fields improving the resolution kernels.

(3) Compute magnitudes or figures of merit based on the temporal course of brain sources instead of the instantaneous local amplitudes and use measures that are independent of the scale factor of the intracranial signals like correlation coefficients.

(4) Evaluate contrasts between experimental conditions or prestimulus versus poststimulus conditions to reduce systematic ghost and lost source effects [31, 89].

(5) Compute correlations between magnitudes derived from the time course of the brain activity and behavioral measurements as reaction times [90].

6. Conclusion

There are many key areas that critically affect the accuracy and precision of source localization. In this paper we discussed the four key areas of EEG/MEG source imaging,

namely, preprocessing, the volume conductor, and the forward and inverse problems. Notwithstanding these wide-ranging components, we emphatically direct the community to allocate attention to these key open issues. Firstly, the conductivity equally affects the forward and inverse solution thus warranting the need for actual conductivity measurements on live tissue to fill the void of these critical parameters. These future studies should accurately document their measurement setups—most especially in terms of moisture and temperature. Secondly, future modeling studies should incorporate how pathologies alter a normal, healthy head model. Lastly, it is critical to select the source model and the inverse procedure based on sound theoretical and experimental basis.

Ultimately, we should make wise decisions to optimize elements of the model that gain the most precision and accuracy in source imaging and suppress those that contribute minimal gains in source localization. After such optimizations, how well do these future models represent their physiological counterpart, that is, the human head? As we proceed forward as a community, we should remember to highlight the shortcomings of future studies reflecting new conductivities, pathologies, source models, and so forth, to prevent any further misinterpretations of those models, while collectively building upon the contributions of past models.

Acknowledgments

This work has been partially supported by the European Project BACS FP6-IST-027140. This paper only reflects the authors' views, and the funding agencies are not liable for any use that may be made of the information contained herein. This work was also supported by the COST Action BM0601 "NeuroMath". Neither the COST Office nor any person acting on its behalf is responsible for the use, which might be made of the information contained in this publication. The COST Office is not responsible for the external websites referred to in this publication.

References

[1] D. Venes, *Taber's Cyclopedic Medical Dictionary*, F. A. Davis Company, Philadelphia, Pa, USA, 20th edition, 2005.

[2] A. M. Dale and M. I. Sereno, "Improved localization of cortical activity by combining EEG and MEG with MRI cortical surface reconstruction: a linear approach," *Journal of Cognitive Neuroscience*, vol. 5, no. 2, pp. 162–176, 1993.

[3] R. Grave de Peralta Menendez, S. L. Gonzalez Andino, and B. Lutkenhoner, "Figures of merit to compare distributed linear inverse solutions," *Brain Topography*, vol. 9, no. 2, pp. 117–124, 1996.

[4] A. J. R. Leal, A. I. Dias, and J. P. Vieira, "Analysis of the EEG dynamics of epileptic activity in gelastic seizures using decomposition in independent components," *Clinical Neurophysiology*, vol. 117, no. 7, pp. 1595–1601, 2006.

[5] P. Anderer, G. Kloesch, G. Gruber, et al., "Low-resolution brain electromagnetic tomography revealed simultaneously active frontal and parietal sleep spindle sources in the human cortex," *Neuroscience*, vol. 103, no. 3, pp. 581–592, 2001.

[6] P. Durka, A. Matysiak, E. M. Montes, P. V. Sosa, and K. J. Blinowska, "Multichannel matching pursuit and EEG inverse solutions," *Journal of Neuroscience Methods*, vol. 148, no. 1, pp. 49–59, 2005.

[7] C. E. Davila and R. Srebro, "Subspace averaging of steady-state visual evoked potentials," *IEEE Transactions on Biomedical Engineering*, vol. 47, no. 6, pp. 720–728, 2000.

[8] O. Bai, M. Nakamura, T. Nagamine, and H. Shibasaki, "Parametric modeling of somatosensory evoked potentials using discrete cosine transform," *IEEE Transactions on Biomedical Engineering*, vol. 48, no. 11, pp. 1347–1351, 2001.

[9] T. W. Picton, *Handbook of Electroencephalography and Clinical Neurophysiology: Human Event-Related Potentials*, Elsevier, Amsterdam, The Netherlands, 1988.

[10] B. H. Jansen, G. Agarwal, A. Hegde, and N. N. Boutros, "Phase synchronization of the ongoing EEG and auditory EP generation," *Clinical Neurophysiology*, vol. 114, no. 1, pp. 79–85, 2003.

[11] S. Rush and D. A. Driscoll, "EEG electrode sensitivity—an application of reciprocity," *IEEE Transactions on Biomedical Engineering*, vol. 16, no. 1, pp. 15–22, 1969.

[12] B. J. Roth, M. Balish, A. Gorbach, and S. Sato, "How well does a three-sphere model predict positions of dipoles in a realistically shaped head?" *Electroencephalography and Clinical Neurophysiology*, vol. 87, no. 4, pp. 175–184, 1993.

[13] A. Crouzeix, B. Yvert, O. Bertrand, and J. Pernier, "An evaluation of dipole reconstruction accuracy with spherical and realistic head models in MEG," *Clinical Neurophysiology*, vol. 110, no. 12, pp. 2176–2188, 1999.

[14] B. N. Cuffin, "EEG localization accuracy improvements using realistically shaped head models," *IEEE Transactions on Biomedical Engineering*, vol. 43, no. 3, pp. 299–303, 1996.

[15] M. S. Hamalainen and J. Sarvas, "Realistic conductivity geometry model of the human head for interpretation of neuromagnetic data," *IEEE Transactions on Biomedical Engineering*, vol. 36, no. 2, pp. 165–171, 1989.

[16] K. Wendel, N. G. Narra, M. Hannula, P. Kauppinen, and J. Malmivuo, "The influence of CSF on EEG sensitivity distributions of multilayered head models," *IEEE Transactions on Biomedical Engineering*, vol. 55, no. 4, pp. 1454–1456, 2008.

[17] K. Wendel, M. Osadebey, and J. Malmivuo, "Incorporating anthropometric and craniometric data into realistically-shaped volume conductor head models," in *Proceedings of the 11th World Congress on Medical Physics and Biomedical Engineering*, Munich, Germany, September 2009.

[18] J. Haueisen, C. Ramon, M. Eiselt, H. Brauer, and H. Nowak, "Influence of tissue resistivities on neuromagnetic fields and electric potentials studied with a finite element model of the head," *IEEE Transactions on Biomedical Engineering*, vol. 44, no. 8, pp. 727–735, 1997.

[19] H. P. Schwan, "Determination of biological impedances," in *Physical Techniques in Biological Research*, W. L. Nastuk, Ed., Academic Press, New York, NY, USA, 1963.

[20] C. Gabriel, S. Gabriel, and E. Corthout, "The dielectric properties of biological tissues—I: literature survey," *Physics in Medicine and Biology*, vol. 41, no. 11, pp. 2231–2249, 1996.

[21] L. A. Geddes and L. E. Baker, "The specific resistance of biological material—a compendium of data for the biomedical engineer and physiologist," *Medical & Biological Engineering*, vol. 5, no. 3, pp. 271–293, 1967.

[22] B. M. Radich and K. M. Buckley, "EEG dipole localization bounds and MAP algorithms for head models with parameter uncertainties," *IEEE Transactions on Biomedical Engineering*, vol. 42, no. 3, pp. 233–241, 1995.

[23] S. P. van den Broek, F. Reinders, M. Donderwinkel, and M. J. Peters, "Volume conduction effects in EEG and MEG," *Electroencephalography and Clinical Neurophysiology*, vol. 106, no. 6, pp. 522–534, 1998.

[24] G. Huiskamp, M. Vroeijenstijn, R. van Dijk, G. Wieneke, and A. C. van Huffelen, "The need for correct realistic geometry in the inverse EEG problem," *IEEE Transactions on Biomedical Engineering*, vol. 46, no. 11, pp. 1281–1287, 1999.

[25] B. Vanrumste, G. Van Hoey, R. Van de Walle, M. D'Havé, I. Lemahieu, and P. Boon, "Dipole location errors in electroencephalogram source analyssis due to volume conductor model errors," *Medical and Biological Engineering and Computing*, vol. 38, no. 5, pp. 528–534, 2000.

[26] N. G. Gencer and C. E. Acar, "Sensitivity of EEG and MEG measurements to tissue conductivity," *Physics in Medicine and Biology*, vol. 49, no. 5, pp. 701–717, 2004.

[27] J. O. Ollikainen, M. Vauhkonen, P. A. Karjalainen, and J. P. Kaipio, "Effects of local skull inhomogeneities on EEG source estimation," *Medical Engineering and Physics*, vol. 21, no. 3, pp. 143–154, 1999.

[28] R. Hoekema, G. H. Wieneke, F. S. S. Leijten, et al., "Measurement of the conductivity of skull, temporarily removed during epilepsy surgery," *Brain Topography*, vol. 16, no. 1, pp. 29–38, 2003.

[29] K. Wendel and J. Malmivuo, "Correlation between live and post mortem skull conductivity measurements," *Proceedings of Annual International Conference of the IEEE Engineering in Medicine and Biology Society*, vol. 1, pp. 4285–4288, 2006.

[30] C. M. Michel, G. Lantz, L. Spinelli, R. Grave de Peralta Menendez, T. Landis, and M. Seeck, "128-channel EEG source imaging in epilepsy: clinical yield and localization precision," *Journal of Clinical Neurophysiology*, vol. 21, no. 2, pp. 71–83, 2004.

[31] S. L. Gonzalez Andino, R. Grave de Peralta Menendez, A. Khateb, T. Landis, and A. J. Pegna, "Electrophysiological correlates of affective blindsight," *NeuroImage*, vol. 44, no. 2, pp. 581–589, 2009.

[32] K. L. Moore and A. F. Dalley, *Clinically Oriented Anatomy*, Lippincott Williams & Wilkins, Philadelphia, Pa, USA, 5th edition, 2005.

[33] T. F. Oostendorp, J. Delbeke, and D. F. Stegeman, "The conductivity of the human skull: results of in vivo and in vitro measurements," *IEEE Transactions on Biomedical Engineering*, vol. 47, no. 11, pp. 1487–1492, 2000.

[34] J. D. Kosterich, K. R. Foster, and S. R. Pollack, "Dielectric permittivity and electrical conductivity of fluid saturated bone," *IEEE Transactions on Biomedical Engineering*, vol. 30, no. 2, pp. 81–86, 1983.

[35] J. D. Kosterich, K. R. Foster, and S. R. Pollack, "Dielectric properties of fluid-saturated bone. The effect of variation in conductivity of immersion fluid," *IEEE Transactions on Biomedical Engineering*, vol. 31, no. 4, pp. 369–374, 1984.

[36] S. I. Goncalves, J. C. de Munck, J. P. A. Verbunt, F. Bijma, R. M. Heethaar, and F. L. da Silva, "In vivo measurement of the brain and skull resistivities using an EIT-based method and realistic models for the head," *IEEE Transactions on Biomedical Engineering*, vol. 50, no. 6, pp. 754–767, 2003.

[37] H. Griffiths, W. R. Stewart, and W. Cough, "Magnetic induction tomography. A measuring system for biological tissues," *Annals of the New York Academy of Sciences*, vol. 873, pp. 335–345, 1999.

[38] N. G. Gencer and M. N. Tek, "Electrical conductivity imaging via contactless measurements," *IEEE Transactions on Medical Imaging*, vol. 18, no. 7, pp. 617–627, 1999.

[39] N. Zhang, *Electrical Impedance Tomography Based on Current Density Imaging*, University of Toronto, Toronto, Canada, 1992.

[40] Y. Z. Ider, S. Onart, and W. R. B. Lionheart, "Uniqueness and reconstruction in magnetic resonance-electrical impedance tomography (MR-EIT)," *Physiological Measurement*, vol. 24, no. 2, pp. 591–604, 2003.

[41] A. Gevins, H. Leong, M. E. Smith, J. Le, and R. Du, "Mapping cognitive brain function with modern high-resolution electroencephalography," *Trends in Neurosciences*, vol. 18, no. 10, pp. 429–436, 1995.

[42] A. Gevins, J. Le, H. Leong, L. K. McEvoy, and M. E. Smith, "Deblurring," *Journal of Clinical Neurophysiology*, vol. 16, no. 3, pp. 204–213, 1999.

[43] F. Babiloni, F. Cincotti, F. Carducci, P. M. Rossini, and C. Babiloni, "Spatial enhancement of EEG data by surface Laplacian estimation: the use of magnetic resonance imaging-based head models," *Clinical Neurophysiology*, vol. 112, no. 5, pp. 724–727, 2001.

[44] C. M. Michel, M. M. Murray, G. Lantz, S. Gonzalez, L. Spinelli, and R. Grave de Peralta Menendez, "EEG source imaging," *Clinical Neurophysiology*, vol. 115, no. 10, pp. 2195–2222, 2004.

[45] A. Gevins, P. Brickett, B. Costales, J. Le, and B. Reutter, "Beyond topographic mapping: towards functional-anatomical imaging with 124-channel EEGs and 3-D MRIs," *Brain Topography*, vol. 3, no. 1, pp. 53–64, 1990.

[46] R. Srinivasan, P. L. Nunez, D. M. Tucker, R. B. Silberstein, and P. J. Cadusch, "Spatial sampling and filtering of EEG with spline laplacians to estimate cortical potentials," *Brain Topography*, vol. 8, no. 4, pp. 355–366, 1996.

[47] F. Babiloni, C. Babiloni, F. Carducci, et al., "High resolution EEG: a new model-dependent spatial deblurring method using a realistically-shaped MR-constructed subject's head model," *Electroencephalography and Clinical Neurophysiology*, vol. 102, no. 2, pp. 69–80, 1997.

[48] O. R. M. Ryynanen, J. A. K. Hyttinen, and J. Malmivuo, "Effect of measurement noise and electrode density on the spatial resolution of cortical potential distribution with different resistivity values for the skull," *IEEE Transactions on Biomedical Engineering*, vol. 53, no. 9, pp. 1851–1858, 2006.

[49] R. Srinivasan, D. M. Tucker, and M. Murias, "Estimating the spatial Nyquist of the human EEG," *Behavior Research Methods, Instruments, & Computers*, vol. 30, no. 1, pp. 8–19, 1998.

[50] Y. Wang and B. He, "A computer simulation study of cortical imaging from scalp potentials," *IEEE Transactions on Biomedical Engineering*, vol. 45, no. 6, pp. 724–735, 1998.

[51] A. Berman and R. Plemmons, *Nonnegative Matrices in the Mathematical Sciences*, SIAM, Philadelphia, Pa, USA, 1994.

[52] W. H. Press, S. A. Teukolsky, W. T. Vetterling, and B. P. Flannery, *Numerical Recipes in C*, Cambridge University Press, Cambridge, UK, 1995.

[53] J. W. Ruge and K. Stüben, "Algebraic multigrid (AMG)," in *Multigrid Methods*, S. F. McCormick, Ed., vol. 3 of *Frontiers in Applied Mathematics*, pp. 73–130, SIAM, Philadelphia, Pa, USA, 1987.

[54] W. L. Briggs, V. E. Henson, and S. F. McCormick, *A Multigrid Tutorial*, SIAM, Philadelphia, Pa, USA, 2000.

[55] A. C. L. Barnard, I. M. Duck, and M. S. Lynn, "The application of electromagnetic theory to electrocardiography—I: derivation of the integral equations," *Biophysics Journal*, vol. 7, pp. 443–462, 1967.

[56] Z. Akalin-Acar and N. G. Gencer, "An advanced boundary element method (BEM) implementation for the forward problem of electromagnetic source imaging," *Physics in Medicine and Biology*, vol. 49, no. 21, pp. 5011–5028, 2004.

[57] Y. Ataseven, Z. Akalin-Acar, C. E. Acar, and N. G. Gencer, "Parallel implementation of the accelerated BEM approach for EMSI of the human brain," *Medical and Biological Engineering and Computing*, vol. 46, no. 7, pp. 671–679, 2008.

[58] S. L. Gonzalez Andino, R. Grave de Peralta Menendez, R. Biscay, J. C. Jimenez, R. D. Pascual, and J. Lemagne, "Projective methods for the magnetic direct problem," in *Advances in Biomagnetism*, New York, NY, USA, 1989.

[59] B. N. Datta, *Numerical Linear Algebra and Applications*, Brooks/Cole, Pacific Grove, Calif, USA, 1995.

[60] W. L. Briggs, *A Multigrid Tutorial*, SIAM, Philadelphia, Pa, USA, 1987.

[61] R. Hoekema, K. Venner, J. J. Struijk, and J. Holsheimer, "Multigrid solution of the potential field in modeling electrical nerve stimulation," *Computers and Biomedical Research*, vol. 31, no. 5, pp. 348–362, 1998.

[62] P. Laarne, J. Hyttinen, S. Dodel, J. Malmivuo, and H. Eskola, "Accuracy of two dipolar inverse algorithms applying reciprocity for forward calculation," *Computers and Biomedical Research*, vol. 33, no. 3, pp. 172–185, 2000.

[63] Y. Saad, *Iterative Methods for Sparse Linear Systems*, SIAM, Philadelphia, Pa, USA, 2nd edition, 2003.

[64] L. A. Neilson, M. Kovalyov, and Z. J. Koles, "A computationally efficient method for accurately solving the EEG forward problem in a finely discretized head model," *Clinical Neurophysiology*, vol. 116, no. 10, pp. 2302–2314, 2005.

[65] J. F. Thompson, B. K. Soni, and N. P. Weatherrill, *Handbook of Grid Generation*, CRC Press, Boca Raton, Fla, USA, 1998.

[66] N. Ottosen and H. Peterson, *Introduction to the Finite Element Method*, Prentice-Hall, Englewood Cliffs, NJ, USA, 1992.

[67] H. I. Saleheen and T. Kwong, "New finite difference formulations for general inhomogeneous anisotropic bioelectric problems," *IEEE Transactions on Biomedical Engineering*, vol. 44, no. 9, pp. 800–809, 1997.

[68] R. Plonsey, "The nature of sources of bioelectric and biomagnetic fields," *Biophysical Journal*, vol. 39, no. 3, pp. 309–312, 1982.

[69] M. Hamalainen, R. J. Ilmoniemi, and J. Sarvas, "Interdependence of information conveyed by the magnetoencephalogram and the electroencephalogram," in *Theory and Applications of Inverse Problems*, H. Hario, Ed., John Wiley & Sons, New York, NY, USA, 1988.

[70] J. Malmivuo, V. Suihko, and H. Eskola, "Sensitivity distributions of EEG and MEG measurements," *IEEE Transactions on Biomedical Engineering*, vol. 44, no. 3, pp. 196–208, 1997.

[71] J. Malmivuo and V. E. Suihko, "Effect of skull resistivity on the spatial resolutions of EEG and MEG," *IEEE Transactions on Biomedical Engineering*, vol. 51, no. 7, pp. 1276–1280, 2004.

[72] A. K. Liu, A. M. Dale, and J. W. Belliveau, "Monte Carlo simulation studies of EEG and MEG localization accuracy," *Human Brain Mapping*, vol. 16, no. 1, pp. 47–62, 2002.

[73] S. Waldert, H. Preissl, E. Demandt, et al., "Hand movement direction decoded from MEG and EEG," *Journal of Neuroscience*, vol. 28, no. 4, pp. 1000–1008, 2008.

[74] M. Hamalainen, R. Hari, R. J. Ilmoniemi, J. Knuutila, and O. V. Lounasmaa, "Magnetoencephalography—theory, instrumentation, and applications to noninvasive studies of the working human brain," *Reviews of Modern Physics*, vol. 65, no. 2, pp. 413–497, 1993.

[75] R. Grave de Peralta Menendez and S. L. Gonzalez-Andino, "A critical analysis of linear inverse solutions to the neuroelectromagnetic inverse problem," *IEEE Transactions on Biomedical Engineering*, vol. 45, no. 4, pp. 440–448, 1998.

[76] S. Supek and C. J. Aine, "Simulation studies of multiple dipole neuromagnetic source localization: model order and limits of source resolution," *IEEE Transactions on Biomedical Engineering*, vol. 40, no. 6, pp. 529–540, 1993.

[77] S. Supek and C. J. Aine, "Spatio-temporal modeling of neuromagnetic data—I: multi-source location versus time-course estimation accuracy," *Human Brain Mapping*, vol. 5, no. 3, pp. 139–153, 1997.

[78] M. S. Hamalainen and R. J. Ilmoniemi, "Interpreting magnetic fields of the brain: minimum norm estimates," *Medical and Biological Engineering and Computing*, vol. 32, no. 1, pp. 35–42, 1994.

[79] O. Hauk, "Keep it simple: a case for using classical minimum norm estimation in the analysis of EEG and MEG data," *NeuroImage*, vol. 21, no. 4, pp. 1612–1621, 2004.

[80] M. Scherg and D. Von Cramon, "Evoked dipole source potentials of the human auditory cortex," *Electroencephalography and Clinical Neurophysiology*, vol. 65, no. 5, pp. 344–360, 1986.

[81] M. Scherg and T. W. Picton, "Separation and identification of event-related potential components by brain electric source analysis," *Electroencephalography and Clinical Neurophysiology. Supplement*, vol. 42, pp. 24–37, 1991.

[82] F. Babiloni, C. Babiloni, L. Locche, F. Cincotti, P. M. Rossini, and F. Carducci, "High-resolution electro-encephalogram: source estimates of Laplacian-transformed somatosensory-evoked potentials using a realistic subject head model constructed from magnetic resonance images," *Medical and Biological Engineering and Computing*, vol. 38, no. 5, pp. 512–519, 2000.

[83] J. Capon, "High resolution frequency-wavenumber," *Proceedings of the IEEE*, vol. 57, no. 8, pp. 1408–1418, 1969.

[84] G. E. Backus and J. F. Gilbert, "The resolving power of gross earth data," *Geophysical Journal of the Royal Astronomical Society*, vol. 16, pp. 169–205, 1968.

[85] K. Sekihara, S. S. Nagarajan, D. Poeppel, and A. Marantz, "Performance of an MEG adaptive-beamformer technique in the presence of correlated neural activities: effects on signal intensity and time-course estimates," *IEEE Transactions on Biomedical Engineering*, vol. 49, no. 12 I, pp. 1534–1546, 2002.

[86] B. Lutkenhoner and R. Grave de Peralta Menendez, "The resolution-field concept," *Electroencephalography and Clinical Neurophysiology*, vol. 102, no. 4, pp. 326–334, 1997.

[87] R. Grave de Peralta Menendez, M. M. Murray, C. M. Michel, R. Martuzzi, and S. L. Gonzalez Andino, "Electrical neuroimaging based on biophysical constraints," *NeuroImage*, vol. 21, no. 2, pp. 527–539, 2004.

[88] N. K. Logothetis and B. A. Wandell, "Interpreting the BOLD signal," *Annual Review of Physiology*, vol. 66, pp. 735–769, 2004.

[89] S. L. Gonzalez Andino, R. Grave de Peralta Menendez, A. Khateb, A. J. Pegna, G. Thut, and T. Landis, "A glimpse into your vision," *Human Brain Mapping*, vol. 28, no. 7, pp. 614–624, 2007.

[90] S. L. Gonzalez Andino, C. M. Michel, G. Thut, T. Landis, and R. Grave de Peralta Menendez, "Prediction of response speed by anticipatory high-frequency (gamma band) oscillations in the human brain," *Human Brain Mapping*, vol. 24, no. 1, pp. 50–58, 2005.

Publication P5

K Wendel, M Osadebey, and J Malmivuo, "Incorporating Craniofacial Anthropometry into Realistically-Shaped Head Models." In *IFMBE Proceedings on the World Congress on Medical Physics and Biomedical Engineering*, O Dössel & WC Schlegel (eds.), Munich, Germany, vol. 25, pp. 1706–1709, September 7–12, 2009.

Oral presentation.

Publication P6

K Wendel, J Väisänen, G Seemann, J Hyttinen, and J Malmivuo. The Influence of Age and Skull Conductivity on Surface and Subdermal Bipolar EEG Leads. Computational Intelligence & Neuroscience, vol. 2010, article ID 397272, 7 pages, 2010.

Hindawi Publishing Corporation
Computational Intelligence and Neuroscience
Volume 2010, Article ID 397272, 7 pages
doi:10.1155/2010/397272

Research Article

The Influence of Age and Skull Conductivity on Surface and Subdermal Bipolar EEG Leads

Katrina Wendel,[1] Juho Väisänen,[1] Gunnar Seemann,[2] Jari Hyttinen,[1] and Jaakko Malmivuo[1]

[1] *Department of Biomedical Engineering, Tampere University of Technology, Korkeakoulunkatu 3, P.O. Box 692, 33101 Tampere, Finland*
[2] *Institute of Biomedical Engineering, Karlsruhe Institute of Technology, 76131 Karlsruhe, Germany*

Correspondence should be addressed to Katrina Wendel, katrina.wendel@tut.fi

Received 1 July 2009; Accepted 8 October 2009

Academic Editor: Fabrizio De Vico Fallani

Bioelectric source measurements are influenced by the measurement location as well as the conductive properties of the tissues. Volume conductor effects such as the poorly conducting bones or the moderately conducting skin are known to affect the measurement precision and accuracy of the surface electroencephalography (EEG) measurements. This paper investigates the influence of age via skull conductivity upon surface and subdermal bipolar EEG measurement sensitivity conducted on two realistic head models from the Visible Human Project. Subdermal electrodes (a.k.a. subcutaneous electrodes) are implanted on the skull beneath the skin, fat, and muscles. We studied the effect of age upon these two electrode types according to the scalp-to-skull conductivity ratios of 5, 8, 15, and 30 : 1. The effects on the measurement sensitivity were studied by means of the half-sensitivity volume (HSV) and the region of interest sensitivity ratio (ROISR). The results indicate that the subdermal implantation notably enhances the precision and accuracy of EEG measurements by a factor of eight compared to the scalp surface measurements. In summary, the evidence indicates that both surface and subdermal EEG measurements benefit better recordings in terms of precision and accuracy on younger patients.

1. Introduction

Clinical electroencephalography (EEG) and evoked potential (EP) recordings such as the visually evoked potentials (VEPs) demand high signal-to-noise ratios (SNRs), minimization of skin artifacts, and high accuracy, to name a few important criteria. Subdermal needle electrodes (a.k.a. subcutaneous needle electrodes) are commonly used in clinical electromyography (EMG), which are inserted into the muscles of interest. It is less commonly known that these subdermal needle electrodes also record continuous EEGs and EPs in intensive care units (ICU) [1–4]. The measurement setup is achieved by inserting the needle nearly tangentially to the skin so that it is stabilized and the recording tip touches the skull. Furthermore, these recordings offer higher SNRs with lower proclivity of standard measurement artifacts when compared with traditional surface measurements and are more suitable for long-term EEG monitoring in the ICU. Higher SNR requires less averaging, thus yielding faster and more accurate diagnostic measurements. We believe that clinical EEGs and EPs such as the VEP could adopt the subdermal measurement setup, thus placing the lead on the skull bypassing the artifact-prone skin.

Previously, we correlated skull conductivity with age (Figure 1) [6]. In that former study, we analyzed the reported skull conductivities of living skull fragments temporarily excised during epilepsy surgery with the age of the patient [5]. We reported a decreasing trend that stabilized in early adulthood. According to medical texts, physiologists explain that the calvarial bone completes the ossification process between the ages of 18 and 20 [7]; therefore, the skull conductivity should nearly approach steady state after adolescence. From the study of Hoekema et al. [5], we extrapolate that the scalp-to-skull conductivity ratio of 5 represents children and a small percentage of adolescents, the ratio of 8 represents adolescents and some adults, the

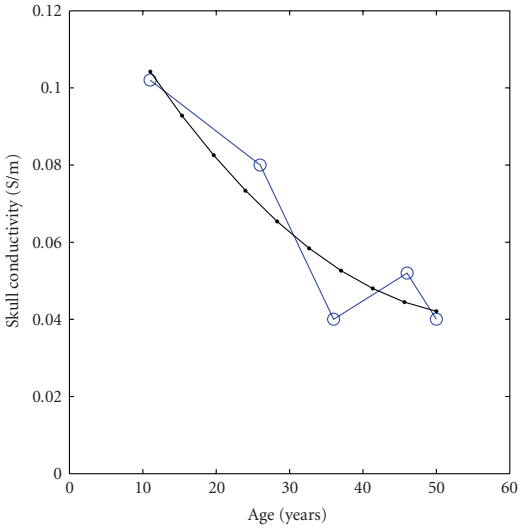

Figure 1: Reported conductivity values of live skull samples temporarily removed during epileptic surgery plotted against patient age [5]. The thick blue trend with circles graphs raw data and the thin gray trend with dots graphs the least squares fit. Reproduced from [6].

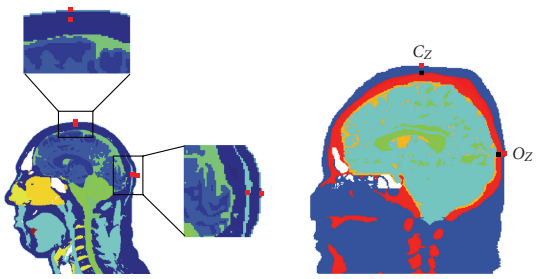

Figure 2: The midsagittal views show the bipolar electrode locations of the surface and subdermal (i.e., on the skull) measurement locations at the apex C_Z and the occipital cortex O_Z. The EEG electrode dimensions are 1 mm × 1 mm × 1 mm. (a) The sagittal slice of the *Visible Human Man* displays all four locations. (b) The sagittal slice of the *Visible Human Woman* also shows the surface and subdermal locations.

ratio of 15 represents most adults, and lastly the ratio of 30 represents cadavers suffering from postcellular death. Ages that overlap scalp-to-skull conductivity ratios accommodate inter- and intrasubject variability [1, 8]. Taking standard skin conductivity values [9, 10] divided by the adult skull conductivity values yields a ratio of 8.5, and then scaled by the living to postmortem factor [6, 11, 12] yields approximately 20 to 26. These ratios fit accordingly with [13], which reported a ratio of 15 for post mortem skulls beyond cellular death.

In the present study we apply the concepts of the half-sensitivity volume (HSV) [14] and region of interest sensitivity ratio (ROISR) [15]. We use these metrics to analyze the effects of EEG electrode implantation on the measurement sensitivity distribution within the brain. Specifically, we aim to compare the sensitivity distributions of the bipolar subdermal EEG measurement with the well-documented surface electrode according to a patient's age [6, 14, 16–19].

2. Methods

2.1. Sensitivity Distribution. The sensitivity distributions of measurement leads in an inhomogeneous volume conductor can be illustrated with lead current fields as defined by [20–22]. The lead vectors define the relationship between the measured signal in the lead and the current sources in the volume conductor such that

$$V_{\mathrm{LE}}(\mathbf{x}) = \int_v \frac{1}{\sigma}\mathbf{J}_{\mathrm{LE}} \cdot \mathbf{J}^i dv, \tag{1}$$

where $V_{\mathrm{LE}}(\mathbf{x})$ is the voltage, for example, measured EEG voltage, in the volume conductor v. The reciprocal current field $\mathbf{J}_{\mathrm{LE}}$ is the lead field, $\mathbf{J}^i$ (A/cm^2) is the impressed current density vector in the volume conductor, and σ is the conductivity (S/m) [17].

The sensitivity distribution in the volume conductor can be established by applying the reciprocity theorem of Helmholtz with Poisson' equation (2) applied to describe quasistatic bioelectric source-field problems [23, 24]. A source distribution, $\mathbf{J}^i$, containing only reciprocal source currents at the measurement electrodes raises a gradient potential distribution, $\nabla\Phi$, that is, measurement sensitivity, according to the linear Poisson equation

$$\nabla \cdot (\boldsymbol{\sigma}\nabla\Phi) = \nabla \cdot \mathbf{J}^i \quad (\text{in } \Omega), \tag{2}$$

setting the Neumann boundary conditions equal to zero on the scalp

$$\boldsymbol{\sigma}(\nabla\Phi)\cdot\mathbf{n}=0 \quad (\text{on } \Gamma_\Omega), \tag{3}$$

where $\boldsymbol{\sigma}$ is the electrical conductivity tensor, Φ is the electrical potential, $\mathbf{J}^i$ is the current source density, $\mathbf{n}$ is a vector normal to the surface, Ω is the volume of the head, and Γ_Ω is the surface of the head [25].

2.2. The Half-Sensitivity Volume. In Malmivuo et al. [14], the concept of the half-sensitivity volume (HSV) was applied to define the volume in which the sensitivity of the measurement lead is concentrated. The HSV is the size of the volume within the source region of the volume conductor, where the magnitude of the sensitivity is at least half of its maximum value. The size of the HSV reflects how focused the region is from which the lead measures bioelectric activity, that is, smaller volumes have a higher measurement resolution and, conversely, larger volumes have a lower measurement resolution. The half-sensitivity volume is thus applied to evaluate the ability of the lead to concentrate the measurement sensitivity.

2.3. The Region of Interest Sensitivity Ratio. Väisänen et al. [15] introduced the concept of the region of interest sensitivity ratio (ROISR), which provides a parameter to analyze the specificity of a measurement system. Equation (4) defines ROISR as a ratio between the average sensitivity of a predefined region-of-interest (ROI) volume v_{ROI} (5) and the average sensitivity in the rest of the source volume, hereafter called a nonROI volume. The ratio is formulated such that

$$\mathbf{ROISR}=\frac{(1/|v_{\text{ROI}}|)\int_{v_{\text{ROI}}}\nabla\Phi_{\text{LE}}(\mathbf{y},\mathbf{x})\,dy}{(1/|v_{\text{nonROI}}|)\int_{v_{\text{nonROI}}}\nabla\Phi_{\text{LE}}(\mathbf{y},\mathbf{x})\,dy}, \tag{4}$$

where v_{ROI} is the ROI source volume (cm^3) and v_{nonROI} is the nonROI source volume (cm^3).

In the case of EEG, the nonROI volume consists of the entire brain source volume excluding the ROI volume. ROISR thus defines how well the measurement sensitivity is concentrated within the selected ROI, that is, how specific the measurement is to the signals generated within the ROI. We define the ROI volume as

$$v_{\text{ROI}}=v_B\bigcap v_S, \tag{5}$$

where v_B is the brain source volume containing the gray and white matters, and v_S is a sphere with a 20 mm radius from the cortical electrode located on the occipital cortex surface (10/20 location, O_Z, Figure 2). Consequently, our ROI contains both gray and white matters. We selected this location due to its relevance in visually evoked studies by Sörnmo and Laguna [26].

2.4. Model and Computations. We calculate the sensitivity distributions in a realistically shaped male and female heads model based on the U.S. National Library of Medicine's Visible Human Project digital male and female anatomical dataset [27–29], VHP. Calculation of the sensitivity distributions is based on the principle of reciprocity and the numerical finite difference method (FDM) solution of EEG electrode sensitivity. In the FDM model, the segmented head data from a magnetic resonance image (MRI) data set is divided into cubic elements forming a resistive network [30]. The conductivities, of the elements correspond to the tissue conductivities and the dimensions of the elements correspond to the resolution of the dataset. The FDM is based on Poisson's equation that can be used to describe the bioelectric quasistatic source field problems [24]. A potential distribution within the model for a specific source configuration is solved with linear equations and iterative methods [31, 32].

EEG source localization and head model simulations significantly depend on the conductivities used in the models. In literature many studies apply a brain-to-skull conductivity ratio between 15 and 80 [33]; however, these two parameters vary widely in their conductivity values. The brain tissue conductivity value ranges from 0.12 S/m to 0.48 S/m [1, 8, 34–40], whereas the skull conductivity value ranges from 0.0042 S/m to 0.3 S/m [5, 8, 11, 13, 34–36, 41]. The scalp (skin) conductivity value varies less in literature from 0.33 S/m to 0.45 S/m [8, 9, 34, 35, 42]. Therefore, in the present study we apply the scalp-to-skull conductivity ratios of 5, 8, 15, and 30 : 1 [1, 6, 13, 38–40, 43]. The tissues and their corresponding conductivity values that we used in this study are listed in Table 1 [10].

We calculate the sensitivity distributions of the brain for each bipolar electrode pair located on the scalp and the skull. The surface electrodes (a.k.a. scalp electrodes) and the subdermal electrodes measure 1 mm × 1 mm × 1 mm, which reflects the size of one pixel. These dimensions represent one type of subdermal recording electrodes that are insulated up to the tip. Our bipolar leads reflect a visually evoked measurement over the occipital cortex (10/20 location O_Z) referenced against an apex electrode (10/20 location C_Z). The sagittal views of the models (Figure 2) show the two bipolar EEG locations: surface electrode on the scalp and the subdermal electrode on the skull.

3. Results

Figures 3 and 4 present the sensitivity distributions of both the scalp and subdermal leads solved with different conductivity ratios. Clearly, the conductivity ratio has a significant impact on the sensitivity distribution when we consider only one type of electrodes. However, the comparison of both types of electrodes diminishes the influence of the conductivity correlated with age, thus indicating the improved measurement resolution of the needle electrodes irrespective of the patient's age.

Optimally placed subdermal electrodes nearly outperform surface electrodes at every age. The smearing effect of the scalp disappears with the subdermal leads because the recording locations are closer to the target region, thus bypassing the skin (Figures 3 and 4). Tables 2 and 3 show that

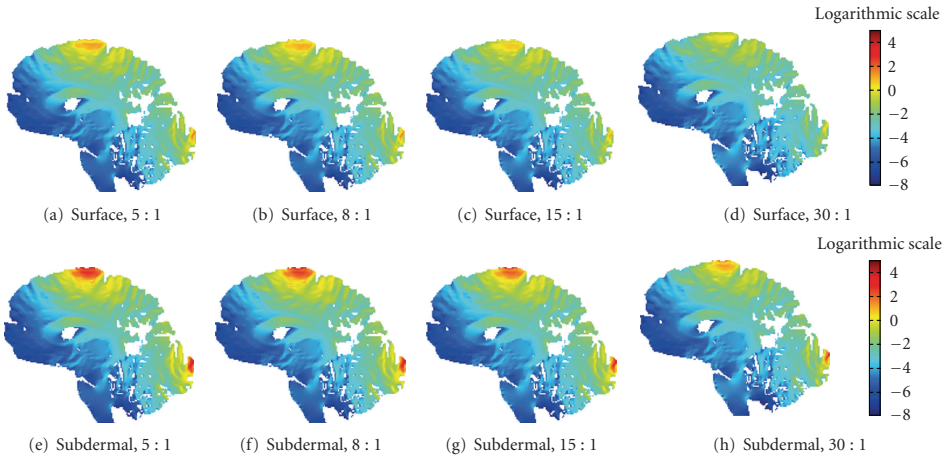

Figure 3: Measurement sensitivity distributions of the *Visible Human Man* mapped in the logarithmic scale: ((a)–(d)) surface electrodes placed on the scalp solved according to the scalp-to-skull conductivity ratio mentioned in the subcaption and ((e)–(h)) subdermal insulated needle electrodes inserted through the skin placing the measuring tip on the skull surface solved according to the scalp-to-skull conductivity ratio mentioned in the subcaption. Scalp-to-skull conductivity ratios are specified in each subcaption: ((a), (e)) 5 : 1, ((b), (f)) 8 : 1, ((c), (g)) 15 : 1, and ((d), (h)) 30 : 1.

Table 1: Tissues and conductivities (S/m) included in our realistic head models [10].

Tissue	Conductivity (S/m)	Tissue	Conductivity (S/m)
Bone marrow	0.046	Scalp	0.43
Fat	0.040	Eye	0.51
Skull/Bones	0.087, 0.054, 0.029, 0.014	Muscles	0.11
White matter	0.14	Blood	1.0
Gray matter	0.33	CSF	1.54
Other neural tissue	0.16		

the subdermal lead's HSV decreases to nearly one-seventh, one-nineth, one-eighth, and one-fourth the size of the scalp lead's HSV. Similarly, we find a 35% to 37% improvement in the subdermal lead's ROISR over the surface lead's ROISR. Figures 3 and 4 illustrate that the subdermal measurement distributions visibly concentrate the measurement sensitivity more efficiently to the target region on the cortex of the younger patient's skull (i.e., lower conductivity values). Moreover, the smearing effect of the skull is reduced with the subdermal leads, and nearly the entire scalp and skull smearing is eliminated when the patient is the youngest (i.e., the skull conducting value is at its peak). Conversely, the older the patient, namely, the higher the scalp-to-skull conductivity ratio, the more the skull conductivity smears the lead field formation. Precisely, the subdermal leads measure neuroelectric activity on or near the gyral cortical surface rather than sulcal or deep sources.

4. Discussion

The present study compares two variables influencing EEG source localization studies: age and electrode location. This study shows that the ratio between the scalp and subdermal measurements regarding the HSV is smallest with the lowest skull conductivity ratio. The correlation between the HSV ratios indicates that measurements will be more localized, that is, increased sensitivity, with higher specificity (ROISR). The subdermal measurement distributions visibly concentrate the measurement sensitivity more efficiently to the target region on the cortex as the skull conductivity increases. The smearing effect of the scalp is reduced with the subdermal leads, and nearly the entire scalp and skull smearing is eliminated when the skull has its highest conducting value [8]. Precisely, the subdermal leads measure neuroelectric activity on or near the gyral cortical surface rather than sulcal or deep sources.

Tissue conductivities such as skin, cortical bone, and brain conductivities change with age [41, 44–50]. Their results indicate a decrease in conductivity between 40.7% and 75.4% from newborn to maturity stages. Furthermore, their results show that the aging process slows during childhood before adolescence after the rapid growth phases of the body have been completed. This is due to the reduction of water content in tissue as a function of age [47, 50]. We believe that the conductivity of the skin changes

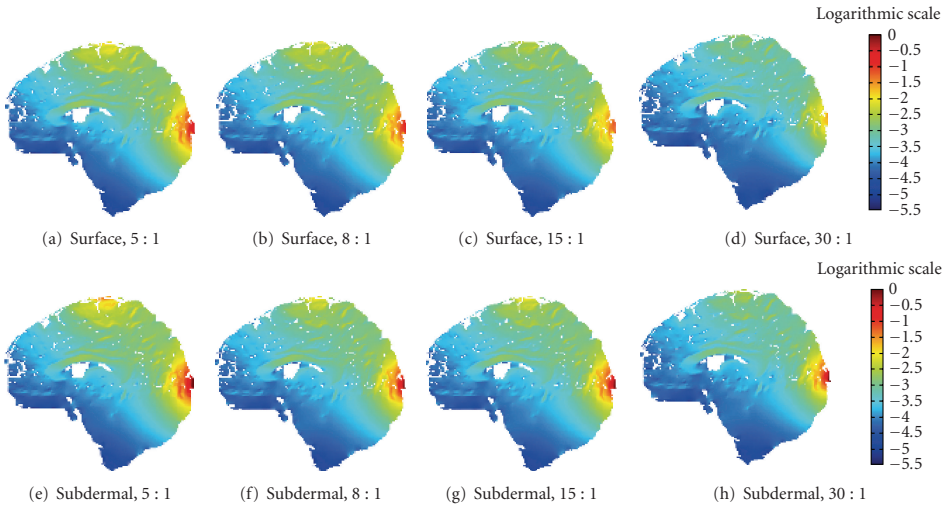

Figure 4: Measurement sensitivity distributions of the *Visible Human Woman* mapped in the logarithmic scale: (a)–(d) surface electrodes placed on the scalp solved according to the scalp-to-skull conductivity ratio mentioned in the subcaption and (e)–(h) subdermal insulated needle electrodes inserted through the skin placing the measuring tip on the skull surface solved according to the scalp-to-skull conductivity ratio mentioned in the subcaption. Scalp-to-skull conductivity ratios are specified in each subcaption: (a), (e) 5 : 1, (b), (f) 8 : 1, (c), (g) 15 : 1, and (d), (h) 30 : 1.

Table 2: Results of the visually evoked bipolar measurement for the surface and subdermal leads of the *Visible Human Man* dataset. All parameters are calculated from the brain region containing both the gray and white matters.

Leads	Conductivity Ratio	Maximum Sensitivity (A/cm^3)	HSV (mm^3)	ROISR
Surface	5 : 1	0.420	4999	2.43
Surface	8 : 1	0.405	5239	2.31
Surface	15 : 1	0.387	4002	2.09
Surface	30 : 1	0.336	2446	1.81
Subdermal	5 : 1	0.85	706	3.17
Subdermal	8 : 1	0.83	586	3.00
Subdermal	15 : 1	0.72	516	2.72
Subdermal	30 : 1	0.54	610	2.39

again in late adulthood, that is, the elderly, particularly decreasing in conductivity. Therefore, the skin conductivity from adolescence onwards should minimally affect this study.

We selected our scalp-to-skull conductivity ratios to span from early childhood through adulthood. Our skull values reflect an 83.9% decrease in the human skull conductivity value compared with the 75.4% change in rats, whereas we kept a fixed conductivity for the brain and skin. When we compare similar sets of measurements such as the surface measurements we obtain an improvement in measurement, resolution between 10.4% and 51.1% for the HSV and an improvement in the measurement accuracy between 25.5% and 38.2% for the ROISR. When we include the subdermal needle measurements, we yield improvements between 75% and 89% in the measurement resolution over the surface electrodes. If we had factored in growth from youth through adolescence to adulthood, then the change in HSV and ROISR would have increased the variation in the results. The additional variables would have plausibly enhanced the measurement precision in childern due to the high water content of their tissues [47].

5. Conclusion

The implantation of EEG electrode on the skull notably increases the measurement sensitivity and accuracy over traditional surface electrodes. These measurements known as subdermal or subcutaneous measurements bypass the artifact prone skin to obtain relatively artifact-free, high-resolution EEG recordings. The measurement sensitivity of the needle electrodes concentrates the subdermal EEG measurements. Consequently, the subdermal electrode reduces the need for the extremely invasive electrocorticogram (ECoG) and minimizes the influence of age on EEG source

Table 3: Results of the visually evoked bipolar measurement for the surface and subdermal leads of the *Visible Human Woman* dataset. All parameters are calculated from the brain region containing both the gray and white matters.

Leads	Conductivity Ratio	Maximum Sensitivity (A/cm^3)	HSV (mm^3)	ROISR
Surface	5 : 1	0.900	221	5.95
Surface	8 : 1	0.775	199	5.41
Surface	15 : 1	0.515	190	4.58
Surface	30 : 1	0.379	198	3.68
Subdermal	5 : 1	1.689	44	6.88
Subdermal	8 : 1	1.671	36	6.60
Subdermal	15 : 1	1.595	27	6.20
Subdermal	30 : 1	1.491	25	5.92

localization. We found that the scalp-to-skull conductivity ratio influenced the subdermal EEG measurement less than the surface EEG measurements. From our correlative study we can definitively claim that children, specifically preadolescent children, would benefit the most from the increased resolution of the subdermal electrodes.

The age plays an important role in the surface electrode measurements, but the change in measurement location to subdermal electrodes irrefutably improves the measurement sensitivity distributions. Succinctly, the subdermal electrodes outperform surface electrodes because they minimize the effect due to the intersubject variability in the scalp-to-skull conductivity ratio associated with the change in age.

References

[1] J. Latikka, T. Kuurne, and H. Eskola, "Conductivity of living intracranial tissues," *Physics in Medicine and Biology*, vol. 46, no. 6, pp. 1611–1616, 2001.

[2] J. R. Ives, "New chronic EEG electrode for critical/intensive care unit monitoring," *Journal of Clinical Neurophysiology*, vol. 22, no. 2, pp. 119–123, 2005.

[3] S. Fossi, A. Amantini, A. Grippo, et al., "Continuous EEG-SEP monitoring of severely brain injured patients in NICU: methods and feasibility," *Neurophysiologie Clinique*, vol. 36, no. 4, pp. 195–205, 2006.

[4] G. Bryan Young, J. R. Ives, M. G. Chapman, and S. M. Mirsattari, "A comparison of subdermal wire electrodes with collodion-applied disk electrodes in long-term EEG recordings in ICU," *Clinical Neurophysiology*, vol. 117, no. 6, pp. 1376–1379, 2006.

[5] R. Hoekema, G. H. Wieneke, F. S. S. Leijten, et al., "Measurement of the conductivity of skull, temporarily removed during epilepsy surgery," *Brain Topography*, vol. 16, no. 1, pp. 29–38, 2003.

[6] K. Wendel and J. Malmivuo, "Correlation between live and post mortem skull conductivity measurements," in *Proceedings of the 28th Annual International Conference of the IEEE Engineering in Medicine and Biology Society*, pp. 4285–4288, August 2006.

[7] K. L. Moore and A. F. Dalley, *Clinically Oriented Anatomy*, Lippincott Williams & Wilkins, Philadelphia, Pa, USA, 5th edition, 2005.

[8] C. H. Wolters, A. Anwander, X. Tricoche, D. Weinstein, M. A. Koch, and R. S. MacLeod, "Influence of tissue conductivity anisotropy on EEG/MEG field and return current computation in a realistic head model: a simulation and visualization study using high-resolution finite element modeling," *NeuroImage*, vol. 30, no. 3, pp. 813–826, 2006.

[9] T. C. Ferree, K. J. Eriksen, and D. M. Tucker, "Regional head tissue conductivity estimation for improved EEG analysis," *IEEE Transactions on Biomedical Engineering*, vol. 47, no. 12, pp. 1584–1592, 2000.

[10] C. Ramon, P. H. Schimpf, and J. Haueisen, "Influence of head models on EEG simulations and inverse source localizations," *BioMedical Engineering Online*, vol. 5, article 10, 2006.

[11] J. D. Kosterich, K. R. Foster, and S. R. Pollack, "Dielectric permittivity and electrical conductivity of fluid saturated bone," *IEEE Transactions on Biomedical Engineering*, vol. 30, no. 2, pp. 81–86, 1983.

[12] J. D. Kosterich, K. R. Foster, and S. R. Pollack, "Dielectric properties of fluid-saturated bone—the effect of variation in conductivity of immersion fluid," *IEEE Transactions on Biomedical Engineering*, vol. 31, no. 4, pp. 369–374, 1984.

[13] T. F. Oostendorp, J. Delbeke, and D. F. Stegeman, "The conductivity of the human skull: results of in vivo and in vitro measurements," *IEEE Transactions on Biomedical Engineering*, vol. 47, no. 11, pp. 1487–1492, 2000.

[14] J. Malmivuo, V. Suihko, and H. Eskola, "Sensitivity distributions of EEG and MEG measurements," *IEEE Transactions on Biomedical Engineering*, vol. 44, no. 3, pp. 196–208, 1997.

[15] J. Väisänen, O. Väisänen, J. Malmivuo, and J. Hyttinen, "New method for analysing sensitivity distributions of electroencephalography measurements," *Medical and Biological Engineering and Computing*, vol. 46, no. 2, pp. 101–108, 2008.

[16] M. F. Suesserman, F. A. Spelman, and J. T. Rubinstein, "In vitro measurement and characterization of current density profiles produced by nonrecesed, simple recessed, and radially varying recessed stimulating electrodes," *IEEE Transactions on Biomedical Engineering*, vol. 38, no. 5, pp. 401–408, 1991.

[17] J. Malmivuo and R. Plonsey, *Bioelectromagnetism: Principles and Applications of Bioelectric and Biomagnetic Fields*, Oxford University Press, New York, NY, USA, 1995.

[18] S. Grimnes and O. G. Martinsen, *Bioimpedance and Bioelectricity Basics*, Academic Press, San Diego, Calif, USA, 2000.

[19] J. O. Ollikainen, M. Vauhkonen, P. A. Karjalainen, and J. P. Kaipio, "Effects of electrode properties on EEG measurements and a related inverse problem," *Medical Engineering and Physics*, vol. 22, no. 8, pp. 535–545, 2000.

[20] R. McFee and F. D. Johnston, "Electrocardiographic leads: I. Introduction," *Circulation*, vol. 8, no. 10, pp. 554–568, 1953.

[21] R. McFee and F. D. Johnston, "Electrocardiographic leads: II. Analysis," *Circulation*, vol. 9, no. 2, pp. 255–266, 1954.

[22] R. McFee and F. D. Johnston, "Electrocardiographic leads: III. Synthesis," *Circulation*, vol. 9, no. 6, pp. 868–880, 1954.

[23] H. L. F. Helmholtz, "Über einige Gesetze der Vertheilung elektrischer Ströme in körperlichen Leitern mit Anwendung auf die thierisch-elektrischen Versuche," *Annalen der Physik und Chemie*, vol. 89, pp. 211–233, 354–377, 1853.

[24] J. Sarvas, "Basic mathematical and electromagnetic concepts of the biomagnetic inverse problem," *Physics in Medicine and Biology*, vol. 32, no. 1, pp. 11–22, 1987.

[25] C. Johnson, M. Mohr, U. Rude, A. Samsonov, and K. Zyp, "Multilevel methods for inverse bioelectric field problems," in *Multiscale and Multiresolution Methods in Computational Science and Engineering*, Springer, Berlin, Germany, 2003.

[26] L. Sörnmo and P. Laguna, *Bioelectrical Signal Processing in Cardiac and Neurological Applications*, Academic Press, San Diego, Calif, USA, 2005.

[27] M. J. Ackerman, "The visible human project," *The Journal of Biocommunication*, vol. 18, no. 2, p. 14, 1991.

[28] National Institutes of Health, "Visible human project," U.S. National Library of Medicine, http://www.nlm.nih.gov/research/visible/visible_human.html.

[29] F. B. Sachse, C. D. Werner, K. Meyer-Waarden, and O. Dössel, "Applications of the visible man dataset in electrocardiology: calculation and visualization of body surface potential maps of a complete heart cycle," in *Proceedings of the 2nd Users Conference of the National Library of Medicine's Visible Human Project*, pp. 47–48, 1998.

[30] X. Franceries, B. Doyon, N. Chauveau, B. Rigaud, P. Celsis, and J.-P. Morucci, "Solution of Poisson's equation in a volume conductor using resistor mesh models: application to event related potential imaging," *Journal of Applied Physics*, vol. 93, no. 6, pp. 3578–3588, 2003.

[31] C. R. Johnson, "Computational and numerical methods for bioelectric field problems," *Critical Reviews in Biomedical Engineering*, vol. 25, no. 1, pp. 1–81, 1997.

[32] P. Kauppinen, J. Hyttinen, P. Laarne, and J. Malmivuo, "A software implementation for detailed volume conductor modelling in electrophysiology using finite difference method," *Computer Methods and Programs in Biomedicine*, vol. 58, no. 2, pp. 191–203, 1999.

[33] S. Rush and D. A. Driscoll, "EEG electrode sensitivity—an application of reciprocity.," *IEEE Transactions on Biomedical Engineering*, vol. 16, no. 1, pp. 15–22, 1969.

[34] C. Gabriel, S. Gabriel, and E. Corthout, "The dielectric properties of biological tissues: I. Literature survey," *Physics in Medicine and Biology*, vol. 41, no. 11, pp. 2231–2249, 1996.

[35] S. Gabriel, R. W. Lau, and C. Gabriel, "The dielectric properties of biological tissues: II. Measurements in the frequency range 10 Hz to 20 GHz," *Physics in Medicine and Biology*, vol. 41, no. 11, pp. 2251–2269, 1996.

[36] S. Gabriel, R. W. Lau, and C. Gabriel, "The dielectric properties of biological tissues: III. Parametric models for the dielectric spectrum of tissues," *Physics in Medicine and Biology*, vol. 41, no. 11, pp. 2271–2293, 1996.

[37] J. A. Latikka, J. A. Hyttinen, T. A. Kuurne, H. J. Eskola, and J. A. Malmivuo, "The conductivity of brain tissues: comparison of results in vivo and in vitro measurements," in *Proceedings of the 23rd Annual International Conference of the IEEE Engineering in Medicine and Biology Society*, vol. 1, pp. 910–912, Istanbul, Turkey, October 2001.

[38] S. Goncalves, J. de Munck, J. P. A. Verbunt, F. Bijma, R. M. Heethaar, and F. H. Lopes da Silva, "In vivo measurement of the brain and skull resistivites using an EIT-based method and realistic models for the head," *IEEE Transactions on Biomedical Engineering*, vol. 50, pp. 754–767, 2003.

[39] S. Gonçalves, J. de Munck, J. P.A. Verbunt, R. M. Heethaar, and F. H. Lopes da Silva, "In vivo measurement of the brain and skull resistivities using an EIT-based method and the combined analysis of SEF/SEP data," *IEEE Transactions on Biomedical Engineering*, vol. 50, no. 9, pp. 1124–1128, 2003.

[40] Y. Lai, W. van Drongelen, L. Ding, et al., "Estimation of in vivo human brain-to-skull conductivity ratio from simultaneous extra- and intra-cranial electrical potential recordings," *Clinical Neurophysiology*, vol. 116, no. 2, pp. 456–465, 2005.

[41] C. Gabriel, A. Peyman, and E. H. Grant, "Electrical conductivity of tissue at frequencies below 1 MHz," *Physics in Medicine and Biology*, vol. 54, no. 16, pp. 4863–4878, 2009.

[42] V. Raicu, N. Kitagawa, and A. Irimajiri, "A quantitative approach to the dielectric properties of the skin," *Physics in Medicine and Biology*, vol. 45, no. 2, pp. L1–L4, 2000.

[43] T. C. Ferree and D. M. Tucker, "Development of high-resolution EEG devices," *International Journal of Bioelectromagnetism*, vol. 1, pp. 4–10, 1999.

[44] A. Peyman, A. A. Rezazadeh, and C. Gabriel, "Chnages in the dielectric properties of rat tissue as a function of age at microwave frequencies," *Physics in Medicine and Biology*, vol. 46, pp. 1617–1629, 2001.

[45] A. Peyman, A. A. Rezazadeh, and C. Gabriel, "Erratum: changes in the dielectric properties of rat tissue as a function of age at microwave frequencies," *Physics in Medicine and Biology*, vol. 47, no. 12, pp. 2187–2188, 2002.

[46] C. Gabriel, "Dielectric properties of biological tissue: variation with age," *Bioelectromagnetics*, vol. 26, supplement 7, pp. S12–S18, 2005.

[47] J. Keshvari, R. Keshvari, and S. Lang, "The effect of increase in dielectric values on specific absorption rate (SAR) in eye and head tissues following 900, 1800 and 2450 MHz radio frequency (RF) exposure," *Physics in Medicine and Biology*, vol. 51, no. 6, pp. 1463–1477, 2006.

[48] A. Peyman, S. J. Holden, S. Watts, R. Perrott, and C. Gabriel, "Dielectric properties of porcine cerebrospinal tissues at microwave frequencies: in vivo, in vitro and systematic variation with age," *Physics in Medicine and Biology*, vol. 52, no. 8, pp. 2229–2245, 2007.

[49] J. Wiart, A. Hadjem, M. F. Wong, and I. Bloch, "Analysis of RF exposure in the head tissues of children and adults," *Physics in Medicine and Biology*, vol. 53, no. 13, pp. 3681–3695, 2008.

[50] A. Peyman, C. Gabriel, E. H. Grant, G. Vermeeren, and L. Martens, "Variation of the dielectric properties of tissues with age: the effect on the values of SAR in children when exposed to walkie-talkie devices," *Physics in Medicine and Biology*, vol. 54, no. 2, pp. 227–241, 2009.

Publication P7

K Wendel, J Väisänen, A Kybartaite, J Hyttinen, and J Malmivuo. The Significance of Relative Conductivity on Thin Layers in EEG Sensitivity Distributions. Biomedizinische Technik (Biomedical Engineering), vol. 55, no. 3, 2010. Published online ahead of print: 5/05/2010, DOI: 10.1515/BMT.2010.012.